

INFORMATION TO USERS

This material was produced from a microfilm copy of the original document. While the most advanced technological means to photograph and reproduce this document have been used, the quality is heavily dependent upon the quality of the original submitted.

The following explanation of techniques is provided to help you understand markings or patterns which may appear on this reproduction.

1. The sign or "target" for pages apparently lacking from the document photographed is "Missing Page(s)". If it was possible to obtain the missing page(s) or section, they are spliced into the film along with adjacent pages. This may have necessitated cutting thru an image and duplicating adjacent pages to insure you complete continuity.
2. When an image on the film is obliterated with a large round black mark, it is an indication that the photographer suspected that the copy may have moved during exposure and thus cause a blurred image. You will find a good image of the page in the adjacent frame.
3. When a map, drawing or chart, etc., was part of the material being photographed the photographer followed a definite method in "sectioning" the material. It is customary to begin photoing at the upper left hand corner of a large sheet and to continue photoing from left to right in equal sections with a small overlap. If necessary, sectioning is continued again — beginning below the first row and continuing on until complete.
4. The majority of users indicate that the textual content is of greatest value, however, a somewhat higher quality reproduction could be made from "photographs" if essential to the understanding of the dissertation. Silver prints of "photographs" may be ordered at additional charge by writing the Order Department, giving the catalog number, title, author and specific pages you wish reproduced.
5. PLEASE NOTE: Some pages may have indistinct print. Filmed as received.

University Microfilms International

300 North Zeeb Road
Ann Arbor, Michigan 48106 USA
St. John's Road, Tyler's Green
High Wycombe, Bucks, England HP10 8HR

77-12,750

MATHAI, Chirathalakal Varughese, 1945-
2.7 MICRON WATER VAPOR BAND ABSORPTION
AND ITS STATIC AND DYNAMIC THERMODYNAMIC
DERIVATIVES.

The University of Oklahoma, Ph.D., 1976
Physics, atmospheric science

Xerox University Microfilms, Ann Arbor, Michigan 48106

THE UNIVERSITY OF OKLAHOMA
GRADUATE COLLEGE

2.7 MICRON WATER VAPOR BAND ABSORPTION AND ITS STATIC
AND DYNAMIC THERMODYNAMIC DERIVATIVES

A DISSERTATION
SUBMITTED TO THE GRADUATE FACULTY
in partial fulfillment of the requirements for the
degree of
DOCTOR OF PHILOSOPHY

BY
CHIRATHALAKAL VARUGHESE MATHAI
NORMAN, OKLAHOMA
1976

2.7 MICRON WATER VAPOR BAND ABSORPTION AND ITS STATIC
AND DYNAMIC THERMODYNAMIC DERIVATIVES

A THESIS

APPROVED FOR THE DEPARTMENT OF PHYSICS

BY

Ingram Prosser
Neal Puffer
Robert M. St. John
Claude E. Dutton
Richard S. Fowler

TO
MY PARENTS, SISTER, BROTHERS
AND MY WIFE

I am grateful to my major advisor, Dr. Sybrand Broersma for his support, understanding, and technical advice. Special thanks are due to Mr. Larry Walls for all his help throughout the course of the experiment and for writing the computer programs. I am thankful to Mr. Paul Hendrickson for his part in the installation of the water vapor cross flow system.

I am thankful to Dr. Fritz Krause and the National Aeronautic and Space Administration for the financial support received. I am grateful to Prof. M. M. Patel and Dr. Jacob Rajan of the Maharaja Sayajirao University of Baroda, India, for training me in atomic and molecular spectroscopy.

I wish to thank all the members of my advisory committee for their help; in particular, I am grateful to Dr. Robert M. St. John for spending so much of his time for me. I also wish to acknowledge Dr. Tom Rhymes for his assistance in plotting the experimental results.

I am pleased to thank my father-in-law, Mr. Isaac K. Kurien for typing the first draft of this thesis. Most of all, I am grateful to my wife, Susy for her encouragement, understanding, support, and patience. I am thankful to her and my daughter, Suma Mary for letting me to take so much of my time which rightly belonged to them.

ABSTRACT

We have measured the absorption and its concentration(c), pressure (P), and temperature(T) dependences over the 2.7 micron vibration-rotation band of water vapor at near atmospheric conditions. For comparison we also have calculated these spectra using a line-by-line method. The line strengths as listed in N. B. S. Monograph 71, should be corrected to account for the non-rigidity of the water vapor molecule. We propose a form

$$F = (0.92 + Z_m)^2$$

for the ratio of the measured to rigid rotator line strengths, the F factor for the ν_3 band of water vapor. Here, $m = J + 1$ for the R branch, $m = -J$ for the P branch, and J is the rotational quantum number of the lower state and $Z = -0.025$.

In addition to the conventional steady state absorption measurements, we have also perturbed the thermodynamic equilibrium of the absorber gas by acoustic excitation. The resulting fluctuations in the transmitted intensity were measured and the pressure derivatives of the absorption under adiabatic conditions, $(\partial A/\partial P)_{ad}$, were derived.

We observe crossover points in the wings of the band, where the absorption and its pressure derivative are independent of the temperature of the water vapor; there is a mild negative T dependence in the core of the band and a strong positive T dependence farther out in the wings. We also see that $(\partial/\partial P(\partial A/\partial P)_{ad})$ is very small in the wings of the band, whereas $(\partial/\partial c(\partial A/\partial P)_{ad})$ is significant. These results can be used to measure the concentration, the pressure, and the temperature of water vapor in the atmosphere.

We have also calculated the absorption and its first and second thermodynamic derivatives for the 3.46 micron hydrogen chloride band. The calculated absorption has also been compared with published results.

TABLE OF CONTENTS

	Page
LIST OF TABLES	viii
LIST OF FIGURES	ix
Chapter	
I. INTRODUCTION	1
II. THEORY	7
A. Introduction	7
B. Vibrational Analysis	8
C. Rotational Analysis	15
1. Rigid Symmetric Top Molecule	16
2. Asymmetric Top Molecule	16
3. Symmetry Properties of Rotational Levels	17
D. Vibration-Rotation Spectra	19
E. Theoretical Line-by-Line Calculation	23
1. 2.7 Micron Water Vapor Band	24
2. 3.46 Micron Hydrogen Chloride Band	25
F. F Factors	25
III. EXPERIMENTAL FACILITIES	30
A. Introduction	30
B. Gas Handling and Vapor Cross Flow System	31
C. Concentration Measurement	33
D. Pressure Measurement and Pressure Control	34
E. Temperature Measurement and Temperature Control	35

F. Pressure Fluctuations and δP Measurements.....	56
G. Optical System	37
H. Electronics	38
IV. THE EXPERIMENTAL METHOD	39
A. Typical Operating Procedure	39
1. The Static Mode	39
2. The Dynamic Mode	41
B. Cell Conditions	42
C. Absorption and its Static Derivatives	43
D. Adiabatic Derivatives	44
E. Data and Data Processing	45
V. ANALYSIS OF RESULTS	48
A. Introduction	48
B. The Static Mode Results	49
C. Static First Derivatives	76
D. Static Second Derivatives	81
E. The Dynamic Mode Results	85
F. Variable δP Analysis	98
G. Discussion of Results	104
H. 3.46 Micron HCl Band Absorption and its Derivatives ...	105
VI. CONCLUSIONS	117
REFERENCES	119

LIST OF TABLES

TABLE	Page
I. Multiplication Table for the Symmetry Operators constituting the C_{2v} Point Group	10
II. Irreducible Representations of the C_{2v} Point Group	11
III. Vibrational Transitions of H_2O at 300^0K	14
IV. Classification of the Energy Levels of the Asymmetric Top Molecule	18
V. Adiabatic Derivatives of the Absorption	23
VI. Table of I Measurements	45
VII. Table of δI Measurements	47
VIII. 2.7 Micron Water Vapor Band Integrated Absorptance for a 1.005 m Column	50

LIST OF FIGURES

FIGURE	Page
1. The Symmetry Elements of the Water Vapor Molecule	9
2. Normal Modes of Vibration of H ₂ O	9
3. Absorptance vs. Wavenumber with Pressure as a Parameter for c = 0.81% and T = 288 ⁰ K	51
4. Absorptance vs. Wavenumber with Pressure as a Parameter for c = 1.62% and T = 288 ⁰ K	52
5. Absorptance vs. Wavenumber with Pressure as a Parameter for c = 0.81% and T = 313 ⁰ K	53
6. Absorptance vs. Wavenumber with Pressure as a Parameter for c = 1.62% and T = 313 ⁰ K	54
7. Absorptance vs. Wavenumber with Pressure as a Parameter for c = 3.24% and T = 313 ⁰ K	55
8. Absorptance vs. Wavenumber with Pressure as a Parameter for c = 0.81% and T = 338 ⁰ K	56
9. Absorptance vs. Wavenumber with Pressure as a Parameter for c = 1.62% and T = 338 ⁰ K	57
10. Absorptance vs. Wavenumber with Pressure as a Parameter for c = 3.24% and T = 338 ⁰ K	58
11. Absorptance vs. Wavenumber with Pressure as a Parameter for c = 4.86% and T = 338 ⁰ K	59
12. Absorptance vs. Wavenumber with Concentration as a Parameter for P = 0.5 atm. and T = 288 ⁰ K	61
13. Absorptance vs. Wavenumber with Concentration as a	

Parameter for $P = 1.0$ atm. and $T = 288^0\text{K}$	62
14. Absorptance vs. Wavenumber with Concentration as a Parameter for $P = 0.75$ atm. and $T = 313^0\text{K}$	63
15. Absorptance vs. Wavenumber with Concentration as a Parameter for $P = 1.0$ atm. and $T = 338^0\text{K}$	64
16. Absorptance vs. Wavenumber with Concentration as a Parameter for $P = 1.25$ atm. and $T = 338^0\text{K}$	65
17. Absorptance vs. Wavenumber with Temperature as a Parameter for $c = 0.81\%$ and $P = 0.5$ atm.	67
18. Absorptance vs. Wavenumber with Temperature as a Parameter for $c = 0.81\%$ and $P = 0.75$ atm.	68
19. Absorptance vs. Wavenumber with Temperature as a Parameter for $c = 0.81\%$ and $P = 1.0$ atm.	69
20. Absorptance vs. Wavenumber with Temperature as a Parameter for $c = 1.62\%$ and $P = 0.75$ atm.	70
21. Absorptance vs. Wavenumber with Temperature as a Parameter for $c = 3.24\%$ and $P = 1.0$ atm.	71
22. F Factor vs. Wavenumber for the ν_1 and ν_3 Bands of H_2O	73
25. Square Root of the F Factor vs. m for the ν_3 Band of H_2O	75
24. Partial Derivative of the Absorption with respect to Pressure times Pressure vs. Wavenumber	77
25. Partial Derivative of the Absorption with respect to Concentration times Concentration vs. Wavenumber	78
26. Partial Derivative of the Absorption with respect to Temperature times Temperature vs. Wavenumber	79
27. Second Partial Derivative of the Absorption with respect	

to Concentration times c^2 vs. Wavenumber	82
28. Second Partial Derivative of the Absorption with respect to Pressure times P^2 vs. Wavenumber	83
29. Mixed Partial Derivative of the Absorption with respect to Concentration and Temperature times cT vs. Wavenumber	84
30. Adiabatic Pressure Derivative of the Absorption times P vs. Wavenumber with Concentration as a Parameter for $P = 1.0$ atm. and $T = 288^0K$ and $T = 295^0K$	86
31. Adiabatic Pressure Derivative of the Absorption times P vs. Wavenumber with Concentration as a Parameter for $P = 1.0$ atm. and $T = 308^0K$	87
32. Adiabatic Pressure Derivative of the Absorption times P vs. Wavenumber with Concentration as a Parameter for $P = 1.0$ atm. and $T = 338^0K$	88
33. Adiabatic Pressure Derivative of the Absorption times P vs. Wavenumber with Temperature as a Parameter for $c = 0.81\%$ and $P = 1.0$ atm.	89
34. Adiabatic Pressure Derivative of the Absorption times P vs. Wavenumber with Temperature as a Parameter for $c = 1.62\%$ and $P = 0.75$ atm.	90
35. Adiabatic Pressure Derivative of the Absorption times P vs. Wavenumber with Temperature as a Parameter for $c = 1.62\%$ and $P = 1.0$ atm.	91
36. Adiabatic Pressure Derivative of the Absorption times P vs. Wavenumber with Temperature as a Parameter for $c = 2.43\%$ and $P = 1.0$ atm.	92

37. Adiabatic Pressure Derivative of the Absorption times P
vs. Wavenumber with Pressure as a Parameter for $c = 1.62\%$
and $T = 293^0\text{K}$ 94

38. Adiabatic Pressure Derivative of the Absorption vs. Wavenum-
ber with Pressure as a Parameter for $c = 1.62\%$ and $T = 293^0\text{K}$ 95

39. Adiabatic Pressure Derivative of the Absorption vs.
Wavenumber with Pressure as a Parameter for $c = 1.62\%$
and $T = 308^0\text{K}$ 96

40. Adiabatic Pressure Derivative of the Absorption vs.
Wavenumber with Pressure as a Parameter for $c = 2.43\%$
and $T = 338^0\text{K}$ 97

41. Second Derivative, $cP(\partial/\partial c(\partial A/\partial P)_{ad.})$ vs. Wavenumber 99

42. Second Derivative, $PP(\partial/\partial P(\partial A/\partial P)_{ad.})$ vs. Wavenumber 100

43. Mixed Derivative, $PT(\partial/\partial T(\partial A/\partial P)_{ad.})$ vs. Wavenumber 101

44. Adiabatic Pressure Derivative of the Absorption times P
vs. Wavenumber with the Fluctuating Pressure as a
Parameter for $c = 3.24\%$, $P = 1.0\text{ atm.}$, and $T = 338^0\text{K}$ 102

45. Fluctuating Intensity vs. Wavelength with Fluctuating
Pressure as a Parameter 103

46. 3.46 Micron Hydrogen Chloride Band Absorptance vs.
Wavenumber with the Absorber Mass as a Parameter 106

47. HCl Band Absorptance vs. Wavenumber for $u = 3.5687$ plotted
along with those of Babrov and Stull and Plass 107

48. Average Energy vs. Wavenumber for the HCl Band 108

49. Partial Derivative, $TA(T)$ vs. Wavenumber with Absorber
Mass as Parameter 109

50. Partial Derivative, $cA(c)$ vs. Wavenumber with Absorber Mass as a Parameter	110
51. Partial Derivative, $PA(P)$ vs. Wavenumber with Absorber Mass as a Parameter	111
52. Adiabatic Derivative, $PA(P)_{ad}$ vs. Wavenumber with Absorber Mass as a Parameter	112
53. Adiabatic Derivative, $PPA(PP)_{ad}$ vs. Wavenumber with Absorber Mass as a Parameter	113
54. Adiabatic Derivative, $PTA(PT)_{ad}$ vs. Wavenumber with Absorber Mass as a Parameter	114
55. Adiabatic Derivative, $cPA(cP)_{ad}$ vs. Wavenumber with Absorber Mass as a Parameter	115

2.7 MICRON WATER VAPOR BAND ABSORPTION AND ITS STATIC
AND DYNAMIC THERMODYNAMIC DERIVATIVES

CHAPTER I

INTRODUCTION

This dissertation deals with research concerning the 2.7 micron water vapor band absorption at near atmospheric conditions. We have measured the static transmitted intensity and its fluctuations, using acoustic excitation, over the entire band. For comparison, we also have theoretically calculated the absorption spectra and its static and dynamic thermodynamic derivatives using a line-by-line method¹. We have investigated the relationship between these spectra and the thermodynamic variables, concentration (c), pressure (P), and temperature (T).

A detailed knowledge of the infrared transmission of planetary atmospheres is of fundamental importance in astrophysics, meteorology, infrared probing, etc. In order to understand how infrared transmission is affected by the atmosphere, it is necessary to learn how and to what extent atmospheric constituents attenuate infrared radiation.

Observations and analyses of spectral measurements of infrared radiation show that the atmospheric absorption at these frequencies is a complex process. The attenuation of infrared radiation in the atmosphere

is mainly due to water vapor, carbon dioxide, and ozone; near infrared radiation also experiences attenuation by fog, haze, dust, and smoke in the atmosphere. This type of attenuation, as well as uncontrollable factors such as temperature and humidity, makes it difficult to obtain quantitative data on true molecular absorption in field studies. Hence, laboratory studies of synthetic or artificial atmospheres are desirable as guide. The absorption in the 2.7 micron region is sufficiently strong so that the water vapor content can be measured spectroscopically at a given location in the atmosphere by various types of instruments such as high altitude balloons or other high altitude vehicles with the sun serving as a radiation source. Good detectors and sources are available for the 2.7 micron region and background emission by the earth and reflected solar radiation are relatively low. Finally our experimental results may be used in the crossed beam correlation technique². Here the atmospheric water vapor is monitored remotely, hoping to estimate water delivery to a certain region and thus predict critical water shortages.

There are two different instrumental approaches in measuring the absorption. (1) Using high resolution, one can determine the exact location of the individual rotational lines and the variation of line strengths and half-widths throughout the absorption band. Interactions between absorbing molecules and other molecules in the absorber path must be considered. On the basis of this information concerning all the absorption lines in the band, it is possible to compute the absorption of radiation for various thermodynamic conditions in the atmosphere. (2) In the second approach, the low resolution method, one experimentally

determines the absorption in small regions of the band containing several rotational lines. Here the effects of fine structure are integrated out. Empirical relations can be obtained, which directly correlate the overall absorption with the thermodynamic variables. The resulting expressions are of immediate use in predicting the overall absorption in the atmosphere. Comparisons of results between these two types of measurements are possible taking into consideration the way in which the instrumentation affects the two types of observations.

In the limit of high resolving power, we define A_ν as the fractional absorption at any given frequency, ν . In practice, because of finite slit width, one deals with a frequency interval. For a given spectrometer setting, one observes a fractional absorption, A'_ν , which is an average value of A_ν for the frequency interval passed by the spectrometer. For an entire vibration-rotation absorption band, it has been shown³ that under fairly general conditions, even for an arbitrary slit function, it is true that

$$\int_{\nu_1}^{\nu_2} A'_\nu d\nu = \int A_\nu d\nu \quad \text{I - (1)}$$

where the first integral represents the area under the observed absorption curve and the limits of integration give a frequency interval $(\nu_2 - \nu_1)$ outside of which there is negligible observed absorption by the band. The second integral is called the total absorption or the equivalent bandwidth, and has limits sufficiently wide to include the entire absorption by the band. Thus the measured total absorption of a band is independent of spectrometer slit width.

Our experiment belongs to approach two while our theoretical

calculations are based on approach one. The experimental spectroscopic region of interest contains three vibration-rotation bands (see Chapter II) of water vapor.

In our experiment we have obtained information in addition to the conventional spectroscopic methods by perturbing the steady state conditions of the absorber gas (introducing known pressure fluctuations using two loudspeakers). This causes fluctuations in the temperature and pressure of the gas. We measure the fluctuation of the transmitted intensity about its mean value, (I) . The experiment was conducted for various c , P , and T values. From this we obtained the absorption spectra and the thermodynamic derivative spectra over the entire 2.7 micron water vapor band.

In the theoretical calculations, we used the line parameters for the 2.7 micron band⁴, line frequencies, line strengths, half-widths, and energies of upper and lower levels to obtain the absorption spectra and the thermodynamic derivative spectra using the line-by-line method¹. These spectra were degraded to 35 cm^{-1} using a triangular slit function so that they could be compared directly with our experimental results. We have shown that the experimental results and the theoretically calculated results show good agreement when adjustments are made in the line strengths (see Chapter II).

The experiment has two parts: in the first part we have measured the I through the sample water vapor for various combinations of thermodynamic variables. Then the absorption is obtained from

$$A = 1 - I/I_0$$

I - (2)

where I_0 is the transmitted intensity with the absorption cell evacuated. By using 2, 3, or 4 of these A versus wavenumber curves, we were able to calculate the static first and second thermodynamic derivative spectra.

In the second part, to be called the pressure fluctuation mode or dynamic mode, known fluctuations are introduced in the absorption cell; and we have measured the fluctuations in the transmitted intensity, δI , as a function of wavelength over the entire 2.7 micron band, for various combinations of static thermodynamic conditions. For the size of the cell and the 14 Hz pressure fluctuation frequency, the acoustic excitation constitutes an adiabatic process (see Chapter II). We then calculate

$$(\partial A / \partial P)_{ad.} = -1 / I_0 (\delta I / \delta P) \quad I - (3)$$

Again, as in the static derivative spectra, we were able to calculate the second derivative spectra using two of these spectra. They are

$$\partial / \partial c (\partial A / \partial P)_{ad.}, \quad \partial / \partial P (\partial A / \partial P)_{ad.}, \quad \text{and} \quad \partial / \partial T (\partial A / \partial P)_{ad.}.$$

These derivative spectra can be of use in the field of environmental science for the detection of small traces of gases. This method is of practical importance because there are fluctuations in the atmosphere in the form of simple pressure and temperature variations with time.

In Chapter II, we discuss the near infrared spectra of asymmetric molecules, water vapor in particular, and also a brief sketch of the method used in our theoretical calculation of the spectra. The experimental set up is explained in Chapter III and the data and data processing methods are in Chapter IV. Experimental results are presented in Chapter V and compared with the theoretical calculations. Chapter V also contains

the results of a similar theoretical calculation we have made for the 3.46 micron fundamental band of hydrogen chloride.

CHAPTER II

THEORY

A. INTRODUCTION

In this chapter we discuss the nomenclature used in the analysis of the near infrared spectrum of asymmetric top molecules with emphasis on the water vapor molecule. We deal first with the vibration and rotation of the molecule separately. Thereafter they are considered together and the interaction of the two types of motion, the fine structure of infrared bands, is examined. The F factors for the 2.7 micron H_2O band are then introduced so that they can be used to correct the line strengths of the rotational lines in our calculation.

A molecule absorbs infrared radiation when a transition between two vibration-rotation energy levels takes place. A vibrating molecule will interact with the electromagnetic radiation, if an oscillating dipole moment is associated with the vibration. A change in dipole moment occurs for a molecule whenever a change in relative position of the centers of positive and negative charges, resulting from the atomic motion, occurs. We shall neglect the quadrupole interaction on account of its much lower probability.

Infrared absorption bands can be related to the motions of the individual atoms that comprise a molecule. The motions of atoms are

generally divided into vibrations and rotations and the former into different types of vibrations. The overall complex motion of all the atoms in a molecule can be approximately resolved into a small number of basic motions which are designated as the normal vibrations or the fundamental vibrations of the molecule.

B. VIBRATIONAL ANALYSIS

Use of group theory and symmetry operations is of great importance in the theory of molecular structure and molecular spectra. The symmetry properties of a body involve two distinct concepts. First, it may possess certain elements of symmetry. Second, given these elements, there are symmetry operations which can be carried out with respect to them.

Let us consider the case of water vapor molecule in particular.

H_2O is a non-linear, planar triatomic molecule as shown in Figure 1, with YZ as the plane of the molecule. The equilibrium values of the HOH angle and O-H distance are given by $104^\circ 27'$ and 0.958×10^{-8} cm. respectively⁵.

The symmetry operations which can be performed on H_2O are: (1) a rotation of π around the two-fold axis, C_2 , (2) a reflection in the vertical plane, σ_v , (3) a reflection in another vertical plane, σ_v' , and (4) the identity, I.

The symmetry operations form the elements of a finite group known as the C_{2v} group. The multiplication table for this group of symmetry operators for H_2O is given in Table I.

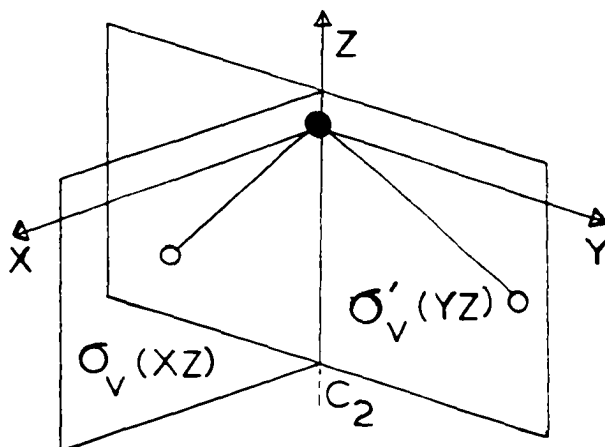


Figure 1. The symmetry elements of the water molecule

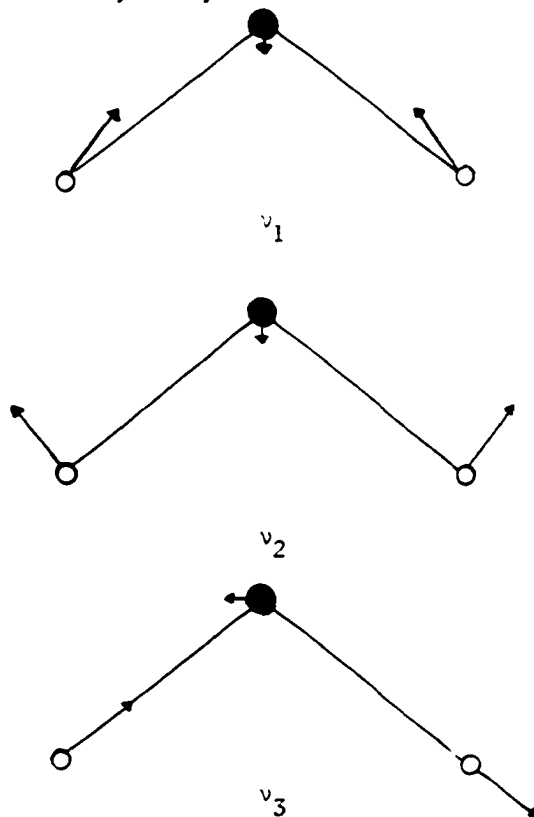


Figure 2. The normal modes of vibration of H_2O

TABLE I
 MULTIPLICATION TABLE FOR THE SYMMETRY OPERATORS
 CONSTITUTING THE C_{2v} POINT GROUP⁶

	I	C_2	σ_v	$\sigma_{v'}$
I	I	C_2	σ_v	$\sigma_{v'}$
C_2	C_2	I	$\sigma_{v'}$	σ_v
σ_v	σ_v	$\sigma_{v'}$	I	C_2
$\sigma_{v'}$	$\sigma_{v'}$	σ_v	C_2	I

If we replace each symmetry operation of an Abelian group (a group is called an Abelian, if all the elements of that group commute) by a number, such that the products of the numbers correspond with laws of multiplication for the group, then that set of numbers is said to form a representation of the group. There are four irreducible representations of the C_{2v} , shown in Table II; these are related to the types of possible molecular vibrations.

TABLE II
 IRREDUCIBLE REPRESENTATIONS OF C_{2v} POINT GROUP

I	C_2	σ_v	$\sigma_{v'}$	Species
1	+1	+1	+1	A_1
1	+1	-1	-1	A_2
1	-1	+1	-1	B_1
1	-1	-1	+1	B_2

In the case of H_2O , a vibration can be either symmetric or anti-symmetric with respect to the symmetry operation, and therefore the only numbers possible are +1 or -1. Each set of numbers along a row (a representation) gives rise to a different type of vibration in the molecule and is referred to as a species of vibration. So, for H_2O , there are four species of vibrations that are possible (though one of these will be eliminated later), each corresponding to an irreducible representation in Table II. The representations are labeled A_1 , A_2 , B_1 , and B_2 .

In the case of any planar molecule, two of the three principal axes lie in the molecular plane, one of which is the C_2 axis, and the third axis is perpendicular to the molecular plane. The three normal modes of vibration of H_2O are: (1) a symmetric stretch, (2) a bend, and (3) an asymmetric stretch. These three and the associated frequencies are

shown in Figure 2. Each of the normal vibrations is represented by the variation in time of one normal coordinate. The normal vibrations for H_2O cannot be degenerate on account of the molecular symmetry⁶. All three vibrations remain unchanged under an identity operation and the reflection in the molecular plane. Vibrations ν_1 and ν_2 are also unchanged under the group operations C_2 and σ_v , and therefore they belong to the A_1 representation or A_1 species. However the direction of all the displacements in ν_3 are reversed under C_2 and σ_v operations, and so this vibration belongs to the B_2 representation.

According to quantum mechanics, the vibrational transition probability is proportional to the square of the transition moment,

$$[\vec{M}]^{v'v''} = \int \psi_{v'} \vec{M} \psi_{v''}^* d\tau \quad \text{II - (1)}$$

where $\psi_{v'}$ and $\psi_{v''}$ are the vibrational eigenfunctions of the upper and lower state respectively. The dipole moment \vec{M} has components,

$$M_x = \sum e_i x_i, \quad M_y = \sum e_i y_i, \quad \text{and} \quad M_z = \sum e_i z_i$$

where e_i is the charge of the particle i at (x_i, y_i, z_i) .

Only those vibrational transitions are allowed for which the transition moment is nonzero, i.e., at least one component of the integrand

$$\psi_{v'} \vec{M} \psi_{v''}^*$$

remains unchanged for any of the four symmetry operations. In other words, at least one of the quantities,

$$\psi_{v'} M_x \psi_{v''}^*, \quad \psi_{v'} M_y \psi_{v''}^*, \quad \psi_{v'} M_z \psi_{v''}^*,$$

should be totally symmetrical for a vibrational transition to be an allowed one. So, a vibrational transition $v' \leftrightarrow v''$ is allowed⁵ only when there is at least one component of the dipole moment \vec{M} that has the same species as the product $\psi_{v'}\psi_{v''}$. Accordingly, the only allowed vibrational transitions for H_2O are A_1 , B_1 , and B_2 ; species A_2 is thus infrared inactive. The same general rule applies to overtone bands also.

The water molecule with three non-degenerate eigenvibrations has vibrational energy⁷ correct to second order, in the anharmonic oscillator approximation, given by

$$G_0(v_1, v_2, v_3) = \sum_{i=1}^3 \omega_i (v_i + 1/2) + \sum_{i=1}^3 \sum_{j>i} x_{ij} (v_i + 1/2) (v_j + 1/2)$$

II - (2)

where the constants ω_i and x_{ij} are⁸

$\omega_1 = 3825.32$	$x_{12} = -20.02$
$\omega_2 = 1653.91$	$x_{13} = -155.06$
$\omega_3 = 3935.59$	$x_{22} = -19.50$
$x_{11} = -43.89$	$x_{23} = -19.81$
	$x_{33} = -46.87$

Accidental degeneracies occur when two or more vibrational states have the same symmetry type or nearly the same energy. This situation does not occur in H_2O for any of the fundamental vibration states, but does occur for the states (002) and (200) and for all subsequent pairs of states, $(v_1 - 2, v_2, v_3 + 2)$ and (v_1, v_2, v_3) . For H_2O the first contribution from the perturbation associated with the resonance comes

from fourth order terms.

Table III lists some of the vibrational transitions, band centers (calculated using the energy equation), relative intensities, and ΔK (see section II - C).

TABLE III
VIBRATIONAL TRANSITIONS OF H₂O AT 300°K⁷

Region	Transition	Band Origin (cm ⁻¹)	Relative Intensity	ΔK
6.3 μ	000→010	1595.0	1.00	+ 1
	010→020	1556.4	9.6 x 10 ⁻⁴	+ 1
	010→100	2056.7	1.9 x 10 ⁻⁵	+ 1
	010→001	2160.6	9.6 x 10 ⁻⁵	0
3.2 μ	000→020	3151.4	1.00	+ 1
	010→030	3073.4	4.8 x 10 ⁻⁴	+ 1
2.7 μ	000→001	3755.8	1.00	0
	000→100	3651.7	0.10	+ 1
	010→011	3737.0	4.8 x 10 ⁻⁴	0
	010→110	3630.0	4.8 x 10 ⁻⁵	+ 1
1.87 μ	000→011	5332.0	1.00	0
	000→110	5225.0	2.0 x 10 ⁻²	+ 1
	000→030	4668.4	6.7 x 10 ⁻³	+ 1
	010→021	5279.0	4.8 x 10 ⁻⁴	0
	010→120	5166.0	9.6 x 10 ⁻⁶	+ 1
	010→040	4551.0	3.2 x 10 ⁻⁶	+ 1
	010→101	5656.6	4.8 x 10 ⁻⁴	0
	010→200	5593.1	3.8 x 10 ⁻⁵	+ 1
	010→002	5847.2	5.8 x 10 ⁻⁵	+ 1

C. ROTATIONAL ANALYSIS

It is customary to label the principal axes of a molecule as a, b, and c so that the principal moments of inertia about these axes have the order

$$I_c > I_b > I_a$$

A molecule in which all the three moments of inertia are equal is called a spherical top; if all three have different values, then it is called an asymmetric top, and if two of them are equal, then it is called a symmetric top. The symmetric tops are divided into two groups: (1) if the two largest moments of inertia are equal, it is a prolate symmetric top, and (2) if the two smallest moments of inertia are equal the molecule is an oblate symmetric top.

We define the rotational constants

$$A = h/8\pi^2cI_a, \quad B = h/8\pi^2cI_b, \quad \text{and} \quad C = h/8\pi^2cI_c$$

where evidently

$$A > B > C.$$

The rotational energy of a molecule can be written in units of cm^{-1} as,

$$E(A, B, C) = A P_a^2 + B P_b^2 + C P_c^2 \quad \text{II - (3)}$$

where P_i are the components of the total angular momentum $\vec{P} \equiv \vec{J}$. For an asymmetric top molecule like H_2O , the rotational energies cannot be expressed as a simple function of the rotational quantum number. It is instructive to look at a less complex symmetric top molecule before we deal with an asymmetric top molecule.

1. Rigid Symmetric Top Molecule

In this case the total angular momentum, \vec{J} , has a constant component K along the top axis of symmetry. The unique axes for prolate and oblate symmetric tops are the a and the c axes respectively. The rotational term values of a prolate symmetric top are⁵

$$F(J, K) = B J (J + 1) + (A - B) K^2 \quad \text{II - (4)}$$

and for an oblate symmetric top, they are

$$F(J, K) = B J (J + 1) + (C - B) K^2 \quad \text{II - (5)}$$

where $J = 0, 1, 2, \dots$ and $K = -J, (-J + 1), \dots, +J$.

All states with $K \neq 0$ are doubly degenerate, and a total of $(2J + 1)$ states exist for each value of J . Since $A > B = C$, for a prolate symmetric top, the energy for a particular J increases with an increase in $|K|$. For an oblate symmetric top the energy for a given J decreases as $|K|$ increases. If we consider a non-rigid symmetric top molecule, the energy levels are⁹

$$F(J, K) = B J (J + 1) + (A - B) K^2 - D_J J^2 (J + 1)^2 - D_{JK} J (J + 1) K^2 - D_K K^4, \quad \text{II - (6)}$$

where the D 's are small compared to A and B .

2. Asymmetric Top Molecule

The total angular momentum for a given energy level is constant in direction and magnitude, but none of the components of \vec{J} are constant. Since there is no longer a preferred direction which carries out a simple rotation about J , the K degeneracy we encountered in the last section is

removed. Thus, for each value of J there are $(2J + 1)$ different energy levels. Since there is no single quantum number having a definite physical meaning, these $(2J + 1)$ levels are distinguished using a subscript τ added to J such that

$$\tau = -J, (-J + 1), \dots, +J \quad \text{II - (7)}$$

The rotational energy can still be written as a function of the rotational constants as before in equation II - (3). Ray¹⁰ has solved the energy equation to obtain the energy levels, by using a change of variables method as,

$$E(A, B, C) = F(J_\tau) = \frac{A + C}{2} J(J + 1) + \frac{A - C}{2} E_\tau(\kappa) \quad \text{II - (8)}$$

$$\text{where } E(\kappa) = \frac{2}{A - C} E(A, B, C) - \left(\frac{A + C}{A - C}\right) J(J + 1) \quad \text{II - (9)}$$

and $\kappa = \frac{2B - A - C}{A - C}$, is called the asymmetry parameter. When $\kappa = -1$ or $+1$, the equation II - (8) reduces to the two equations obtained for the prolate symmetric top and oblate symmetric top respectively.

3. Symmetry Properties of Rotational Levels

The symmetry properties, and hence the selection rules for rotational transitions, are obtained from the behavior of the rotational eigenfunction, ψ_τ . The equation II - (3) remains unchanged when any of the components P_a , P_b , or P_c are replaced by their negatives. This can be accomplished by two-fold rotations about each of the three principal axes of the molecule. These three rotations plus the identity operation constitute the D_2 point group whose character table is given in Table IV, along with the different notations for each species used in the literature.

TABLE IV
 CLASSIFICATION OF THE ENERGY LEVELS OF THE
 ASYMMETRIC TOP MOLECULE⁵

I	Behavior			Species Designation		
	C_2^c	C_2^b	C_2^a	Dennison	Mulliken	King, Hainer, and Cross
1	+	+	+	++	A	e e
1	+	-	-	+-	B_c	o e
1	-	-	+	-+	B_a	e o
1	-	+	-	--	B_b	o o

The first sign in Dennison notation (+ or -) refers to the behavior of ψ_r with respect to C_2^c , and the second refers to C_2^a . In the King, Hainer, and Cross¹¹ notation, the energy levels are labeled by a set of quantum numbers, J, K_{-1} , and K_{+1} where K_{-1} and K_{+1} are the limiting prolate and oblate symmetric top quantum numbers, respectively. The first letter, e or o, refers to the parity of K_{-1} and the second letter to the parity of K_{+1} , e standing for even and o for odd.

Molecules like H_2O have only one two-fold axis about which a rotation interchanges identical atoms. The sub-group C_2 of the D_2 point group gives either a symmetric or an antisymmetric species, A or B respectively. The ++ and -- belong to an A species and +- and -+ belong to a B species.

In a set with a given J value, the levels are alternately antisymmetric or symmetric, and the lowest and the highest levels are symmetric or antisymmetric depending on whether J is even or odd. Thus we can obtain the symmetry of each rotational level.

The total eigenfunction for H_2O , which must obey Fermi statistics must be of species B. For one pair of identical nuclei of spin $1/2$, there are three nuclear spin functions of species A and one of species B. In order to construct a total eigenfunction of species B, we have to combine the A rotational functions with the B spin functions or combine B rotational functions with the A spin functions. Thus B rotational levels have three times the statistical weight of the A levels.

D. VIBRATION - ROTATION SPECTRA

So far we have considered that the vibration and rotation of the molecule take place independently, i.e., pure vibrational and rotational spectra. Now we consider the interaction of the vibration and rotation. In this case, a number of rotational levels are associated with each vibrational state. For a transition between two vibrational states, a number of rotational level pairs may be involved according to the selection rules on the quantum numbers of these levels. Thus we obtain the fine structure of the vibrational band which is discussed next.

We will limit our discussion to asymmetric triatomic molecules and H_2O in particular. First, only a molecule which possesses a permanent dipole moment can exhibit a rotational spectrum. In the case of H_2O the dipole moment is directed along the C_2 symmetry axis.

The energy of a vibrating and rotating molecule, to a good approximation, can be written as the sum of the pure vibrational energy and the rotational energy calculated with effective values of the rotational constants, i.e.,

$$T = G(v_1, v_2, v_3) + F_v(\kappa).$$

The interaction of vibration and rotation will be taken into account by allowing for the periodic change of the moment of inertia during the vibration. We can write for the effective rotational constants,

$$\begin{aligned} A_{(v)} &= A_e - \sum_i \alpha_i^A (v_i + 1/2) \\ B_{(v)} &= B_e - \sum_i \alpha_i^B (v_i + 1/2) \\ C_{(v)} &= C_e - \sum_i \alpha_i^C (v_i + 1/2) \end{aligned} \quad \text{II - (10)}$$

where A_e , B_e , and C_e are the rotational constants referring to the equilibrium position and the α_i 's are small compared to A_e , B_e , and C_e .

We may write,

$$\alpha_i = \alpha_i^{(\text{harmonic})} + \alpha_i^{(\text{anharmonic})} + \alpha_i^{(\text{Coriolis})} \quad \text{II - (11)}$$

The $\alpha_i^{(\text{anharmonic})}$ term results from the anharmonicity of the vibrations which in turn produces the change in equilibrium moment of inertia and hence in the rotational constant. The $\alpha_i^{(\text{Coriolis})}$ term is of importance to our problem of H_2O , in which two vibrational levels of different species lie close together. Though they cannot interact in the rotationless state ($J = 0$ levels), they will indeed interact producing an

increasing repulsion of the rotational levels of the same J with increasing J . The effective rotational constants will be changed from unperturbed values even though there is no shift of the pure vibrational levels. It should be pointed out that only rotational levels of the same overall species and the same J value can perturb one another. Consequently, we have strong Coriolis interaction between ν_1 and ν_3 for H_2O .

The Infrared Spectrum

The infrared spectrum of water vapor is composed of spectral lines corresponding to transitions between different vibration - rotation energy levels. The frequency of a spectral line is determined by the difference between the energies of the two levels involved, according to Bohr's condition, $E_2 - E_1 = h\nu$.

The selection rules governing the allowed transitions for a triatomic molecule are⁵

$$\Delta J = 0, \pm 1 \quad \text{and} \quad J = 0 \nleftrightarrow J = 0 \quad \text{II - (12)}$$

If the alternating dipole moment lies along the axis of least moment of inertia, resulting in A type bands, we have the additional condition,

$$+ + \leftrightarrow - + \quad \text{and} \quad + - \leftrightarrow - - \text{ only.} \quad \text{II - (13)}$$

If the alternating dipole moment lies along the axis of intermediate moment of inertia, resulting in B type bands, we have the additional condition,

$$+ + \leftrightarrow - - \quad \text{and} \quad + - \leftrightarrow - + \text{ only.} \quad \text{II - (14)}$$

These additional conditions for A and B type bands in the King, Hainer and Cross notation are given elsewhere¹². Finally, type C bands are forbidden for any planar triatomic molecule.

The 2.7 micron spectral region consists of three vibration - rotation bands of water vapor: ν_3 , ν_1 and $2\nu_2$ with relative strengths, 120:12:1, and with the band origins at 3755.92 cm^{-1} , 3657.08 cm^{-1} , and 3151.60 cm^{-1} respectively¹³. The ν_3 band is an A type band and ν_1 and $2\nu_2$ are B type bands. The energy level diagrams for the first few J values for these bands are given by Herzberg⁵. Unlike the bands of linear and symmetric top molecules, there is no regularity in line spacing of the P, Q, and R branches of the vibration rotation spectra of an asymmetric molecule except when the asymmetry is very small. The asymmetry of water vapor molecule is not small; κ has a value of -0.4377^4 .

High resolution experimental investigations have been conducted by many workers at Ohio State University^{12,14}. Theoretically calculated, extensive tables for the infrared absorption of water vapor are given in Reference 15. The single largest collection of calculated line parameters for the 2.7 micron band of H_2O are given by Gates et al.⁴

In our experiment, we used a wide slit and thus have low resolution to the extent that the fine structure of the vibration - rotation band is not resolved. Our aim is to determine the behavior of the absorption spectra due to the variations in the thermodynamic conditions.

E. THEORETICAL LINE-BY-LINE CALCULATION

As mentioned in Chapter I, we have also calculated the absorption spectra and their thermodynamic derivatives¹. The reader is referred to that reference for details. The calculations were done on a remote teletype terminal connected to the University of Oklahoma computers.

The absorption and its first and second thermodynamic derivatives are obtained using the tables of Reference 1, with the line parameters of Reference 4 as input data. The dynamic or the adiabatic derivatives are obtained using the relations of Table V, and assuming,

$$\frac{C_p - C_v}{C_p} = 0.28$$

for nitrogen.

TABLE V

ADIABATIC DERIVATIVES OF THE ABSORPTION

$P[\partial A/\partial P]_{ad.}$	$= P \partial A/\partial P + 0.28 T \partial A/\partial T$
$c_P \partial/\partial c [\partial A/\partial P]_{ad.}$	$= c_P \partial^2 A/\partial c \partial P + 0.28 c T \partial^2 A/\partial c \partial T$
$P^2 \partial/\partial P [\partial A/\partial P]_{ad.}$	$= P^2 \partial^2 A/\partial P^2 + 0.28 [PT \partial^2 A/\partial P \partial T - T \partial A/\partial T]$
$PT \partial/\partial T [\partial A/\partial P]_{ad.}$	$= PT \partial^2 A/\partial P \partial T + 0.28 [T \partial A/\partial T + T^2 \partial^2 A/\partial T^2]$

1. 2.7 Micron Water Vapor Band

Reference 4 lists line positions, ν (cm^{-1}); intensity, S (cm/g); half-width, α (cm^{-1}); and energy level of lower state, E (cm^{-1}). There are about 3,500 lines in the region 3335 cm^{-1} to 4100 cm^{-1} with line strengths varying from 9,222 to 0.001. From these, we chose the strongest lines, 720 in total. In the wings of the band (3335 to 3550 cm^{-1} and 3950 to 4100 cm^{-1}) these were lines with intensity $3(\text{cm/g})$ and above, while in the core region of the band (3550 to 3950 cm^{-1}) all the lines with intensity $7 (\text{cm/g})$ and above were included in the calculation.

The calculated spectra are degraded to 35 cm^{-1} by using a triangular slit function. The average absorptance at a wave number ν_j is

$$A(\nu_j) = 1/1225 \left(\sum_i w_i (35 - |\nu_i - \nu_j|) \right) \quad \text{II - (15)}$$

where w_i is the equivalent line width (see Reference 1). The summation is over all lines such that

$$|\nu_i - \nu_j| < 35 \text{ cm}^{-1}.$$

The computer programs for these calculations were first written for the 6.3 micron H_2O band by W. L. Walls¹ in PL/1 computer language. We have modified these for the 2.7 micron H_2O band. For each of the five concentrations, we have obtained the absorption spectrum, three first derivative spectra, three second derivative spectra, and three mixed derivative spectra. We have also obtained the integrated values (the area under the curve) for each of these spectra.

The results of these computations are given in Chapter V.

2. Computer Calculations of 3.46 Micron Hydrogen Chloride Band Absorption

Theoretical calculations were also performed to obtain the absorption and its thermodynamic derivatives of HCl 3.46 micron fundamental band. The choice of this band was based on its importance to propulsion related problems¹⁶.

The line parameters for this band are collected from several sources. Line positions of HCl³⁵ are given in Reference 17, and that of HCl³⁷ in Reference 18. The energy levels of the upper and lower levels are calculated using the formulae in Reference 19 and the rotational constants of Reference 17. Line strengths ($\text{cm}^{-2}/\text{atm}^{-1}$) are taken from References 20, 21, and 22. Line widths ($\text{cm}^{-1}/\text{atm}^{-1}$) are taken from References 23 and 24.

There are 57 lines of HCl³⁵ and HCl³⁷ combined, included in this calculation with line strengths ranging from 10 to 0.001, at 300°K. The values of absorber mass, u , were chosen from 3.5687 (g/cm^2) to 28.5496 in multiples of 2. The values of $n = 0.5$, $m = 1.0$, and $kT/hc = 208.53 \text{ cm}^{-1}$ (see Reference 1) are used in the calculations to obtain the absorption and its thermodynamic derivatives at 1 atmosphere and 300°K. The results of these calculations and their comparison with other published results are presented in Chapter V.

F. F FACTORS

The rotational line parameters for the 2.7 micron water vapor band used in the theoretical calculation of the absorption and its thermodynamic derivatives were taken from the National Bureau of Standards Monograph 71

by Gates et al.⁴ They have used the rigid-rotator approximation to obtain the different parameters of all the lines except for lines arising from levels which were very highly perturbed because of accidental resonance. This amounted to the assumption that the interaction between vibration and rotation was negligible.

For the fundamental bands of polyatomic molecules, several mechanisms cause departure from rigid-rotator intensities. They include centrifugal stretching, Coriolis interactions, and Coriolis perturbations of vibration rotation states of different bands which accidentally have the same, or nearly the same, energy (resonance or near resonance). Marked departures from rigid rotator intensities were observed in several cases including the ν_1 and ν_3 bands of water vapor, such that intensities in one sub-branch are enhanced while those in the opposite sub-branch are decreased. Accordingly, corrections to the calculated values of intensities of lines have to be applied to obtain the true intensities.

Gates et al.⁴, have recognized this error and pointed out that these effects may result in an overestimate of intensities of many high J value lines in the high frequency branches by as much as 200 to 300 percent and in underestimates of the highest J lines in the low frequency branches by 50 to 100 percent.

Maclay²⁵, Babrov and Casden²⁶, and Babrov and Healy²⁷ have shown that large deviations from rigid-rotator strengths exist for the two fundamental bands of water vapor in the 2.7 micron region.

Benedict and Calfee²⁸ have applied corrections for the rigid-rotator assumption in a compilation of line parameters for the 6.3 and 1.9 micron

bands of water vapor. Equations describing these corrections are briefly discussed below.

The intensity of any line at frequency ν may be expressed, in a purely formal way, as:

$$S_{VR} = \frac{\nu}{\nu_0} \cdot S_V^0 \cdot S_R \cdot F, \quad \text{II - (16)}$$

where S_V^0 is the vibrational intensity of a nonrotating molecule at the vibrational origin, ν_0 ; S_R is the rotational intensity for a rigid nonvibrating molecule, and F is the correction factor to account for the vibration - rotation interaction. If there is no vibration - rotation interaction, then $F = 1$.

The rotational intensity²⁸ S_R is

$$S_R = L_R \cdot g \cdot [\exp(-E''/kT)] / Q_R \quad \text{II - (17)}$$

where L_R is the rotational transition line strength, such that

$$\sum_{J'_\tau} L_R(J'_\tau, J''_\tau) = (2J'' + 1) \quad \text{II - (18)}$$

and the rotational partition function, Q_R , is

$$Q_R = \sum_{J''} (2J'' + 1) \cdot g \cdot [\exp(-E''/kT)] \quad \text{II - (19)}$$

The values of g , the statistical weight factor, are:

$$\begin{aligned} g &= 1 \text{ for even } \tau \\ g &= 3 \text{ for odd } \tau \end{aligned} \quad \text{II - (20)}$$

Also

$$\sum_R S_R = 1 \quad \text{II - (21)}$$

Since the intensity is proportional to the square of the transition moment, we have²⁸

$$F = [1 + \phi (J'_\tau, J''_\tau)]^2 \quad \text{II - (22)}$$

F factor correction will be necessary whenever ϕ cannot be neglected in comparison with unity.

In the case of water vapor, the three types of effects which contribute to the F factor are (1) the stretching effect, (2) the Coriolis effect, and (3) the $\Delta\kappa$ effect, in order of decreasing importance.

The stretching about each of the three inertial axes, $\rho = a, b,$ and $c,$ in any rotational state J_τ is proportional to $\langle P_\rho^2 \rangle / I_\rho$. The rotation in each state, J_τ , will therefore lead to a shift in the position of the potential minimum. The first order approximation for this contribution to the F factor is²⁶

$$F = [1 - \alpha (\delta J_a) - \beta (\delta J_b) - \gamma (\delta J_c)]^2 \quad \text{II - (23)}$$

where $\delta J_a, \delta J_b,$ and δJ_c are the differences of the effective angular momenta, i.e.,

$$\delta J_a = \langle (P_a^2)' - (P_a^2)'' \rangle, \text{ etc.} \quad \text{II - (24)}$$

The constants $\alpha, \beta,$ and γ depend on the first two coefficients in the power series expansion of the dipole moment function and the coefficients which express the interaction of rotation about each axis on the normal

vibration. Babrov and Casden²⁶ obtained the values of -0.075, -0.035, and -0.028 for α , β , and γ respectively.

Rotations that induce mixing of vibrational wave functions of opposite symmetry types are classified as Coriolis interactions. In H_2O , the only such rotation in first-order is about the C axis and this effect is negligible for the ν_1 band. A complete quantum mechanical treatment of this effect is given in Reference 29.

The value of the asymmetry parameter, κ differs for all upper vibrational states from its value for the ground state. Again, this $\Delta\kappa$ effect is negligible in the 2.7 micron H_2O band region.

We have found the ratio of the degraded experimental absorptance and the degraded calculated absorptance at 5 cm^{-1} intervals, thereby obtaining the F factors indirectly. These F factors are in good agreement with those obtained elsewhere^{26, 27}. It should be pointed out that these two references quote F factors for individual rotational lines, whereas we obtained them using the degraded absorptance. The results are presented in Chapter V.

CHAPTER III
EXPERIMENTAL FACILITIES

A. INTRODUCTION

The apparatus used in our experiment is a modified version of an optical absorption cell with variable path length and temperature³⁰, built during the years 1966-69 at the Illinois Institute of Technology Research Institute and later adapted for a vapor cross flow in our laboratory during 1972-73. An important feature of the cell is the fact that the problems of adsorption and desorption of water vapor by the walls of the cell are eliminated with the cross flow system. A complete description of the original cell is given elsewhere.^{32,33}

The absorption cell is divided into three parts: (1) the left end chamber, (2) the right end chamber, and (3) the middle cell space. Each one of these three sections can be evacuated separately. The middle cell space is made of a 5-inch stainless steel tube, connected to the identical end chambers using two short 3-inch stainless steel tubes and four flanges and O rings. The distance between the two calcium fluoride windows inside the cell and attached to two identical mullite tubes, whose other ends are connected to the end chambers, gives the absorber path length of 1.005 m.

B. GAS HANDLING AND THE VAPOR CROSS FLOW SYSTEM

Two factors make it more difficult to work with samples containing water vapor than most other gases which occur in the atmosphere. The first is the relatively low saturated water vapor partial pressure which occurs near room temperature. The second difficulty arises from the adsorption of water vapor on the walls of the container. Adsorption makes sampling of H_2O vapor difficult, since the amount may be great, depending upon the nature of the surface and the temperature. Furthermore, the adsorption or the desorption process may require several hours to come to equilibrium¹³.

In order to overcome this second difficulty, we have used a continuous vapor-cross-flow system.

Sample water vapor is produced in a 'Vapour-Temp' controlled temperature and humidity chamber, which controls the relative humidity to within 1% of its value. With proper combination settings of the dry bulb temperature, the wet bulb temperature, and the power range selector, the chamber produced satisfactorily the relative humidity required for our experiment^{34, 35}. Slightly more dry nitrogen is fed into the humidity chamber than the wet nitrogen taken out of the chamber, in order to keep a slight overpressure and to prevent carbon dioxide from leaking into the humidity chamber.

Dry nitrogen is injected through a flowmeter and allowed to mix with the wet nitrogen drawn from the humidity chamber in the desired ratio. The resulting sample gas goes either straight to the hot or cold temperature bath or through a compressor, for cell operations above

0.75 atmosphere pressures. The sample gas then enters a gas handling manifold which enables us to measure the water vapor concentrations before the sample gas enters the absorption cell, after it leaves the cell, or completely bypassing the cell. The gas is finally ejected with a pump through a flowmeter which shows the flow rate at any time. The gas handling manifold, associated valves and tubing, and the dew point hygrometer sensor are enclosed in a plexiglass box. The interior of this box is heated with electrical heating tapes and maintained at a temperature which is approximately equal to that of the sample gas.

The sample gas enters the absorption cell through 80 orifices drilled in a stainless steel tube of 1.2 cm. diameter and over one meter long. This tube extends towards and is supported by the flanges at the ends of the 5-inch cell. A similar tube is placed parallel to the first tube, at a distance of 10 cm. The infrared beam passes through the space in between these two tubes, parallel to the tubes. Thus, the sample gas flows across the infrared beam from the orifices in the first tube towards the orifices in the second tube.

Initially, we made a model of the cell flow system with plexiglass and substituted smoke for sample gas. We found that the smoke flow rate was uniform over the entire absorption path when the sample gas entered at the right end of the cell and exited at the left end.

The diffusion of water molecules in the nitrogen across the cell diameter of 5-inches can be expected to take place in about five minutes. Moreover, at a flow rate of 2 liters/minute, the vapor in the 11 liter cell convectively exchanges with a time constant of 5 minutes. Hence,

an equilization to within 1% of the final equilibrium vapor concentration could be expected within 30 minutes³¹.

In order to check this, three hygristors, whose resistance increases with humidity were mounted inside the cell, one at each end and the third at the middle of the cell. The graphs of time versus resistances of these hygristors from the moment the sample gas was introduced into an evacuated cell showed that the humidity reached a constant value in about 40 minutes with a flow rate of about 1 1/2 liters/minute. To some extent, the walls and connections could act as a sink of sample gas and a source of contamination. But at the flow rate used, the gas column of 4.1 cm diameter, path of the infrared beam, in the cell approximated unbounded space quite well. A flow rate of 1 1/2 liters/minute was adequate to suppress wall effects, yet not too fast to give rise to turbulence inside the cell.

C. CONCENTRATION MEASUREMENT

Concentrations of the water vapor samples are measured using a Dew Point Hygrometer. It is an automatic, optically sensed, thermoelectrically cooled, condensation dew point hygrometer. This unit measures the dew point of a sample gas by the primary defining technique; namely, it presents a cooled metal surface to the gas sample so that the temperature of the gas at the metal surface is at the temperature of the metal.

The temperature of the sensor surface is measured by means of an embedded precision thermistor which, in turn, forms a part of an electrical bridge circuit. A zero to fifty millivolts output is

available from the bridge circuit, in addition to a front panel meter graduated in degrees.

Soluble contaminants, such as salts or acids, will change the temperature at which equilibrium occurs, and will result in higher than actual dew points. Insoluble contaminants in the sample gas, such as dust or dirt will not produce an error in the dew point measurement. We have checked the sensor for both kinds of contaminants and found only some dust on it.

The manufacturer had provided us with a calibration curve and our own calibration did not show any significant difference from that curve. We have also checked the calibration regularly for any possible errors and found none.

The dew points of the sample gas were measured both before and after the gas entered the cell. It took about one to one and a half hours to obtain steady state conditions depending on the static pressure. The dew points were also continuously monitored during the course of each run at the outlet side of the cell, to ascertain the constancy of the concentration during the course of the experiment. A different static condition with the same concentration and temperature but higher pressure was obtained after 20 to 30 minutes. The dew points for each static thermodynamic condition, were calculated beforehand.

D. PRESSURE MEASUREMENT AND PRESSURE CONTROL

The pressures in each section of the cell were monitored using NRC 804 thermocouple gauges. In addition, the sample gas pressures were

also measured using an alphanatron gauge and a Bourdon type Heise gauge. The latter could be separated from the system by a vacuum valve, and was pumped out to adjust the zero reading, everytime a pressure measurement was made. Both left and right end chambers and the monochromator were pumped continuously during the experiment to a vacuum of less than 5 microns so that desorption from the walls had no effect.

At the right end of the cell was connected another Heise gauge, a pressure regulator (Mano-watch), and a vacuum pump. The Mano-watch actuated a solenoid valve which regulated the rate at which the gas exhausted through the vacuum pump. Under typical operating conditions the solenoid valve opened and closed once every 5 to 15 seconds and controlled the pressure of the gas in the cell to the precision of 0.2 mm of Hg.

All the static measurements were done at $1/2$, $3/4$, 1, and $5/4$ atmospheric pressures. At lower temperatures, higher concentrations and higher pressures were avoided because of possible condensation inside the cell.

E. TEMPERATURE MEASUREMENT AND TEMPERATURE CONTROL

As mentioned in Section B, the sample gas passed through a hot or cold bath before it entered the cell space. Liquid from the hot or cold bath itself was also circulated by a pump through copper tubing soldered onto the outside walls of the cell. All parts of the thermal equipment and cell walls were carefully insulated.

The heating bath was operated with three commercial heating coils

which were regulated by a proportional electronic temperature controller (Versa-Therm). The Versa-Therm control sensitivity was better than 0.2°C . For temperatures below 25°C , a Blue M cooling unit was used. By adding a heat load it was possible to obtain an appropriate duty cycle and temperature regulation of the cold bath within 0.2°C .

The temperatures of the hot and cold baths were measured using mercury thermometers. The temperatures inside the cell were measured with eight copper-constantan thermocouples in ceramic tubes placed along its length supported by the mullite tubes. The thermocouple wires were connected to two terminal blocks and then to a common temperature reference junction. With melting ice providing the reference temperature, a potentiometer was used to measure the thermoelectric emf's. The temperature variations along the cell were less than 1°C while fluctuations at a given point were about 0.1°C .

F. PRESSURE FLUCTUATIONS AND δP MEASUREMENTS

Pressure fluctuations inside the cell were generated by two 12-inch reinforced cone loudspeakers mounted on the top plate of a foot deep cylindrical tank. A 40-inch long tube connected the speaker cavity to the cell space. The two speakers were connected in series with and actuated by a Dynakit 40 watt amplifier. The amplitude of the pressure fluctuation was adjusted at 14Hz by changing the input voltage to the speakers.

The pressure fluctuations were measured by a model 701A Kistler pressure transducer mounted inside the absorption cell. It measured the

fluctuations about the mean value of the pressure in the cell. This unit was a high sensitivity quartz pressure transducer for dynamic pressure measurements. The pressure transducer outputs were amplified using a model 566 Kistler multirange electrostatic charge amplifier. The sensitivity of the pressure transducer was set at 5.25 picocoulombs/PSI at 15.1 Hz by the factory.

G. OPTICAL SYSTEM

The infrared radiation source was a globar element of silicon carbide, powered by a Hewlett-Packard D. C. power supply. The globar was normally operated at 4 amperes and 45 volts with a resultant source color temperature of about 1400°K .

A chopper produced a light signal in the form of a square wave of 320 Hz; the frequency was measured using a digital counter. A reference signal was also obtained with the chopper and fed into a type A 102B Ad-Yu preamplifier.

The plane reflection grating used had 300 lines/mm and was blazed at 2 microns. The grating provided a reciprocal linear dispersion of 106.1 Angstroms/mm and a resolution of 2.4×10^{-4} microns with 10 micron x 4mm slits.

The entrance and exit slits were both 2 mm wide and 12 mm high. A long wave pass filter with a 2.1 micron cut on, coated on a silicon substrate, was mounted on a plexiglass holder just outside the exit slit. This filter was used to eliminate higher orders of lower wavelength spectra and other stray radiation. Finally, the infrared beam fell on an ellipsoidal mirror which focussed the radiation on to a diffused junction, photovoltaic,

indium antimonide (InSb) detector cooled to liquid nitrogen temperature.

The output from the detector was connected directly to a model 213 Princeton Applied Research (PAR) preamplifier having an input impedance of 10 megohms. The output impedance of the detector, 1000 ohms, and the preamplifier input impedance were matched by connecting a variable resistance R to the output terminal of the detector. For a value of $R = 1500$ ohms, we found that the detector output was increased by a factor of three and that this factor decreased when R was increased or decreased. But for $R = 800$ ohms, the noise in the output decreased by a factor of four compared to the noise with $R = 0$ and $R = 1500$ ohms. We used an 800 ohms resistance thereafter.

H. ELECTRONICS

All the measurements were made using a PAR Lock-in-Amplifier (LIA) and a PAR preamplifier. A PAR selective amplifier was also added for the dynamic mode measurements. These amplifiers were powered by a PAR Nim Bin. The LIA output was recorded by a Honeywell Elektronik 15 dual pen solid state strip-chart recorder.

CHAPTER IV

THE EXPERIMENTAL METHOD

In this chapter, we give the details of the experimental operating procedures, conditions under which the data were taken, and the data processing methods.

A. TYPICAL OPERATING PROCEDURE

In the static mode we have measured mean value intensities, I , and in the dynamic mode we have measured the fluctuations in the mean intensity, δI , about the mean values. First a group of static mode data were taken and their thermodynamic derivatives calculated. Thereafter a group of static and dynamic mode data sets were taken at the same time to obtain I and δI values.

1. Static Mode

Since no dynamic mode data were taken in the first group of data, the speaker cavities and the speaker connections were disconnected. Thus the time required for the conditioning of the cell was reduced by almost half.

The near square wave of frequency 320 Hz, passed through the sample gas in the cell and then through the monochromator where the spectrum was formed. The light reflected from the grating was focussed on the detector

which created an electrical signal proportional to the transmitted light incident on it. The detector output was fed to the preamplifier and then on to the lock-in-amplifier. The selective amplifier was not used for this group of data.

The reference signal, synchronous with the chopped optical signal was connected to the reference channel of the LIA. The phase of this signal with respect to the optical signal was adjusted mechanically by the proper positioning of the reference lamp and correct choice of the Ad-Yu preamplifier. The output of the LIA was recorded with a strip chart recorder.

In order to obtain a reference point, the monochromator was first set at a wavelength on the far wing of the band where the absorptance by water vapor is very small. This was set at 2.33 microns and the LIA output at that point was always adjusted to be 7.5 volts. A scan was made from 2.33 to 3 microns at a speed of 0.2 microns per minute. At the end of the scan, the monochromator was set back to the reference point to check any change in the transmitted intensity at that point. If it had changed by more than one half of one percent, that scan was discarded and a new one was made. This procedure was repeated for 41 different combinations of concentration, pressure, and temperature of the sample gas.

In addition a similar scan, I_0 , was also made at the beginning of the runs each day with the cell space fully evacuated. After every two I scans, the cell was again evacuated and another I_0 scan was made. So we obtained the scans in the order of I_{01} , I_1 , I_2 , I_{02} , I_3 , I_4 , and

I_{O3} . The I_{O1} , I_{O2} , and I_{O3} were taken to check the 100% transmitted intensity for any effects due to absorption by the CaF_2 windows because of condensation of water vapor on them. From all the I_0 scans, we were assured that there was no condensation on the windows for the water vapor concentrations used in our experiment.

2. Dynamic Mode

After the first group of static mode of operation was completed, much effort was expended to improve the signal to noise ratio. The typical operating procedure in this mode was to take an I_0 scan, an I scan and then immediately a δI scan. The additional I_0 and I scans were necessary to calculate the derivatives of the absorption.

The selective amplifier was tuned to the LIA in its internal mode at 14 Hz. The LIA in this mode provided the voltage to operate the two loud speakers connected to the cell space. The (nonchopped) modulated optical signal was fed into the electronics and a δI scan was obtained. For details, see Reference 33. The amplitude of the pressure fluctuation, δP , was also recorded on the stripchart recorder at the beginning and end of each δI scan. The value of δP was fixed at 5.57 mm of Hg., peak to peak. This value of δP was chosen to obtain sufficient pressure fluctuations in the cell, but not to create any turbulence. A δI scan was completed in about an hour, including electronics adjustments. Additional information such as thermodynamic conditions, gain settings of the amplifiers, calibration factors, ambient conditions, LIA integration time, etc., were also recorded for each scan on a separate 'information sheet'.

B. CELL CONDITIONS

It was important that a steady state water vapor condition was established in the cell. As explained in section III - G, this could be achieved. Thus all uncertainties about the sample gas concentration in the cell were avoided. The first steady state for a particular c , P , and T was obtained in about 2 to 3 hours after start up. It was very essential to maintain the room temperature within about 1°F .

The ratio of the partial pressures of the water vapor, p , and nitrogen, the latter almost equal to the total pressure, P , was always adjusted to be a constant; i.e.,

$$p/P = c = \text{constant} \qquad \text{IV - (1)}$$

So an increase in one meant a proportionate increase in the other.

The frequency of the pressure fluctuations of 14 Hz was dictated by the geometry of the absorption cell. With two speakers, the resonance peak for the cell space was at 14 Hz, and the half width of the peak was larger than that with one speaker alone, with the peak at 10 Hz. We were interested in having the resonance frequency at least at 14 Hz, because the S/N ratio for the optical signal at higher frequencies was higher and the electronics operated better. Introducing the pressure fluctuations at both ends of the cell created a more uniform symmetric case.

It can be shown that the pressure fluctuations produced in the cell constitute an adiabatic process; i.e., there is no gain or loss of heat

in the system during a change in pressure³³.

We also assume that the pressure fluctuation is uniform over the entire length of the cell. Laplace's expression gives for the speed of sound

$$v = (kT/m)^{1/2} \quad \text{IV - (2)}$$

where k is the Boltzman constant and m is the mass of the molecule. The speed of sound changes from 340 m/sec. at 288°K to 368 m/sec. at 338°K. The corresponding wavelengths for a 14 Hz sound wave are 24.3 and 26.3 m. respectively. Since the absorption cell is considerably shorter than the wavelength of the sound waves, we conclude that the waves produced inside the cell are reasonably uniform over the cell space at all temperatures encountered in our experiment.

C. ABSORPTION AND ITS STATIC DERIVATIVES

We have the absorption equation,

$$A = 1 - I/I_0 \quad \text{IV - (3)}$$

By choosing a proper wavenumber interval, we can calculate the absorptance over the entire band. The area under the curve of absorption versus wavenumber, gives the integrated band absorptance. Since the experimental band pass changed from about 23 cm⁻¹ at 3 microns to about 35 cm⁻¹ at 2.3 microns, all the experimental results are degraded to 35 cm⁻¹, as in the case of the calculated spectra.

With the aid of the measured transmittance for various combinations

of the thermodynamic variables, it is now easy to obtain the thermodynamic derivative spectra. The static first derivatives can be obtained from two absorptance spectra, with the averages of c , P , and T of the two curves serving as the reference point. Using three absorptance spectra, one can interpolate to find a different c , P , and T point. Experimental second and mixed static derivatives are obtained from 3 or 4 absorptance spectra spaced at regular c , P , and T intervals. Again, the averages of c , P , and T values serve as the reference point.

Using a power law, $A \propto y^{Z(\nu)}$ to express the c , P , and T dependence, we can calculate the experimental spectrum at a different thermodynamic condition^{34,35}. The exponent $Z(\nu)$ is obtained by taking the ratio of the calculated first derivative, $y (\partial A/\partial y)$, and A . Similarly the ratio of the second derivative $y^2 (\partial^2 A/\partial y^2)$ and the first derivative $y (\partial A/\partial y)$ equals $[Z(\nu) - 1]$.

D. ADIABATIC DERIVATIVES

We have the equation

$$(\partial A/\partial P)_{ad.} = -(1/I_0) (\delta I/\delta P) \quad \text{IV - (4)}$$

The value of δP is known and we have measured δI and I_0 . So the magnitude of $(\partial A/\partial P)_{ad.}$ can be calculated.

Thermodynamic second derivatives and mixed derivatives are obtained as before in the static case. Accordingly, we can obtain

$$\partial/\partial c (\partial A/\partial P)_{ad.}, \partial/\partial P (\partial A/\partial P)_{ad.}, \text{ and } \partial/\partial T (\partial A/\partial P)_{ad.}.$$

We can also use a power law to obtain $(\partial A/\partial P)_{ad.}$ spectrum at a desired

thermodynamic condition from a known $(\partial A/\partial P)_{ad}$ spectrum at a different thermodynamic condition.

E. DATA AND DATA PROCESSING

Table VI shows the thermodynamic conditions for each of the 41 static spectra recorded.

TABLE VI
TABLE OF I MEASUREMENTS

Concentration C	Pressure P	Temperature		
		288 ^o K	313 ^o K	338 ^o K
0.81%	0.50	x	x	x
	0.75	x	x	x
	1.00	x	x	x
	1.25	x	x	x
1.62%	0.50	x	x	x
	0.75	x	x	x
	1.00	x	x	x
	1.25		x	x
3.24%	0.25	x	x	
	0.50	x	x	x
	0.75		x	x
	1.00		x	x
	1.25		x	x
4.86%	0.25	x	x	
	0.50		x	x
	0.75		x	x
	1.00			x

These concentration values correspond to 0.000622, 0.001244, 0.002488, and 0.003732 precipitable cm. absorber masses, u (g/cm^2), at 288°K .

In each case, the dew point temperature set the upper concentration and pressure limit. In particular, at 288°K , we were restricted to lower pressures and concentrations. The highest temperature at which the dew point hygrometer could be operated was 343°K .

The I and I_0 data were digitized at intervals of 0.005 microns, with a total of 135 points per run. The computer programs enabled us to get tables of degraded absorptance and wavenumber at 5 cm^{-1} intervals, as well as the integrated band absorptance. The absorptance values for all 41 spectra were then stored in three different computer files. Thereafter other computer programs were used to obtain the thermodynamic derivative spectra.

Table VII shows the combinations of the thermodynamic variables used for the δI measurements.

In order to obtain the experimental $(\partial A/\partial P)_{\text{ad}}$ spectra we had to use the I_0 data taken under static conditions and δI and δP data taken under dynamic conditions. Therefore, we have reduced all the measurements to the absolute outputs at the detector. Taking into consideration the different wave forms used in the static and dynamic modes of operations and the calibration and gain factors of each of the amplifiers, we have to multiply I_0 data by 2.2214×10^{-2} , δP data by 1.393×10^{-2} , and δI data by 1.414×10^{-5} for the lower two concentrations and by 2.828×10^{-5} for the upper two concentrations. The strip chart of 100 marked divisions were digitized in units of zero to 1000.

In the dynamic mode, the data were digitized at intervals of 0.004

TABLE VII
TABLE OF δI MEASUREMENTS

Concentration C	Pressure P	Temperature			
		288 ^o K	293 ^o K	308 ^o K	338 ^o K
	0.75	x			
0.81%	1.00	x		x	x
	1.25	x			
	0.75		x	x	x
1.62%	1.00		x	x	x
	1.25		x	x	x
	0.75			x	x
2.43%	1.00			x	x
	1.25			x	x
3.24%	1.00			x	x

microns, with a total of 160 points per run. These data were fed into the computer and $P (\partial A / \partial P)_{ad.}$ spectra, degraded to 35 cm^{-1} , were calculated. Again, as in the static case, the second and mixed derivatives of these adiabatic derivative spectra were obtained using other computer programs.

All the spectra were plotted using the plotter attached to the minicomputer in the Physics department at the University of Oklahoma.

CHAPTER V
ANALYSIS OF RESULTS

A. INTRODUCTION

In this chapter we present the results of our experiment and the theoretical calculations for the 2.7 micron water vapor band and the 3.46 micron hydrogen chloride band. The calculated spectra for the 2.7 micron band are all at 288°K and for the HCl band, all at 300°K. In this chapter we will use the following notations: A = absorptance, c = concentration, P = total pressure, T = absolute temperature, and E = energy of the lower state of the absorption process. Also partial derivatives $cT \partial A / \partial c$ ($\partial A / \partial T$) will be written as $cT A(c)$, and similarly for the other derivatives as $c A(c)$, $P A(P)$, $T A(T)$, $PP A(PP)$, $cP A(cP)$, $PT A(PT)$, $TT A(TT)$ and $cc A(cc)$. The multiplication by $c, P,$ and T cancels units and the magnitudes fall into the range of values of the absorption. Finally the abbreviation, "ad." stands for adiabatic.

The graphical display of our results gives the dependence of the absorption and its thermodynamic derivatives upon $c, P,$ and T . We shall search for spectral regions, where the absorption or its derivatives are simple functions of the concentration, pressure, and temperature. We will show how, in particular, the $(\partial A / \partial P)_{ad.}$ spectra can be used for a

spectral inversion to obtain the thermodynamic variables.

B. STATIC MODE RESULTS

First we give the results for the static mode of the experiment and compare these with our theoretical calculations. Then, the more important dynamic mode results are presented. Finally, the results of the hydrogen chloride calculations are given.

Table VIII lists the band integrated absorptance for our 1.005 m column of water vapor over the 2.7 micron region. The experimental values are compared with our calculated values as well as those of References 36 and 37. The agreement between the experimental values and the others are well within expected accuracy. At lower temperatures the errors in the experiment, which are mainly due to the short term fluctuations in the concentration and in the global intensity, cause a departure from the calculated values. However, at the higher concentrations, the error in the calculation is larger and the experimental values are more reliable. Table VIII shows that the discrepancy is always less than 5%.

The short term fluctuation errors in the concentration and the global intensity are about 0.3 percent and 0.2 percent respectively. Hence, in a single reading the error does not exceed 0.6 percent. Also, since each absorptance spectrum is obtained from an I scan and an I_0 scan, the maximum possible error in the value of absorptance is 1.2 percent. The maximum value of the absorptance obtained in our experiment was about 0.65; and the maximum absorptance obtained for the lowest concentration and pressure was about 0.25. So, for an average value of the

TABLE VIII

2.7 MICRON WATER VAPOR BAND INTEGRATED ABSORPTANCE FOR A 1.005 M COLUMN

Concentration (c)	Pressure (P) atm	INTEGRATED ABSORPTANCE (cm ⁻¹)							
		288°K				313°K		388°K	
		Expt.	Calc.	Ref. 36	Ref. 37	Expt.	Ref. 36	Expt.	Ref. 36
0.81%	0.50	34.6				33.2		30.6	
	0.75	51.8				49.0		47.5	
	1.00	68.6	68.96	71.0		66.3	68.0	63.7	65.5
	1.25	85.3				83.8		78.5	
1.62%	0.50	55.8				52.7		49.9	
	0.75	81.9				75.8		73.9	
	1.00	108.1	104.6	110.0	95.0	105.3	106.0	102.7	103.0
	1.25					128.6		126.2	
3.24%	0.25	40.8							
	0.50	80.9							
	0.75								
	1.00		153.5	163.0	139.0	155.8	156.0	149.0	150.0
	1.25					183.6		176.3	
4.86%	0.25	50.7				48.2			
	0.50					104.7			
	0.75					151.8			
	1.00		188.8	198.0	173.0		190.0	182.4	183.0

2.7 MICRON WATER VAPOR BAND ABSORPTION

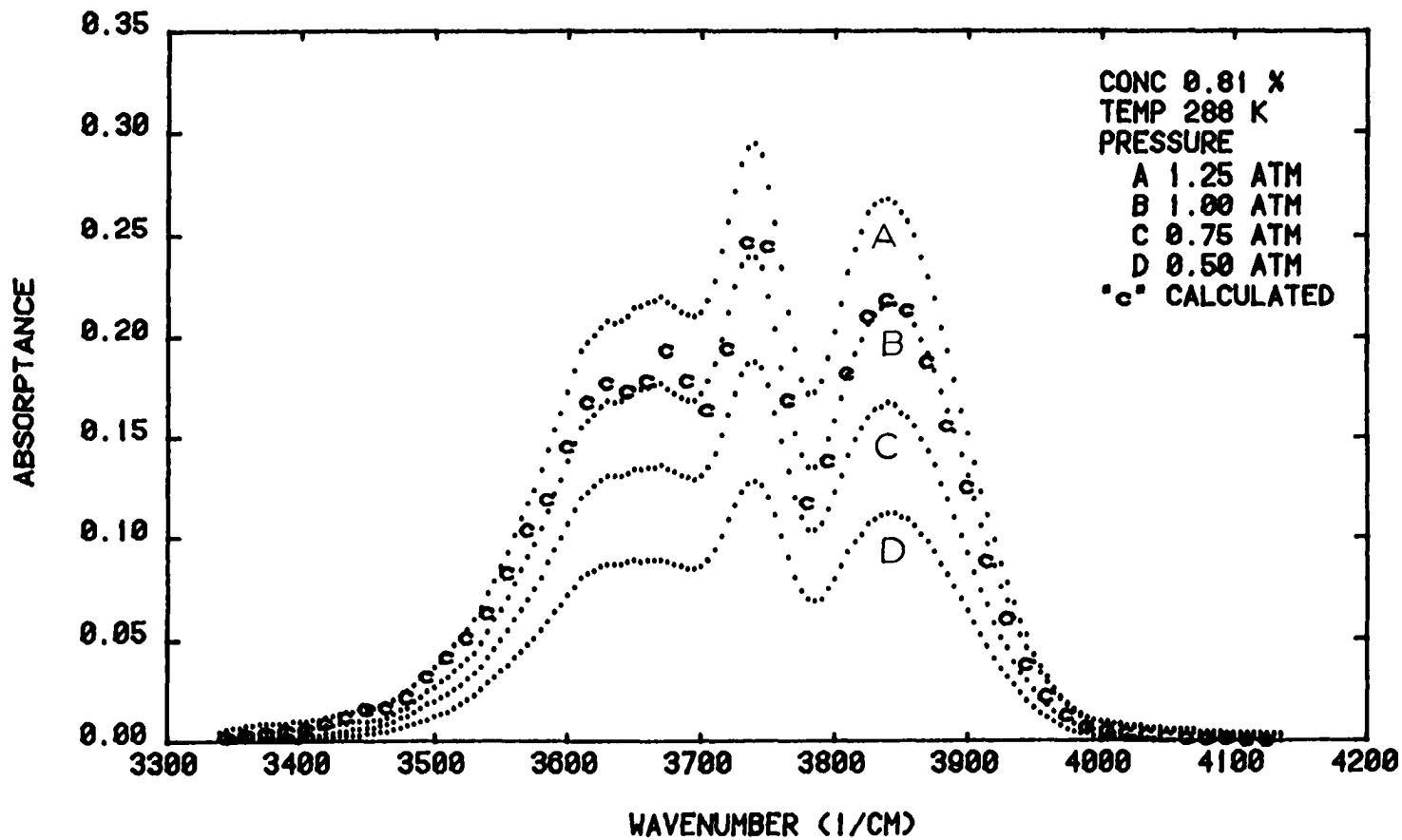


Figure 3

2.7 MICRON WATER VAPOR BAND ABSORPTION

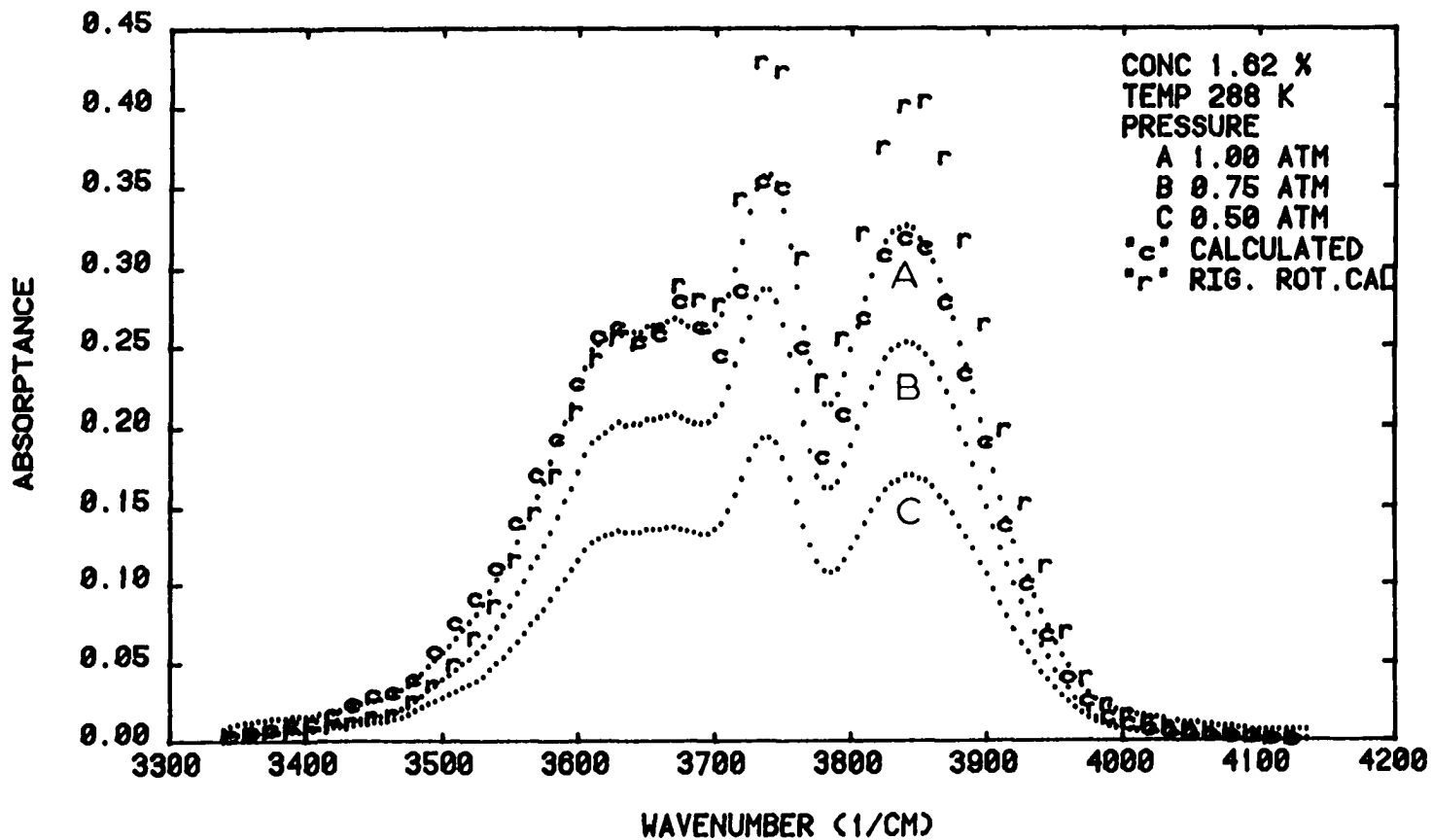


Figure 4

2.7 MICRON WATER VAPOR BAND ABSORPTION

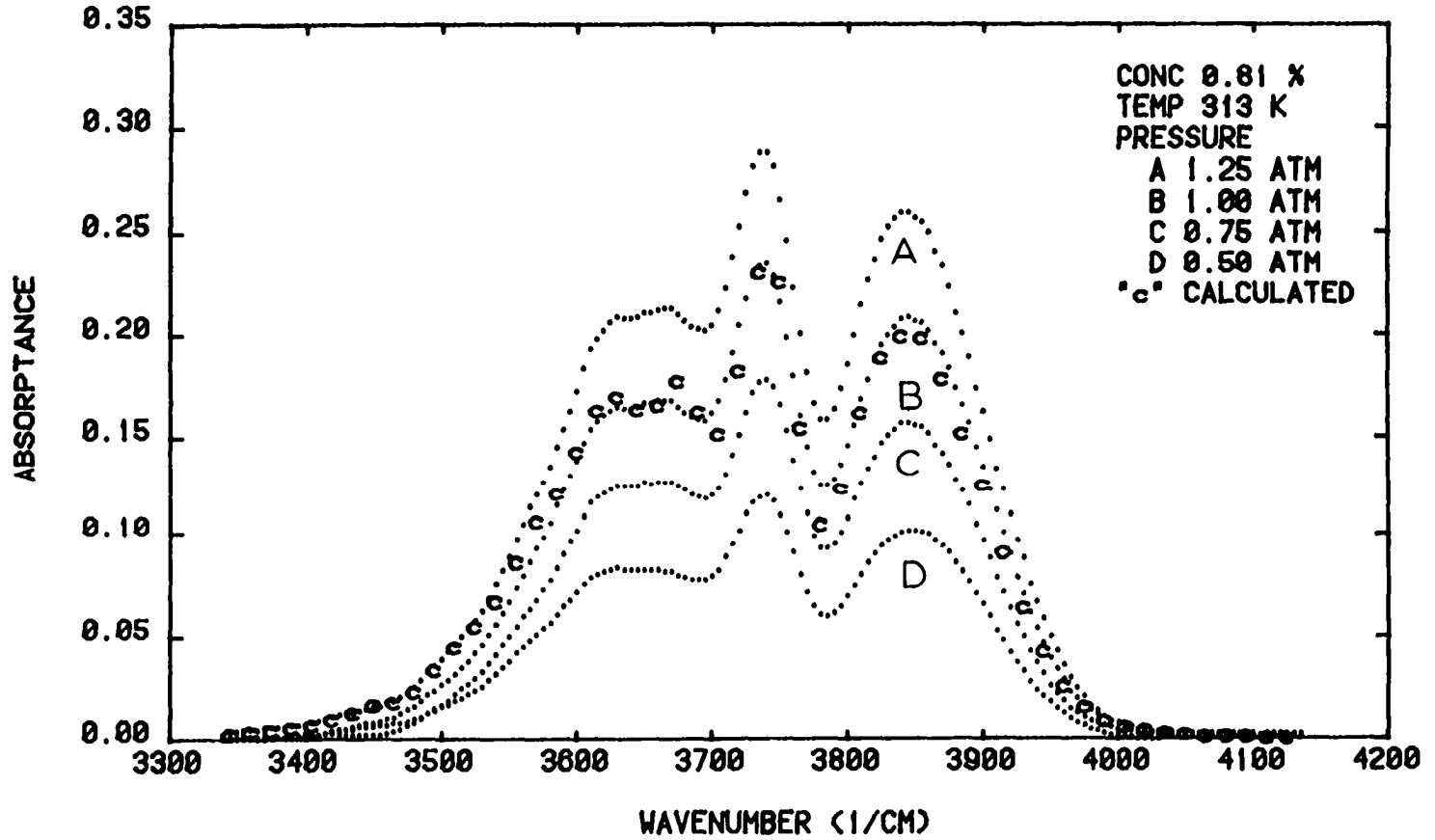


Figure 5

2.7 MICRON WATER VAPOR BAND ABSORPTION

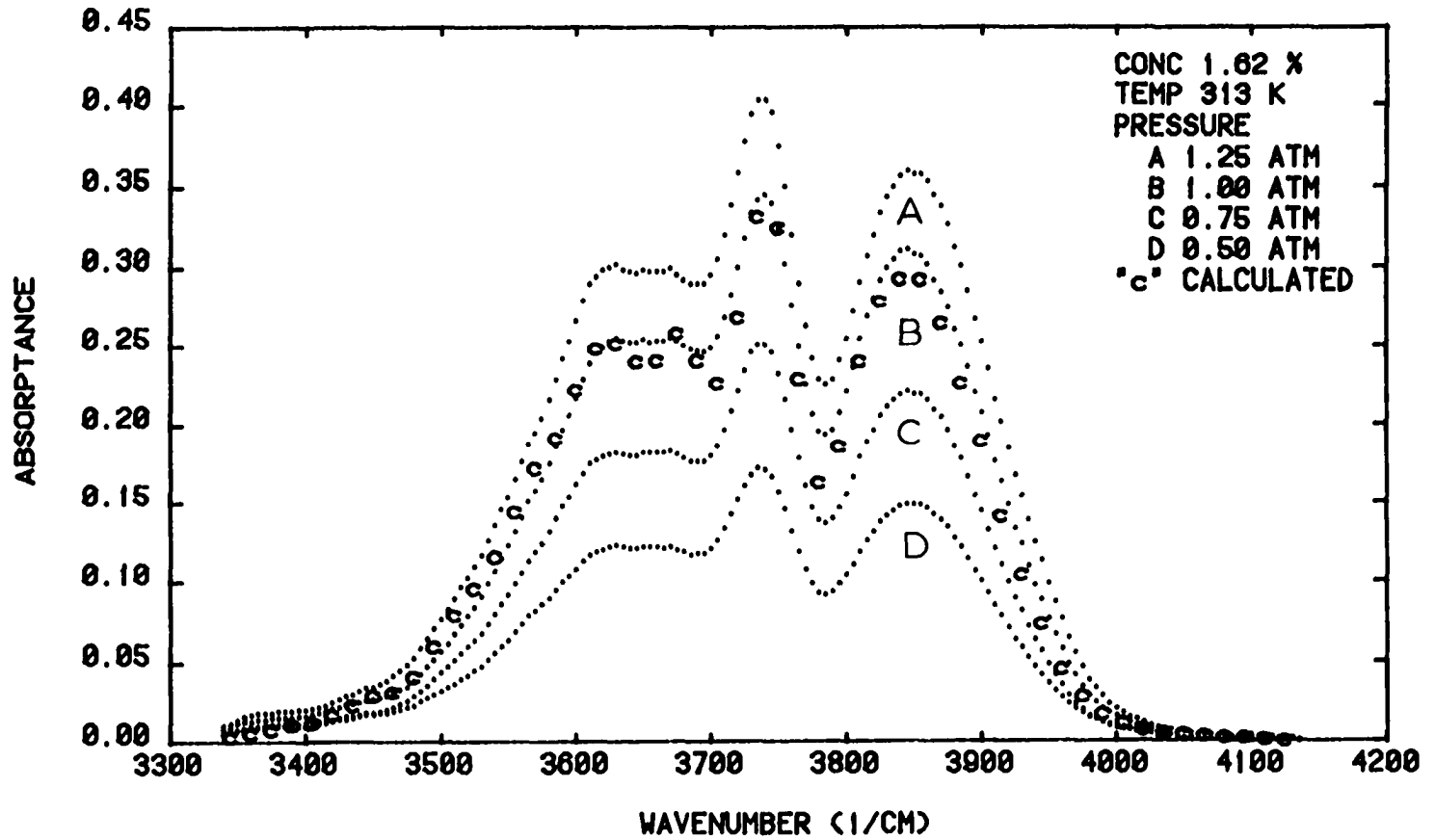


Figure 6

2.7 MICRON WATER VAPOR BAND ABSORPTION

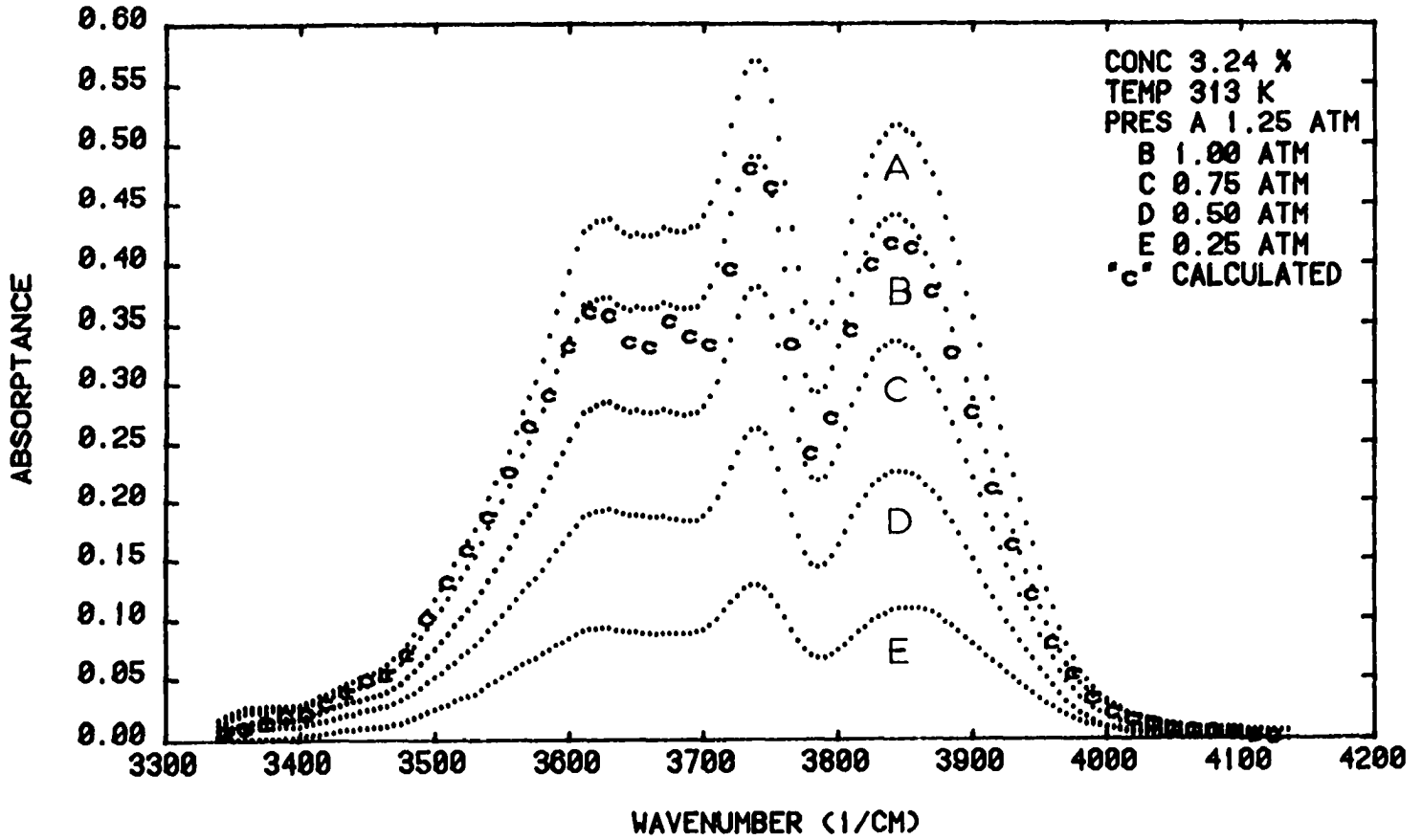


Figure 7

2.7 MICRON WATER VAPOR BAND ABSORPTION

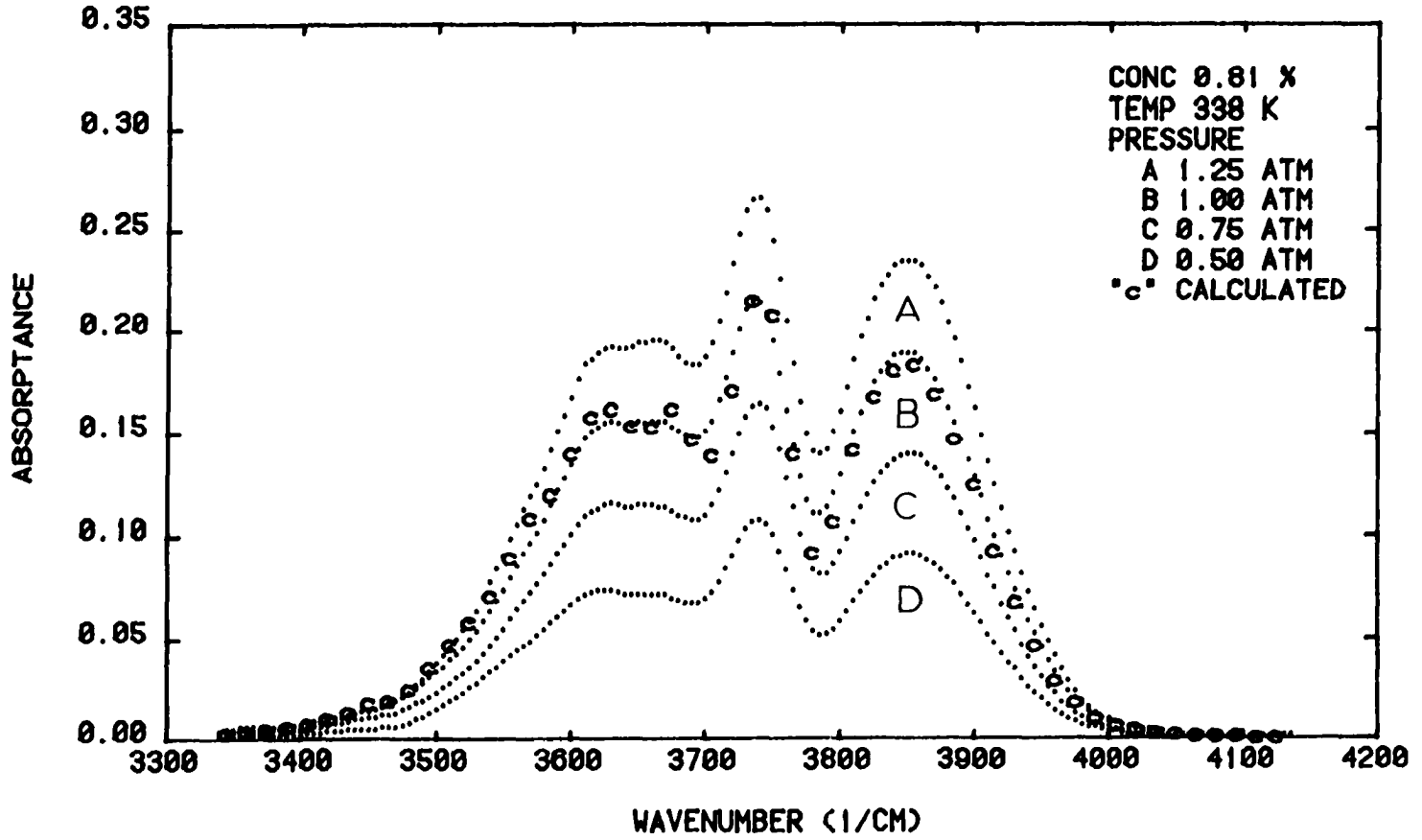


Figure 8

2.7 MICRON WATER VAPOR BAND ABSORPTION

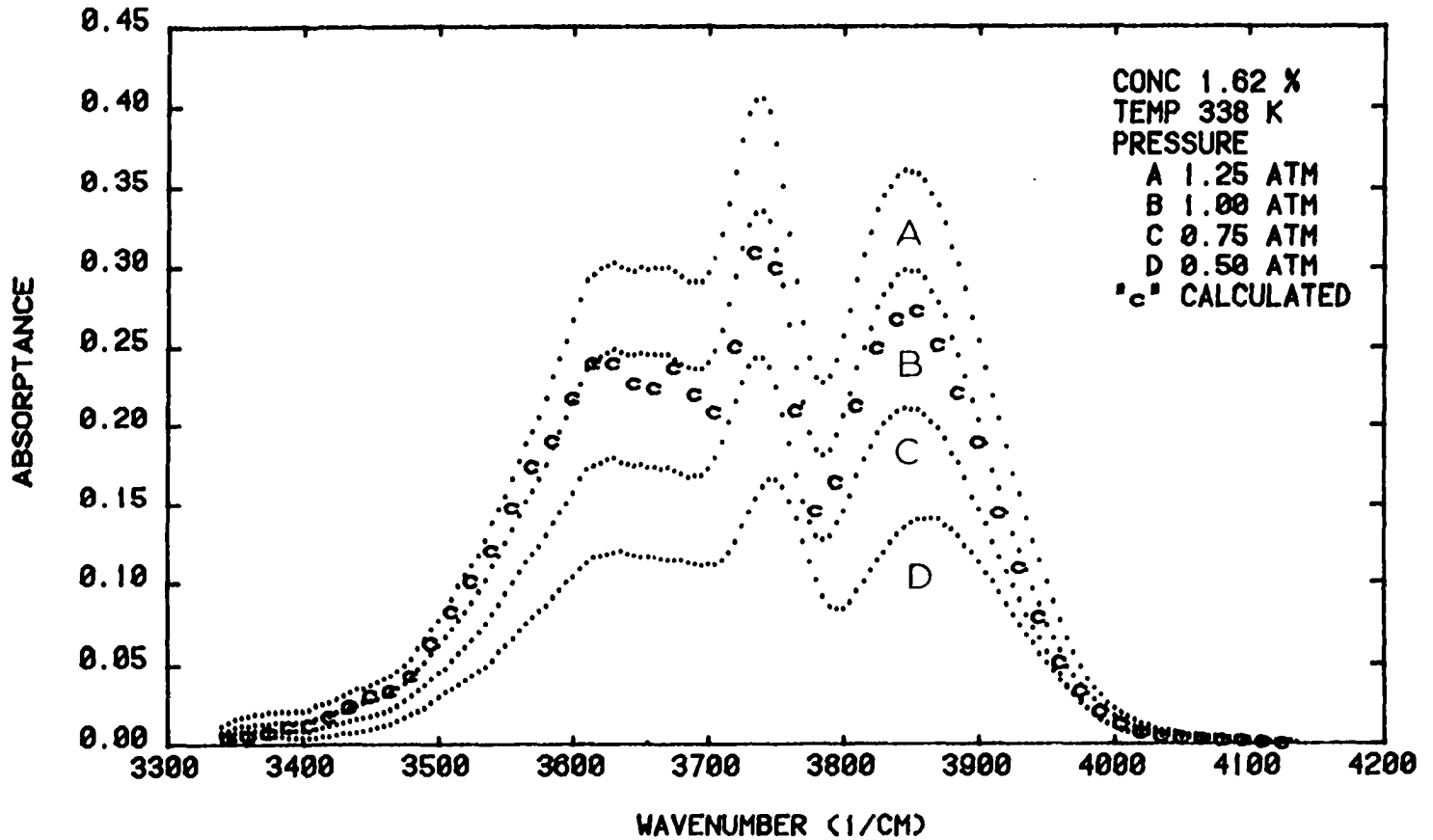


Figure 9

2.7 MICRON WATER VAPOR BAND ABSORPTION

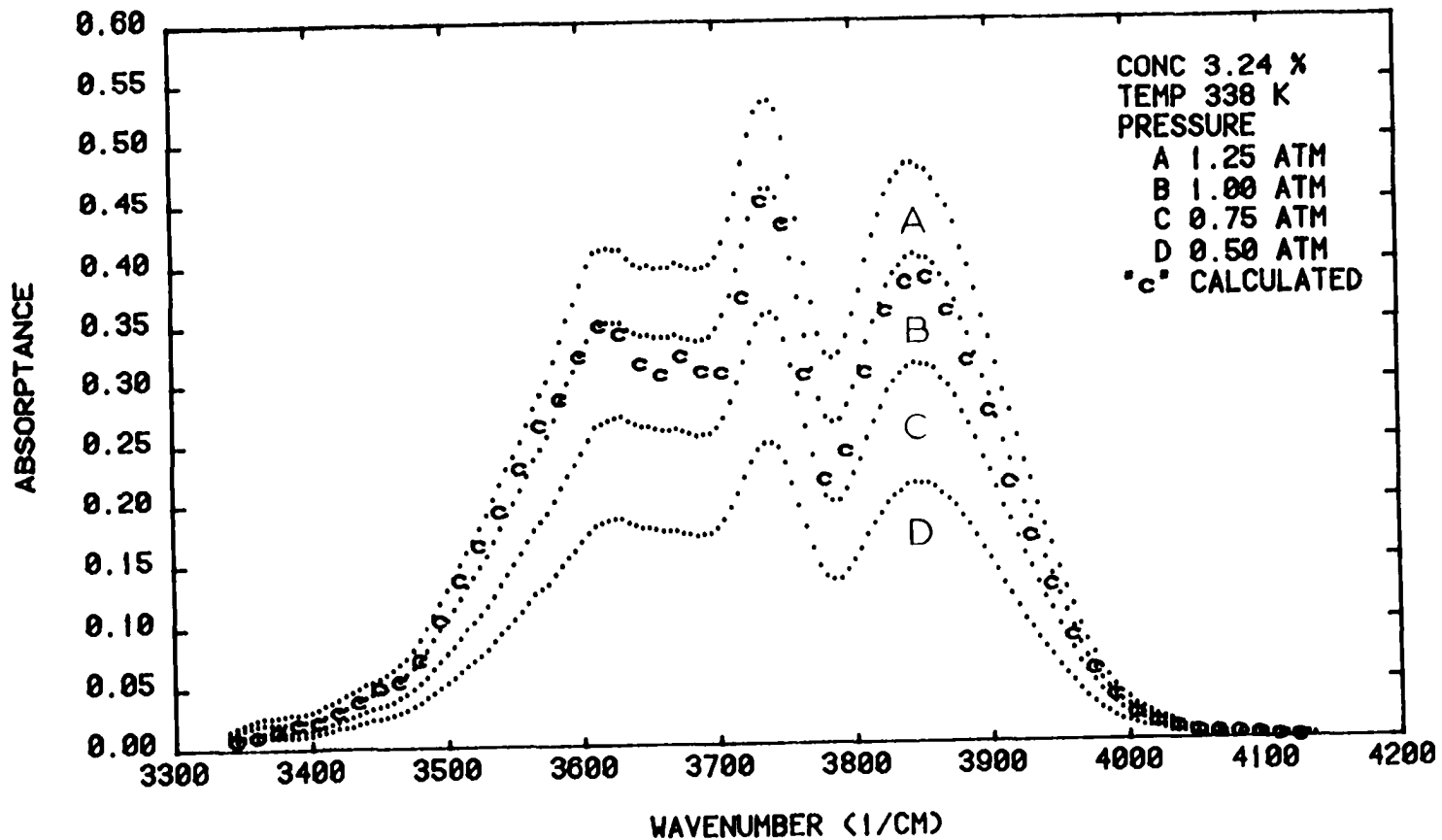


Figure 10

2.7 MICRON WATER VAPOR BAND ABSORPTION

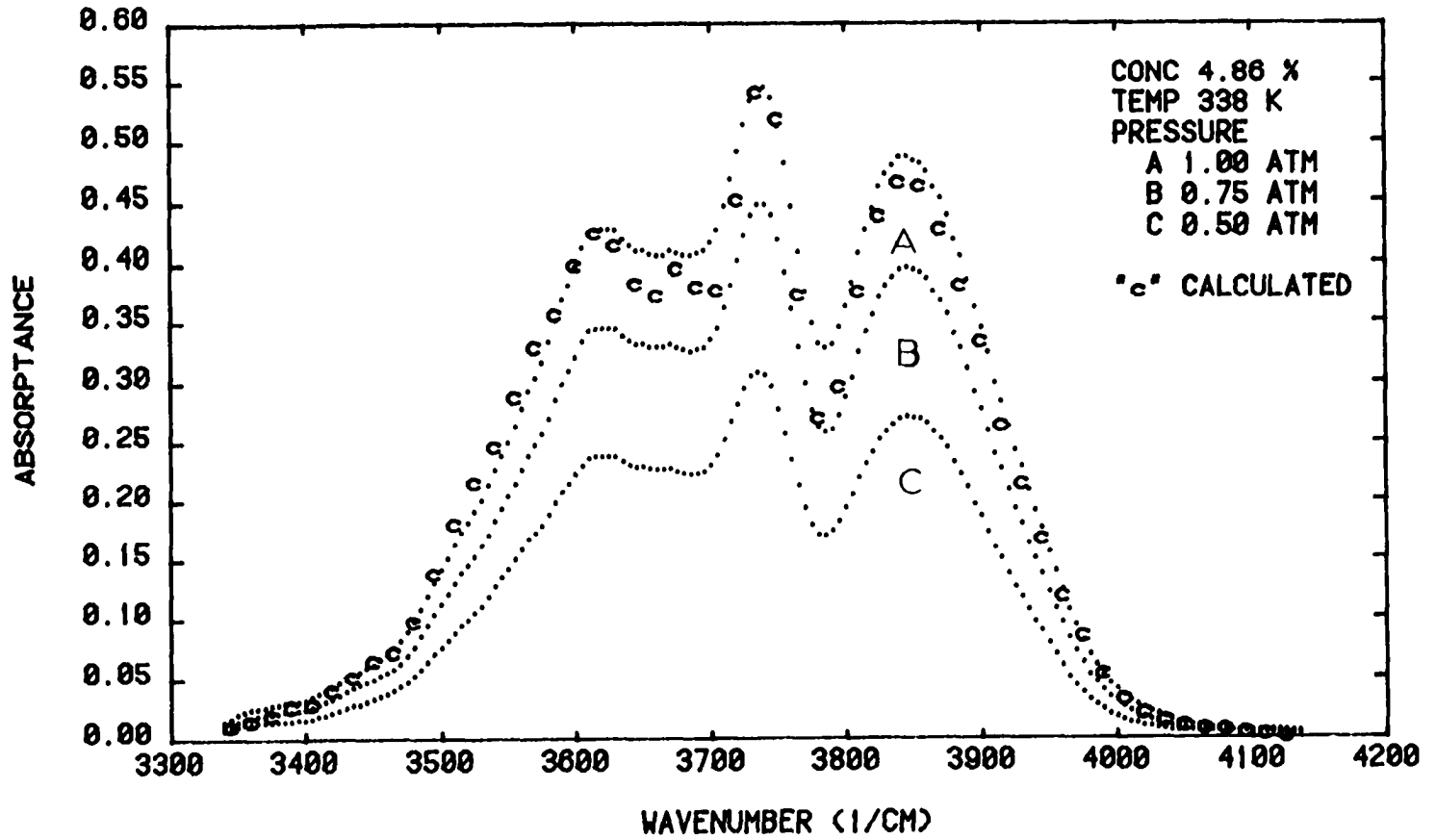


Figure 11

maximum absorptance of 0.45, there is an absolute error of 5.4×10^{-3} . Then, the absolute error in the first derivative, ∂A , is 1.1×10^{-2} and that in the second derivative, $\partial^2 A$, is 2.2×10^{-2} .

Figures 3 through 11 show absorptance (all degraded to 35 cm^{-1}) plotted against wavenumber with the pressure of the sample gas, P , as a parameter for the temperatures of 288°K , 313°K , and 338°K . The curve marked "r" in Figure 4 is the calculated absorptance spectrum obtained using the rigid rotator line strengths of Gates, et al.⁴ The curves marked "c" are the calculated absorptance spectra obtained using the F factor corrected line strengths for the 2.7 micron H_2O band. Since the theoretical calculations are at 288°K , the absorptance at the experimental temperatures had to be computed using the first derivative of the absorptance with respect to the temperature. The agreement between the experimental spectra and the F corrected calculated spectra is excellent.

We assume that the absorptance is approximately related to the pressure through a power law,

$$A = \text{constant} \times P^{Y(\nu)} \quad \nu - (1)$$

The exponent, $Y(\nu)$, may be obtained by taking the ratio of $PA(P)$ to A . The value of $Y(\nu)$ varies slowly from about 1.00 at 3400^{-1} and reaches about 0.8 at the middle of the band (around 3800 cm^{-1}), and then increases back to 1 at about 4100 cm^{-1} .

Figures 12 to 16 show the computer plotted absorptance versus wavenumber with concentration as a parameter for 288°K , 313°K , and 338°K .

2.7 MICRON WATER VAPOR BAND ABSORPTION

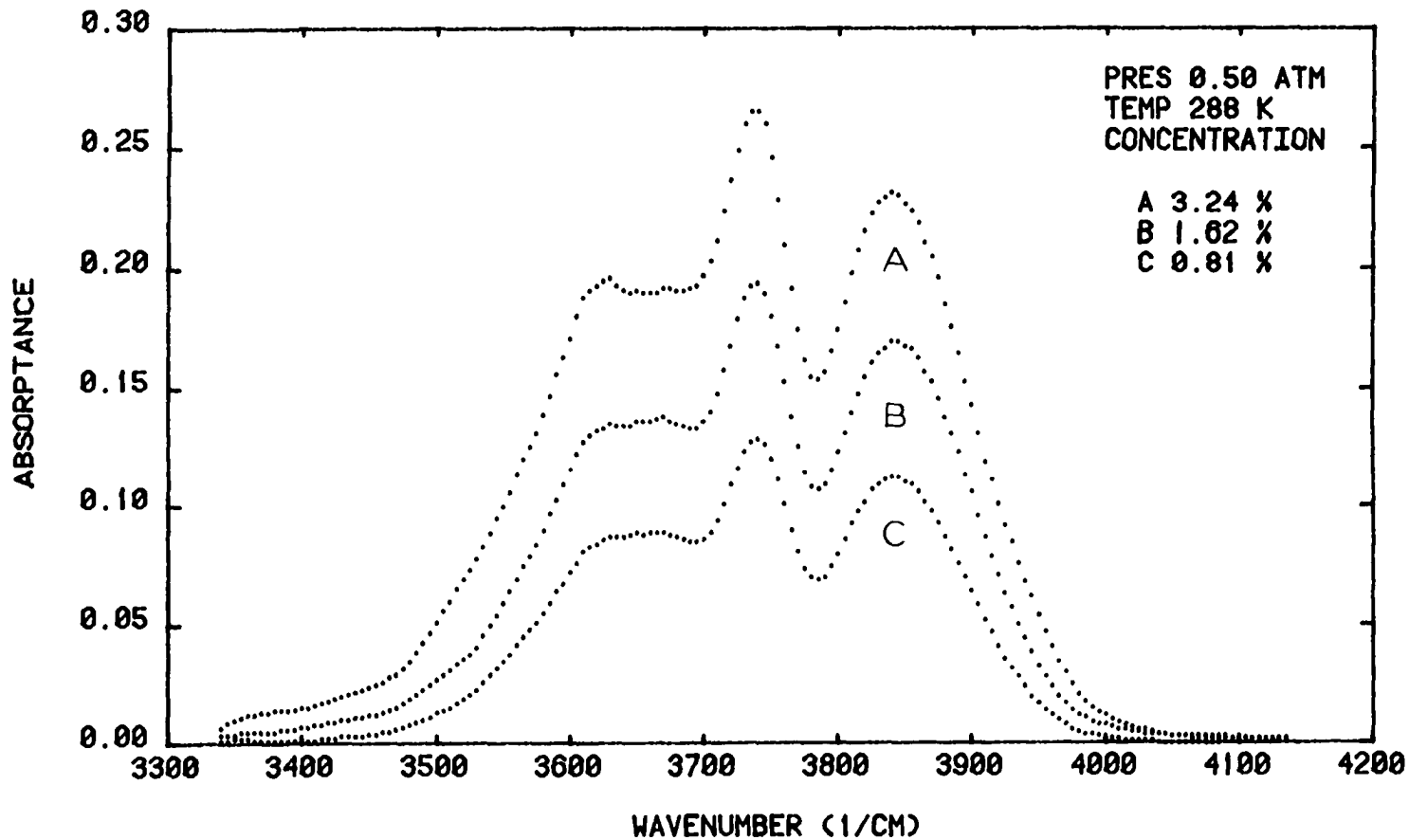


Figure 12

2.7 MICRON WATER VAPOR BAND ABSORPTION

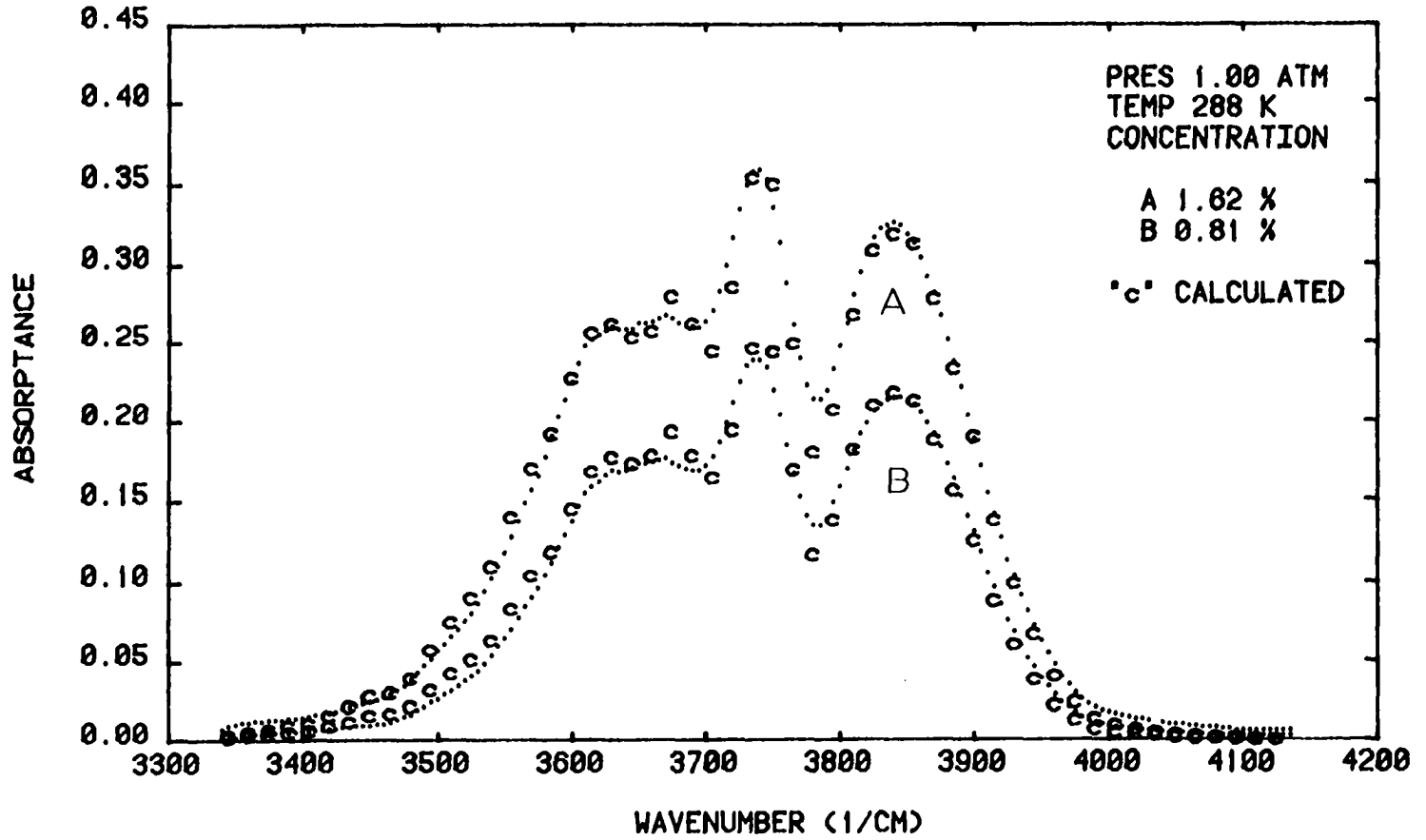


Figure 13

2.7 MICRON WATER VAPOR BAND ABSORPTION

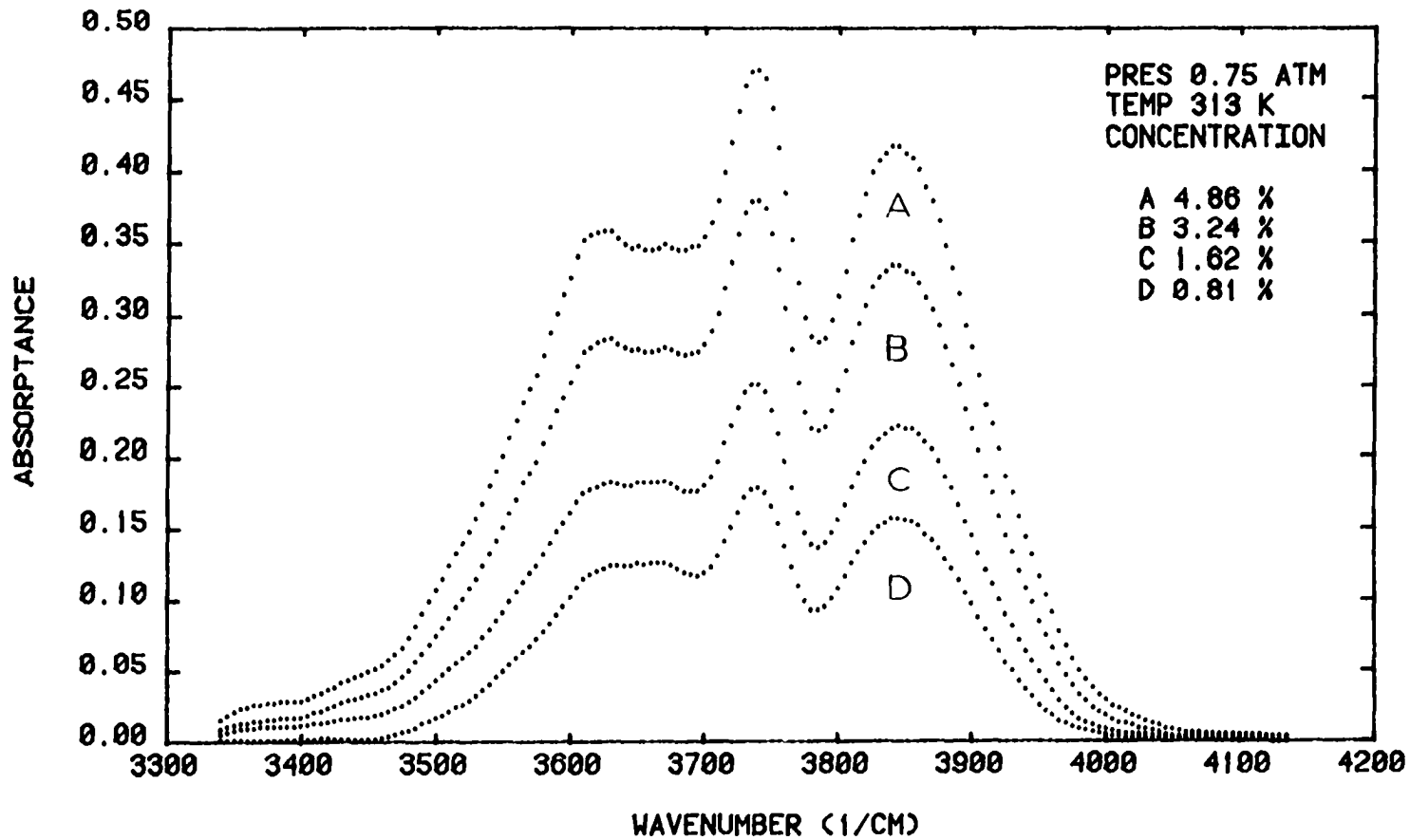


Figure 14

2.7 MICRON WATER VAPOR BAND ABSORPTION

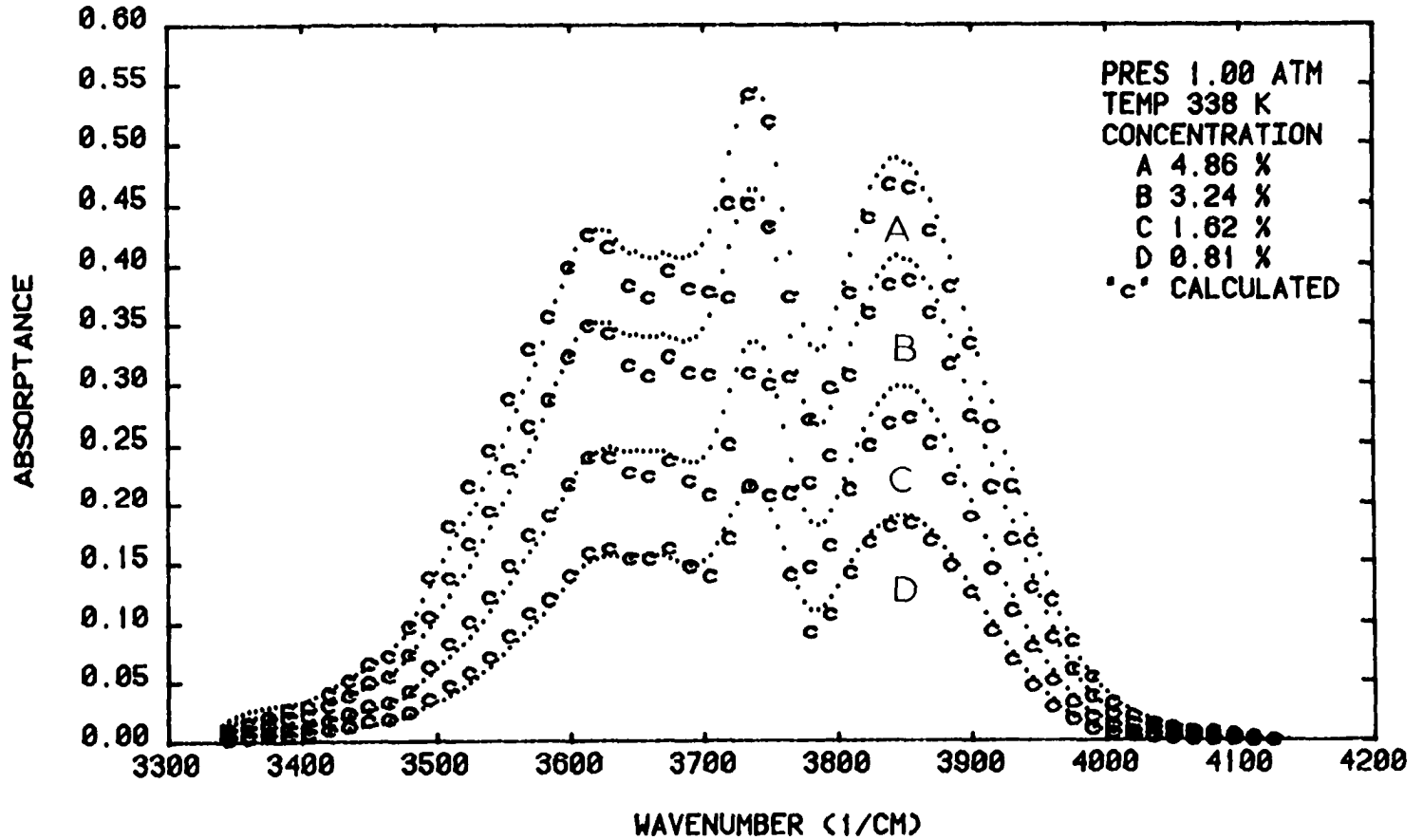


Figure 15

2.7 MICRON WATER VAPOR BAND ABSORPTION

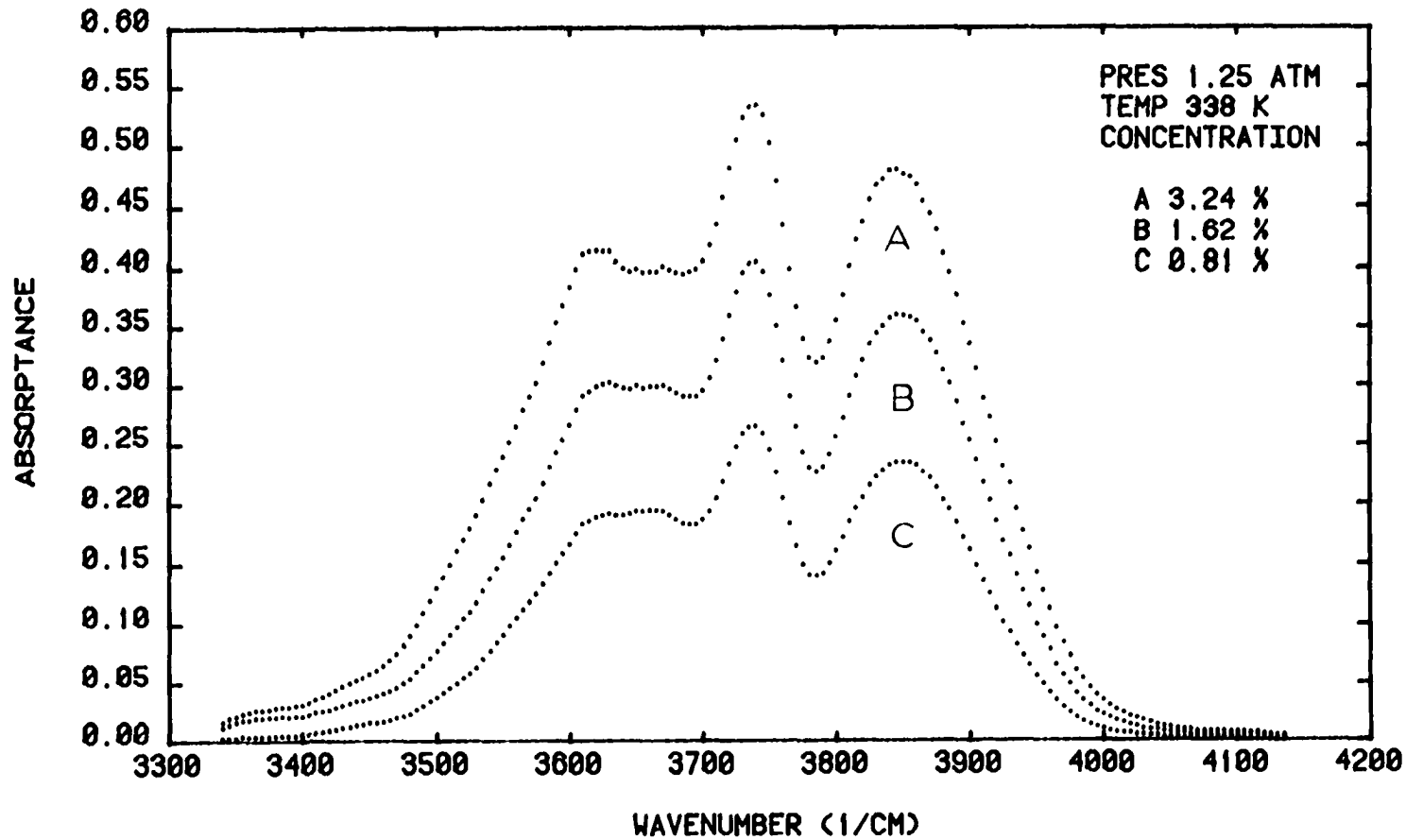


Figure 16

There is a strong dependence of absorption upon the concentration, which is fairly uniform along the entire band. We write the relation between the absorptance and the concentration as a power law,

$$A = \text{constant} \times c^{X(\nu)}, \quad V - (2)$$

where $X(\nu)$ is another parameter. This parameter $X(\nu)$ may be obtained by taking the ratio of $cA(c)$ to A . We found that the value of $X(\nu)$ decreases approximately uniformly from about 1 at 3400 cm^{-1} to about 0.47 at the middle of the band and then increases nearly uniformly back to 1 at about 4100 cm^{-1} . Hence, there is a strong concentration dependence of the absorption throughout the entire band.

Figures 17 through 21 show computer plotted absorptance versus wavenumber with the temperature as a parameter. These graphs show that there are two regions on each wing of the band where the absorption is nearly independent of the temperature of the sample gas. These are the so called 'crossover points'. Between the crossover points there is a mild negative dependence of the absorption on the temperature and beyond the crossover points, in the wings, there is a strong positive dependence of the absorption on the temperature. The T dependence is the most variable of the three as we will see below. As before, we may write the absorptance temperature relationship as a power law,

$$A = \text{constant} \times T^{Z(\nu)} \quad V - (3)$$

where $Z(\nu)$ is another parameter. This parameter may be found by taking the ratio of $TA(T)$ to A . The value of $Z(\nu)$ varies considerably with

2.7 MICRON WATER VAPOR BAND ABSORPTION

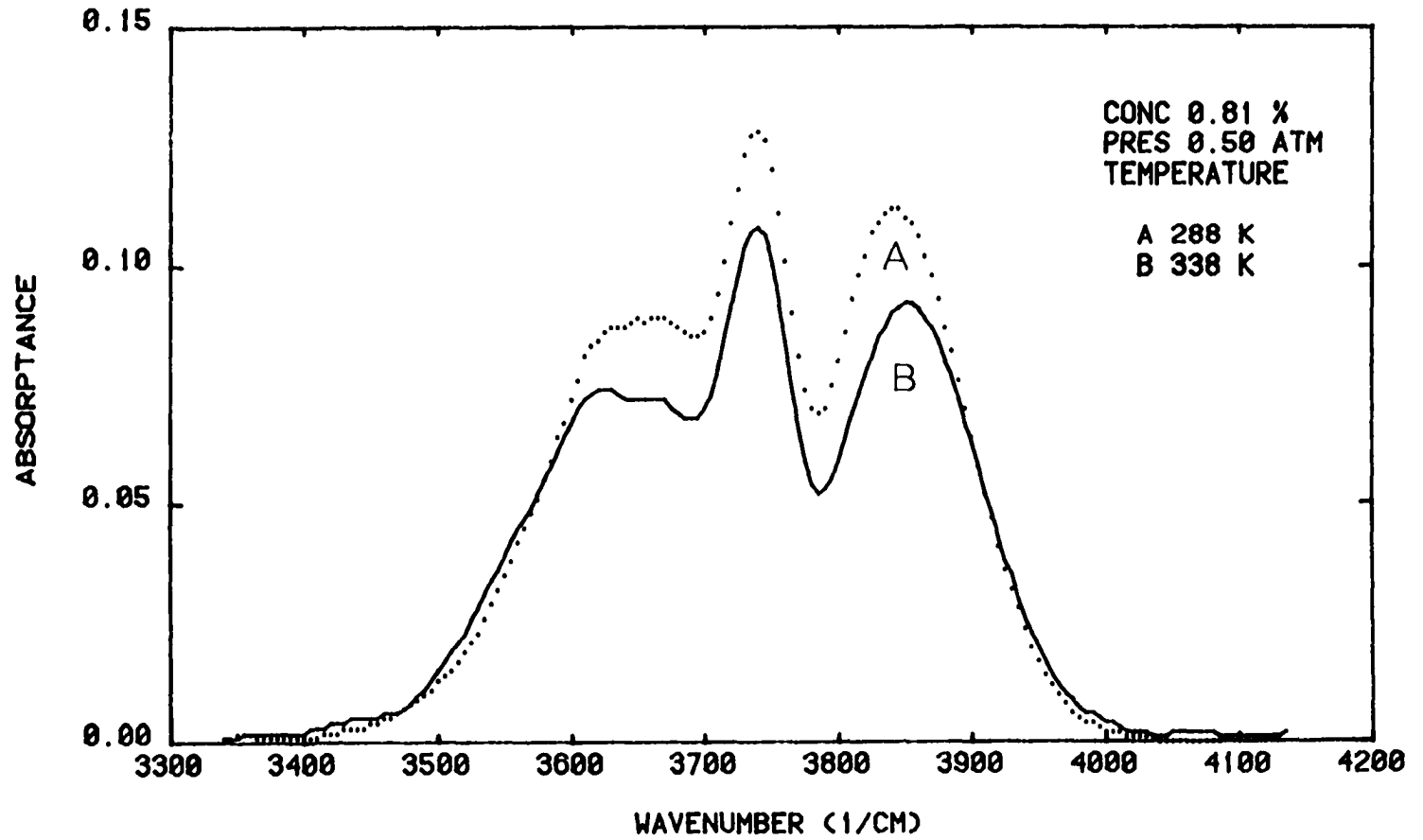


Figure 17

2.7 MICRON WATER VAPOR BAND ABSORPTION

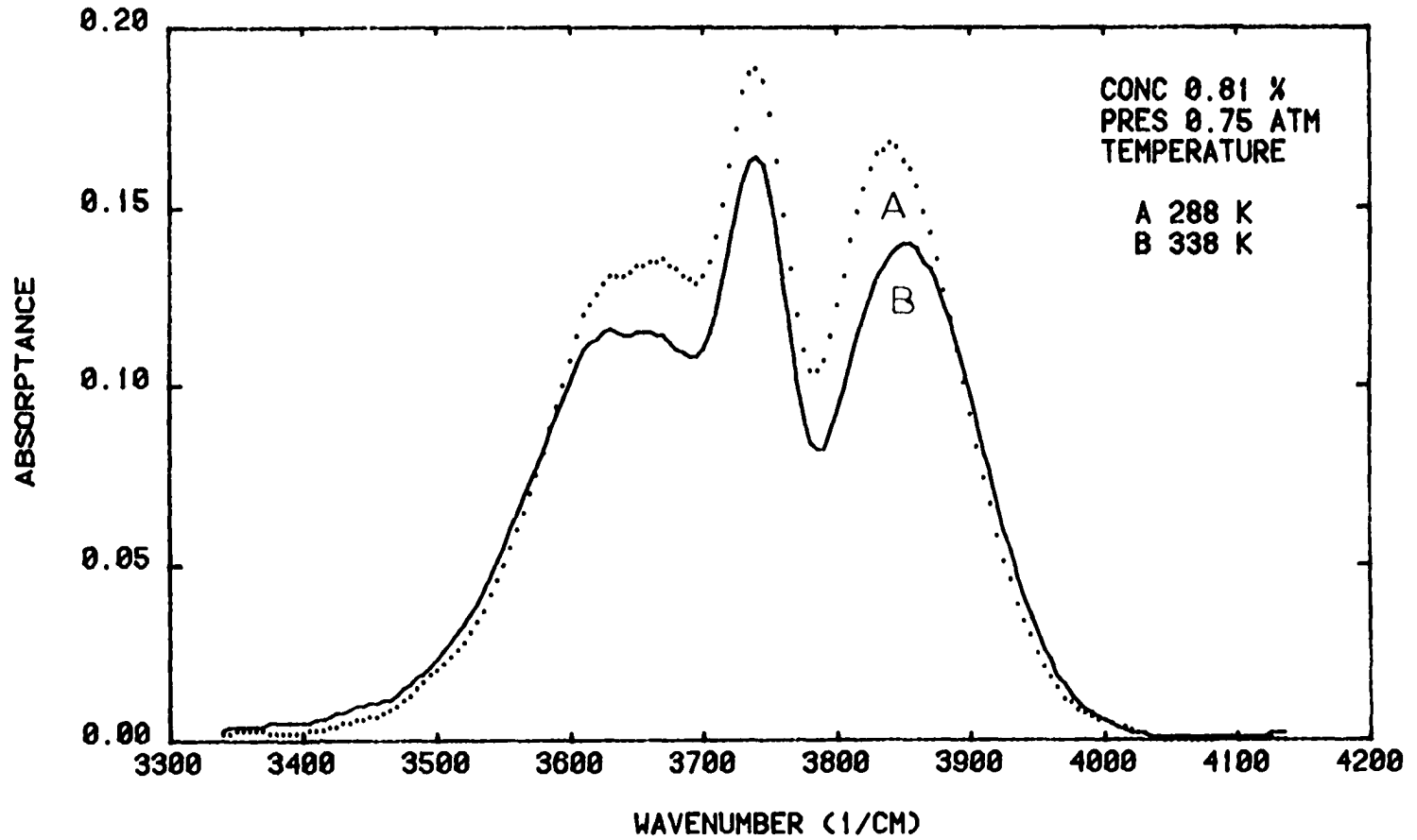


Figure 18

2.7 MICRON WATER VAPOR BAND ABSORPTION

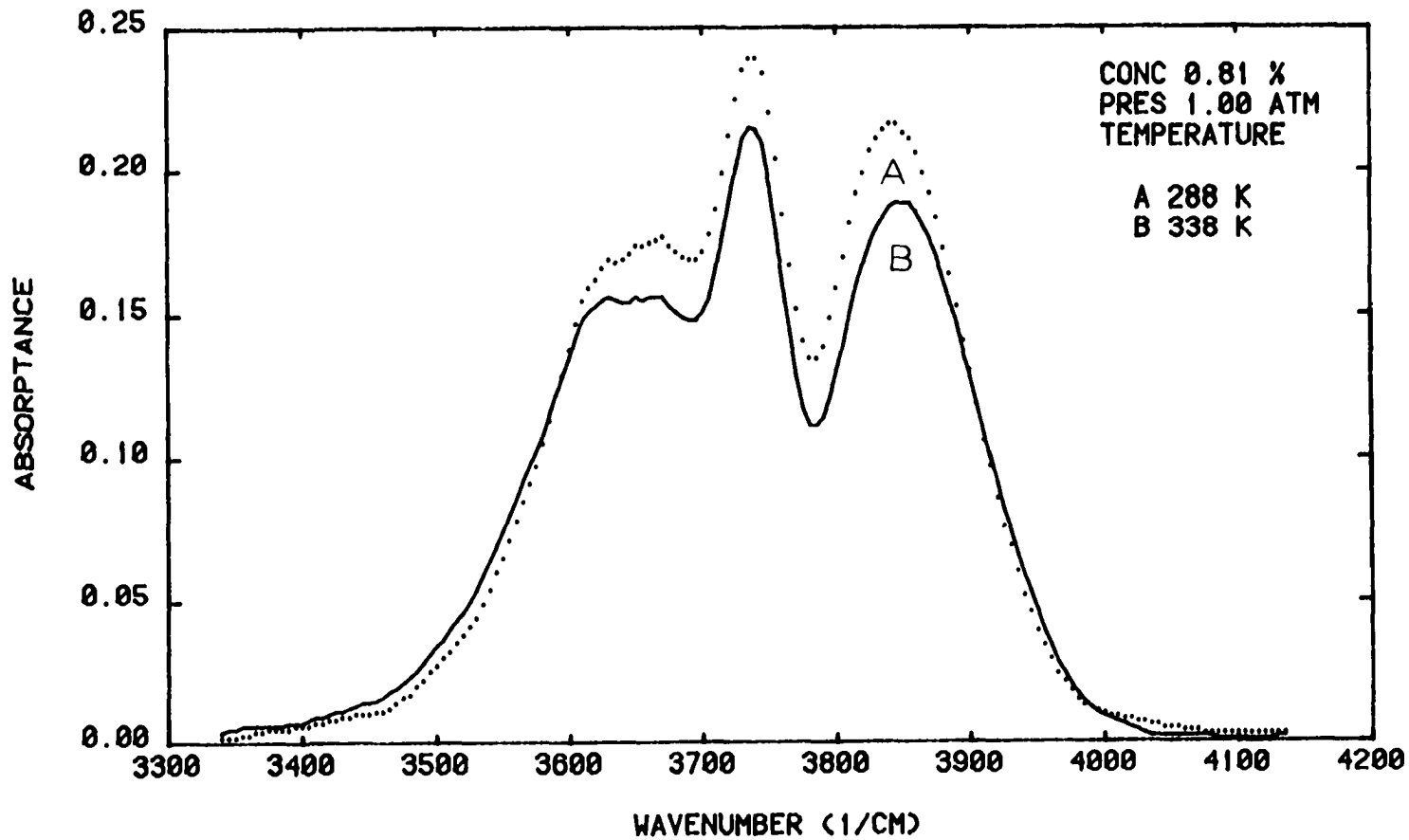


Figure 19

2.7 MICRON WATER VAPOR BAND ABSORPTION

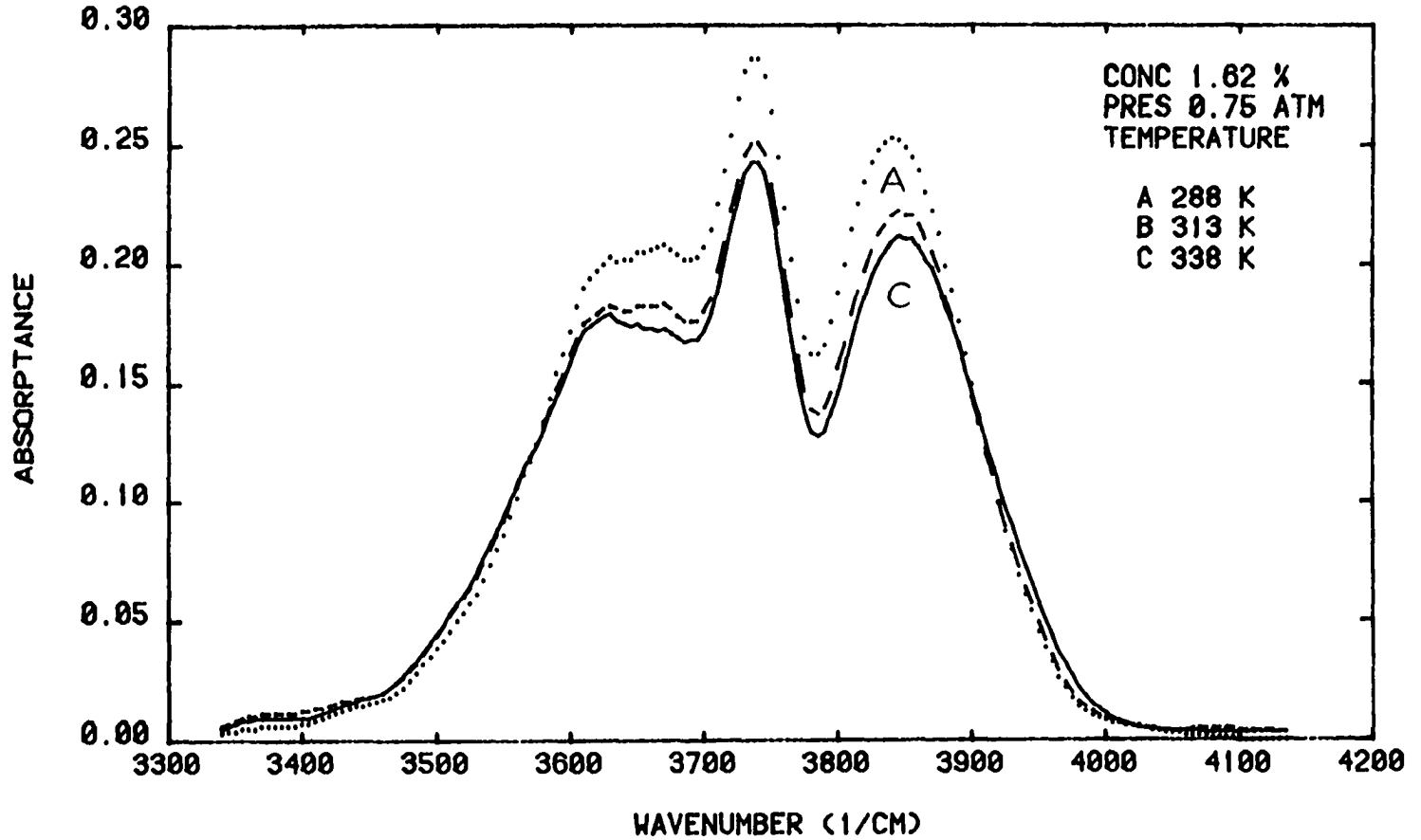


Figure 20

2.7 MICRON WATER VAPOR BAND ABSORPTION

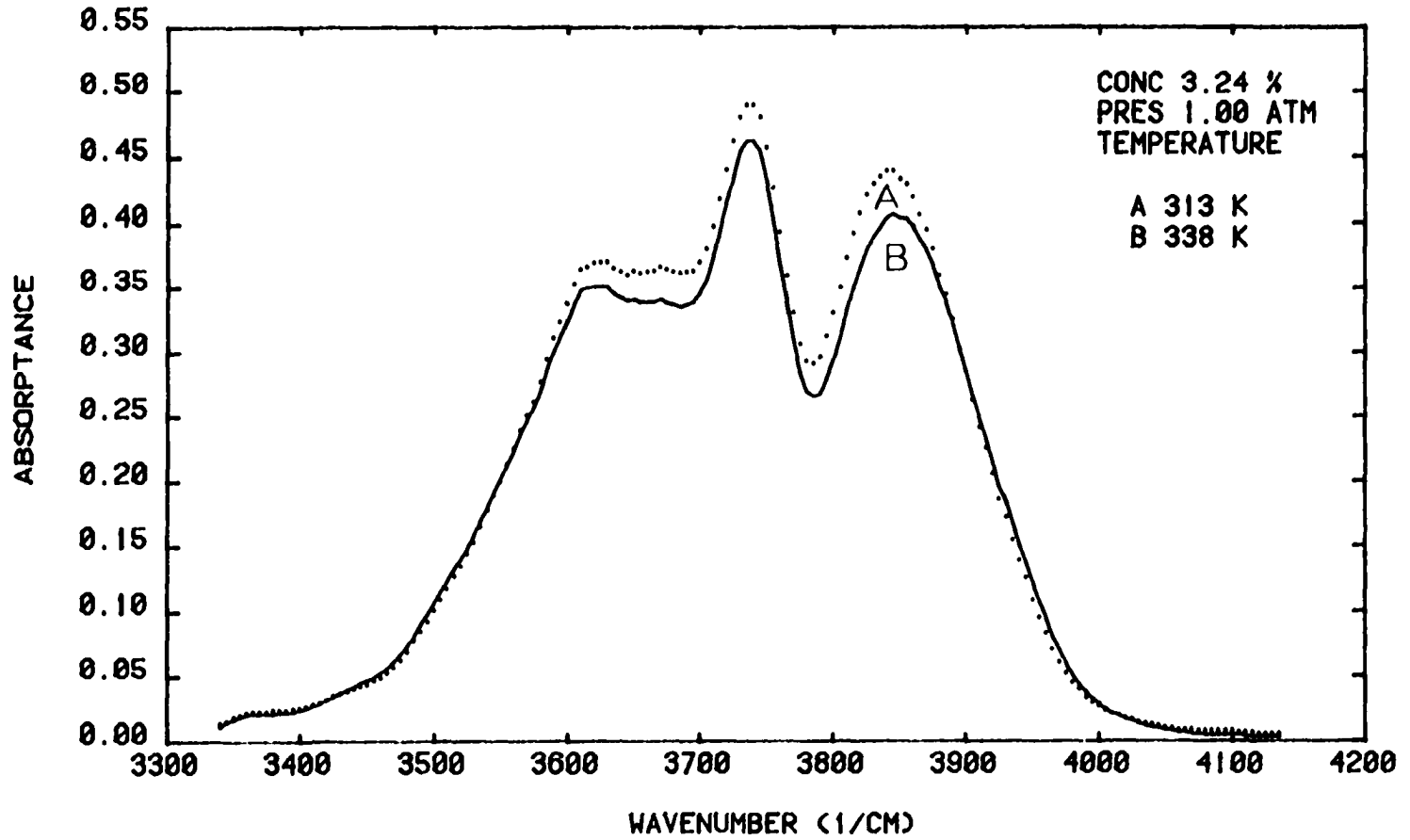


Figure 21

wavenumber along the band. It increases from about 0.3 at 3400 cm^{-1} to 0.6 at about 3515 cm^{-1} , then decreases rapidly reaching 0.0 at about 3575 cm^{-1} , continues decreasing to about -1.1 at the middle of the band, increases to 0.0 at about 3910 cm^{-1} and then to about 0.6 at 4100 cm^{-1} before decreasing again. The crossover points are approximately at the region where the value of $Z(\nu)$ goes to zero. So the temperature dependence is very different from the concentration and pressure dependences.

Figure 22 shows the F factor plotted against wavenumber. In this figure, the dots and crosses are the values obtained by References 26 and 27, for the ν_3 band and the ν_1 band respectively. Since we are doing low resolution work, we could find only the ratio of the measured and calculated absorptance at 5 cm^{-1} intervals, with a degrading of 35 cm^{-1} , the drawn curve is the result of this. There is substantial agreement over a large portion of this curve and the References 26 and 27.

Maclay wrote the F factor as

$$F = 1 \pm (am_a + bm_b + cm_c), \quad V - (4)$$

where a, b, and c are constants, while the m_i is the quantum number for the angular momentum about the i axis. One could include higher order terms of m_i in the above relation. It was assumed²⁵ for the case of $m_a, m_b \ll m_c$

$$S = S_R (1 - cm) \quad V - (5)$$

F FACTOR (MEAS. STR./RIGID ROT. STRENGTH)

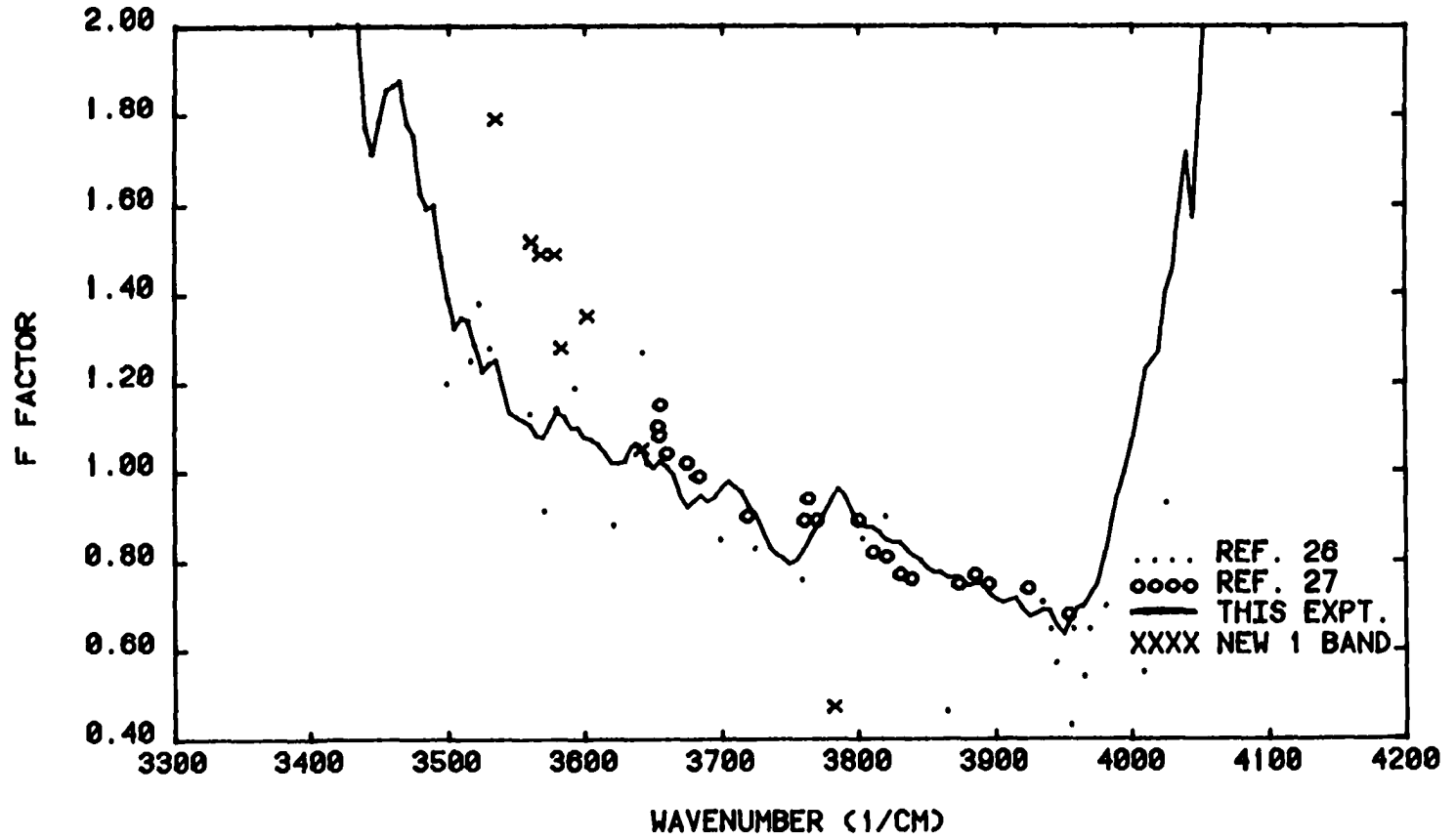


Figure 22

where S is the true strength of a rotational line, and designating m by m_c ; m is given by,

$$m = J + 1 \text{ for the R branch}$$

$$m = -J \text{ for the P branch,}$$

and J is the rotational quantum number of the lower state. Maclay found that equation V - (5) holds for two values of m , $m = -11$ and $m = +14$, with a value of 0.0433 for c .

We are proposing a relation for the F factor as

$$F = (1 + Zm)^2 \quad \text{V - (6)}$$

where Z is a constant and m is defined as before.

Figure 23 is a plot of $(F)^{1/2}$ versus m , obtained from Figure 22 for the ν_3 band alone. A straight line is drawn as the best fit for this.

A correction to the strengths of the weaker ν_1 fundamental band was also applied using the F factors for this band given by Babrov and Casden²⁶. Babrov and Casden had shown that the F factor for this band is a smooth function of wavenumber, as shown in Figure 22. This correction is satisfactory because the ratio of the relative strengths of ν_3 to ν_1 is 10:1.

Our straight line graph for $(F)^{1/2}$ does not pass through $(F)^{1/2} = 1$ for $m = 0$. Recalculating the absorption spectrum several times, we found that the best fit with the experimental spectrum is obtained using F given by

SQUARE ROOT OF F FACTOR VS. m

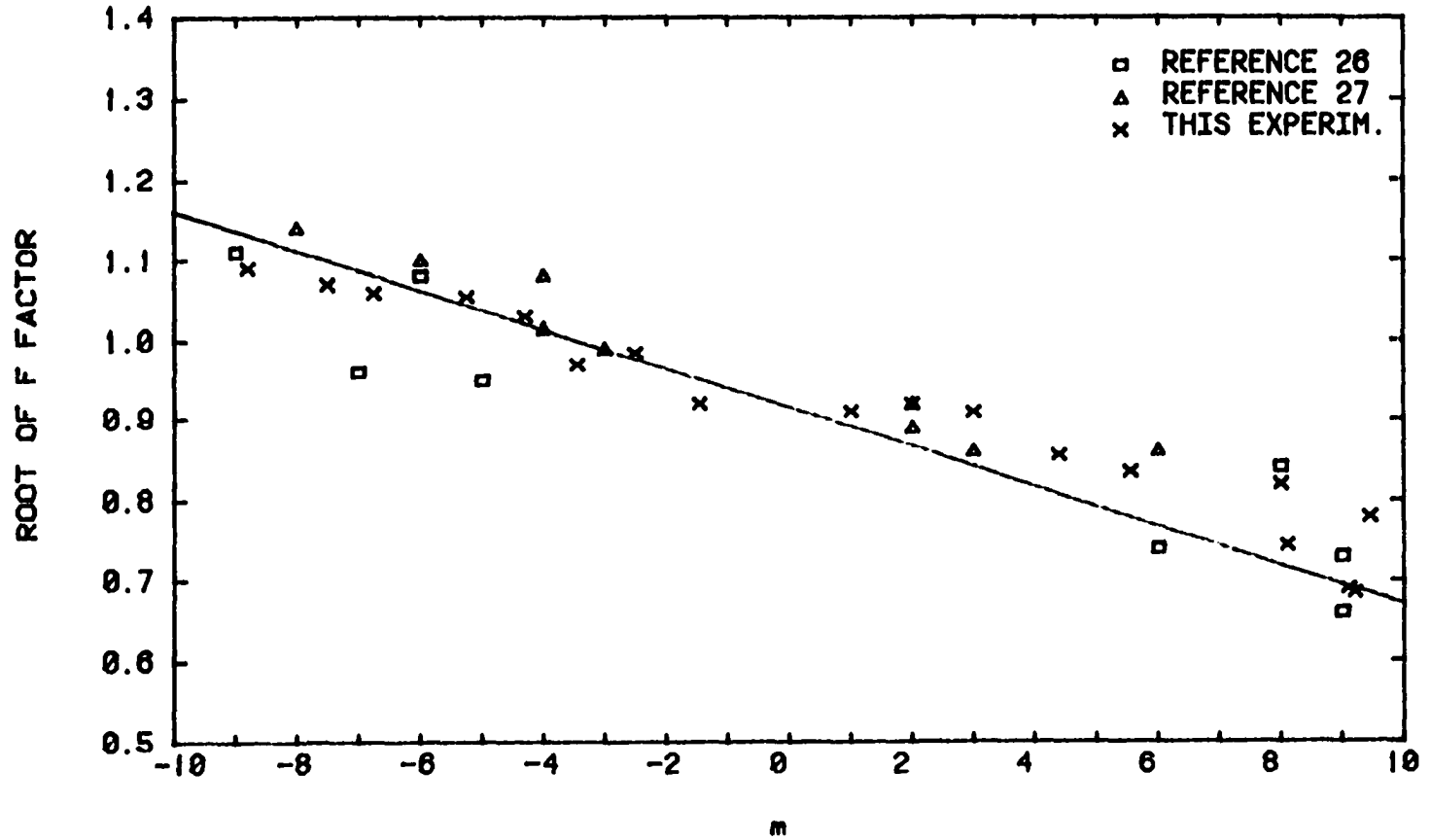


Figure 23

$$F = (0.92 + Z_m)^2, \quad V - (7)$$

with a value of $Z = -0.025$.

The line strengths of Reference 4 are corrected for each transition using the F factor obtained for that transition, for both ν_1 and ν_3 bands, as explained. The absorption and its thermodynamic derivatives are recalculated with these new line strengths, and they are plotted by the computer along with the experimental curves. These curves are marked as "c", and are all for one atmosphere pressure only, and for various concentrations and temperatures as shown in Figures 3 through 11. The agreement between the calculated and our experimental spectra is very good.

C. STATIC FIRST DERIVATIVES

Now, we turn to the static first derivatives which are obtained from two absorption spectra whose averages of c , P , and T serve as the reference point. Using three absorption spectra one can interpolate to find the derivatives at a different c , P , and T point³⁸.

Figure 24 shows the partial derivative of the absorption with respect to P times P plotted against wavenumber, with pressure as a parameter at 313°K and a concentration of 3.24%. The calculated first derivative is computed for the experimental temperature using calculated first and second derivatives assuming a Taylor series expansion and keeping only terms of order two and less. The computed values plotted as "c" show excellent agreement with the measured values.

DERIVATIVE OF 2.7 MICRON BAND ABSORPTION

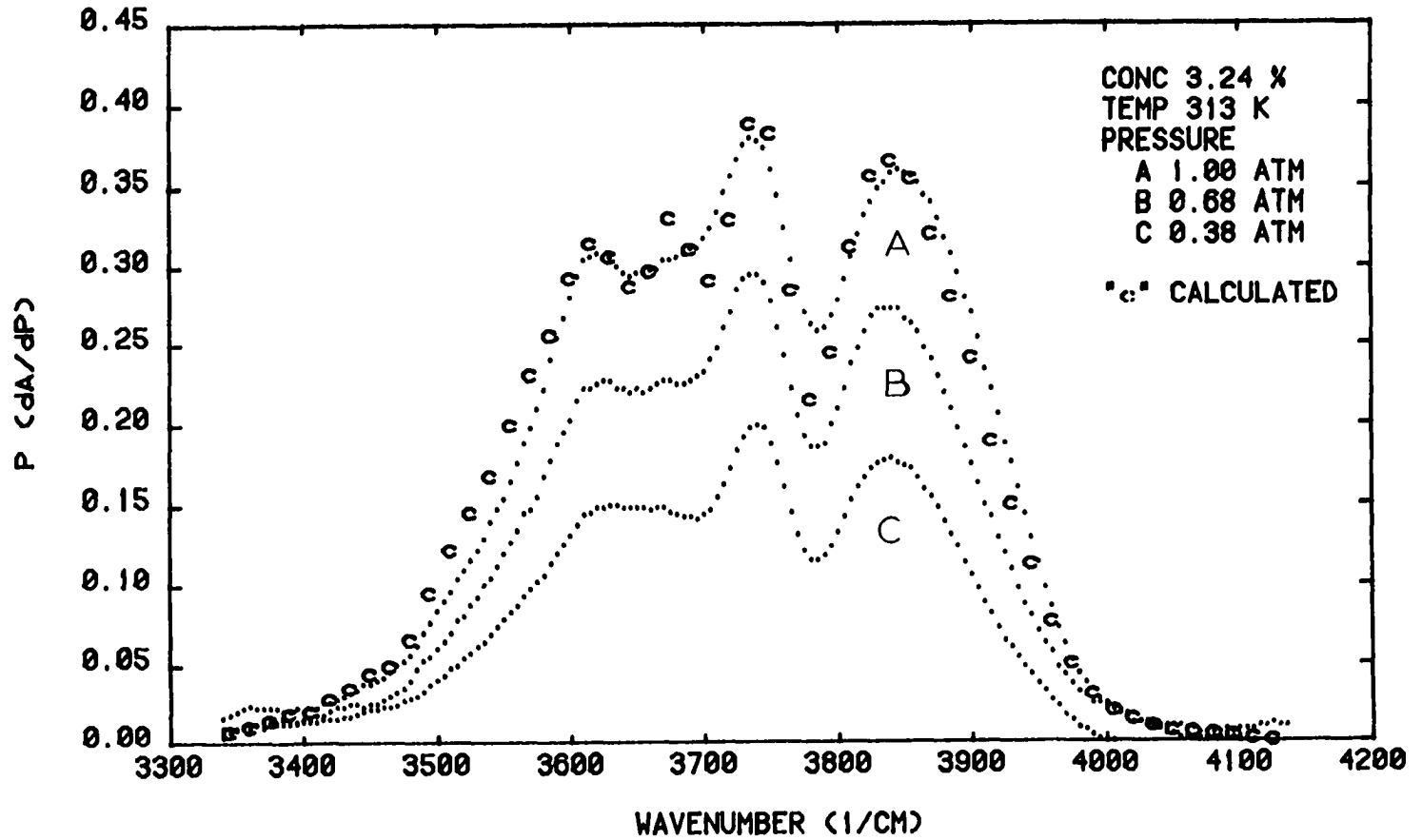


Figure 24

DERIVATIVE OF 2.7 MICRON BAND ABSORPTION

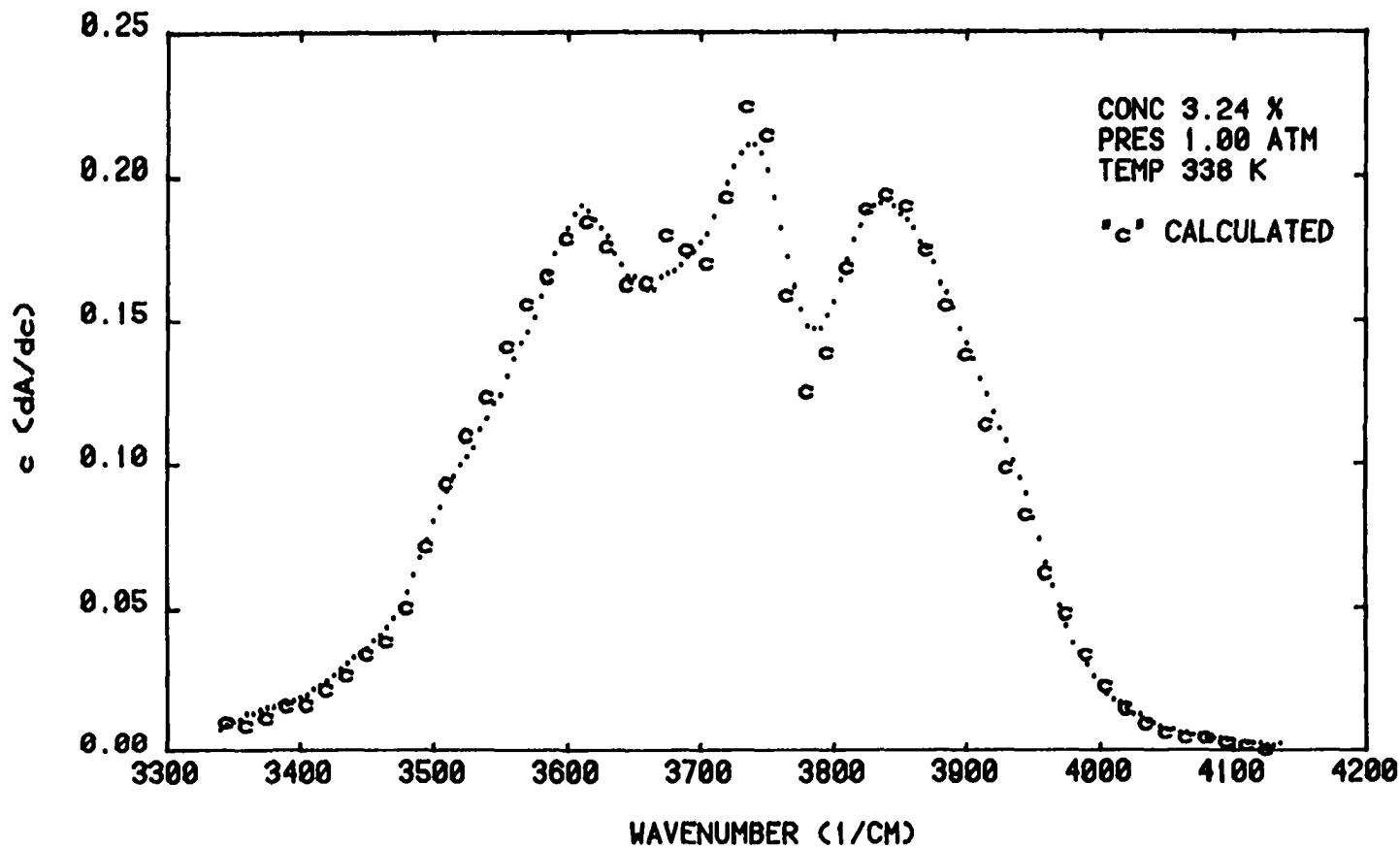


Figure 25

DERIVATIVE OF 2.7 MICRON BAND ABSORPTION

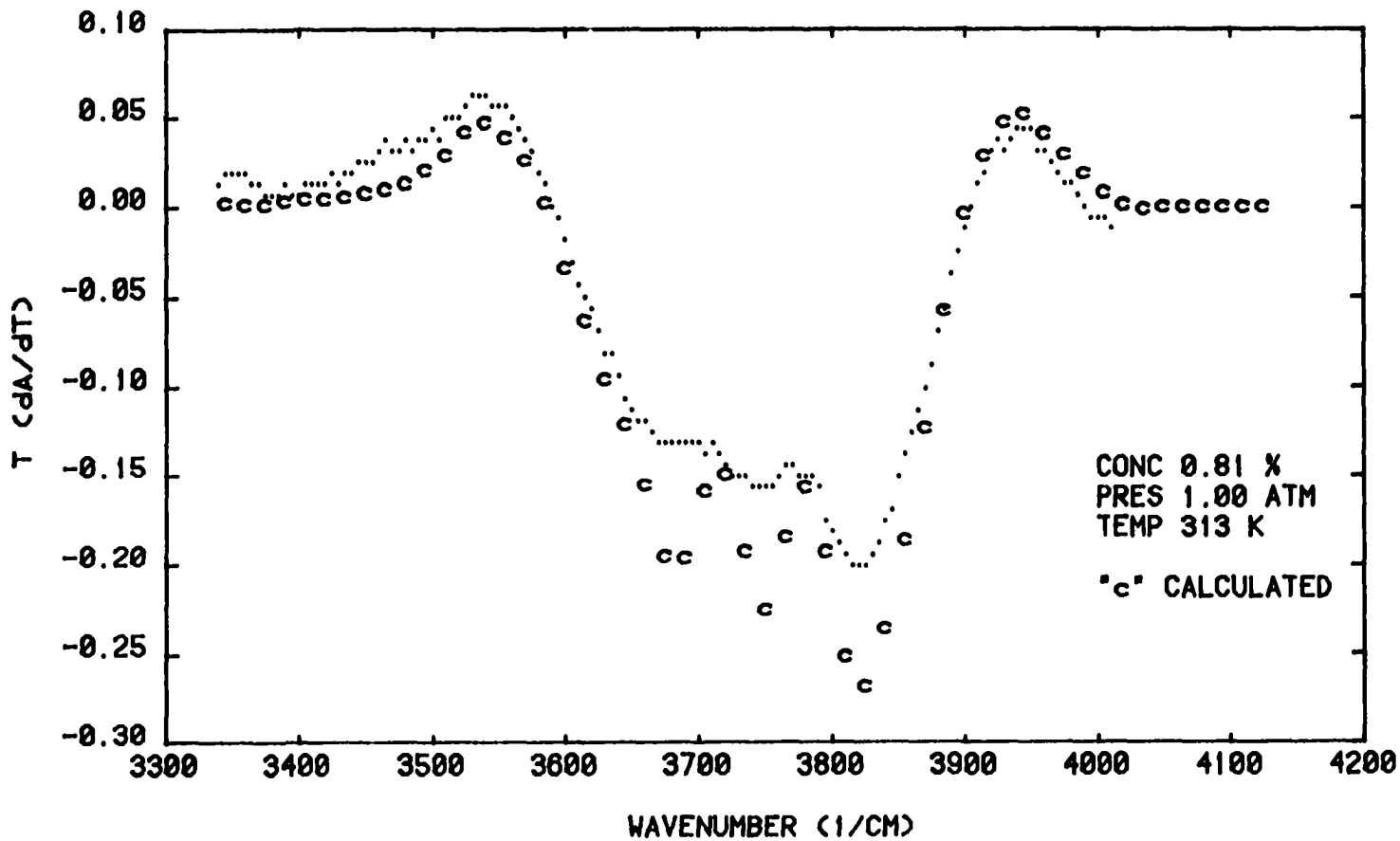


Figure 26

Figure 25 shows the partial derivative of the absorption with respect to c times c versus wavenumber for one atmosphere pressure and at 338°K . Again, as before, the curve marked "c" is the calculated spectrum, computed for the experimental temperature, using calculated first and second derivatives. The agreement between experimental and calculated values is very good. It is clear from these curves that there is a strong dependence of the absorption on the concentration, over the entire band.

Figure 26 shows the partial derivative of the absorption with respect to temperature times the temperature plotted against wavenumber for $c = 0.81\%$, $P = 1$ atmosphere, and $T = 313^{\circ}\text{K}$. The curve marked "c" is the calculated spectrum computed for the experimental temperature.

Earlier in this chapter we concluded that there are two regions in the wings of the band, where the temperature dependence of the absorption is minimal; or even the absorption is independent of the temperature of the sample gas. So we expect the first derivative of the absorption with respect to the temperature at these regions to be zero. Indeed, the $TA(T)$ curve cuts the x-axis at the middle of these regions, at about 3575 cm^{-1} and 3910 cm^{-1} . The value of $TA(T)$ is negative between these two points and is positive everywhere else in the wings.

The difference between the experimental and calculated values of $TA(T)$ is well within our error estimates. Since, we had only a small temperature range available in our experiment, we have,

$$\frac{T}{\Delta T} = \frac{313^{\circ}\text{K}}{50^{\circ}\text{K}} = 6.25$$

Therefore, $\frac{T}{\Delta T}$ times the possible maximum error in ∂A of 1.1×10^{-2} gives the maximum error in the value of T ($\partial A/\partial T$) to be about 0.07. This is larger than the maximum difference between the curves of Figure 26. It should be recalled that the calculated T ($\partial A/\partial T$) at the experimental temperature was computed using calculated first and second derivatives only, neglecting higher order terms. Also, we have not included the possible errors in the calculated first and second derivatives.

D. STATIC SECOND DERIVATIVES

The experimental second derivatives and mixed derivatives are obtained from three or four absorption curves spaced at regular c , P , and T intervals, with the averages of the c , P , and T values serving as the reference points.

Figure 27 shows the second derivative of A with respect to concentration times c^2 , with c as a parameter. Again, the "c" marks are the calculated $c^2 A(cc)$ values. Even for the second derivatives, we have good agreement between the calculated and experimental values, showing the quality of the measured values.

Figure 28 shows the second partial derivative of the absorption with respect to pressure at 338°K for a concentration of 4.86%, with pressure as a parameter. We notice that the PPA(PP) are very small in the wings and small in the core of the band.

The calculated PPA(PP) are marked "c" for one atmosphere. There is very poor agreement between the calculated and experimental values. The authors of Reference 1, have recognized this error in the calculation

SECOND DERIVATIVE OF 2.7 MICRON BAND ABSORPTION

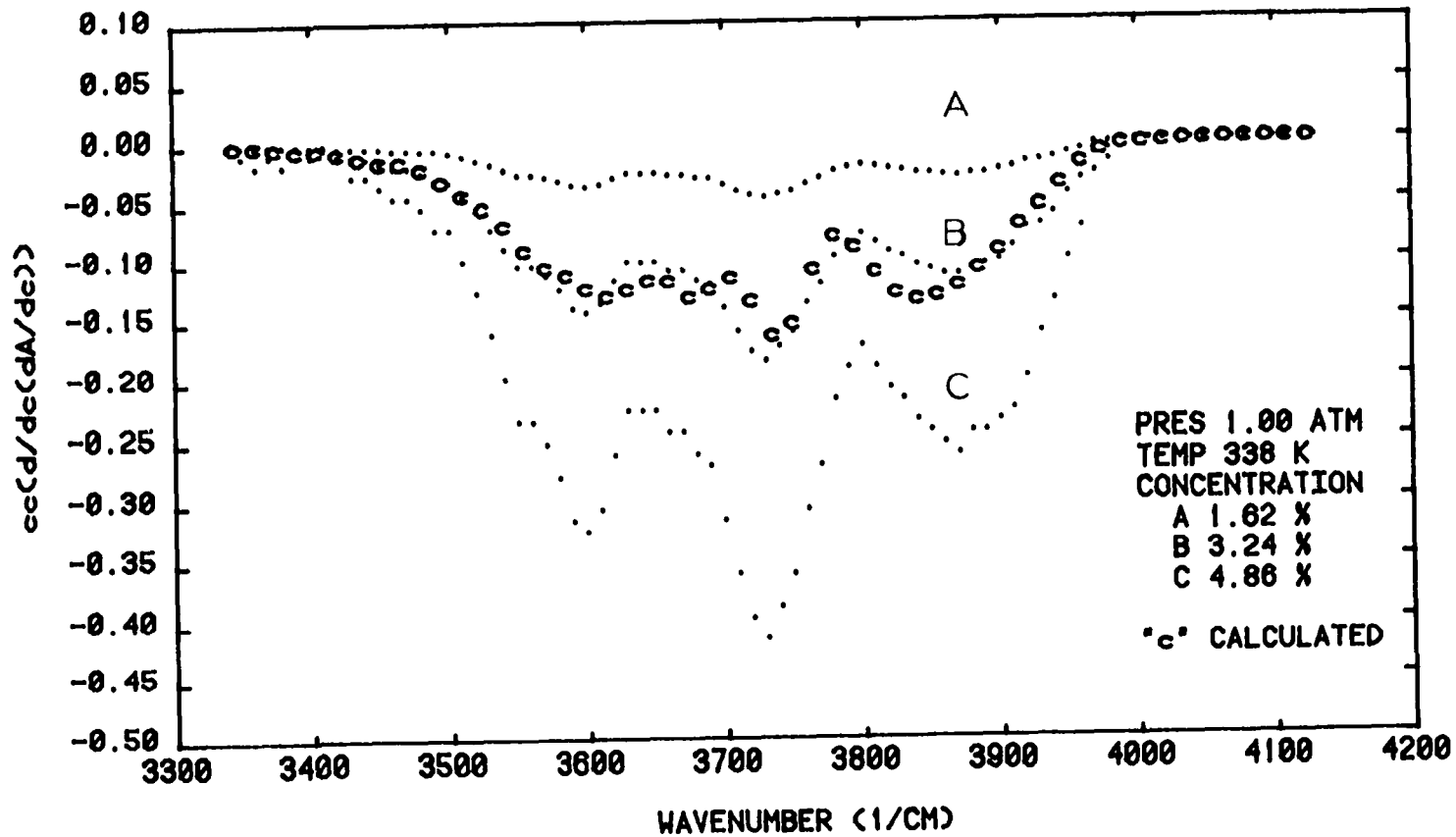


Figure 27

SECOND DERIVATIVE OF 2.7 MICRON BAND ABSORPTION

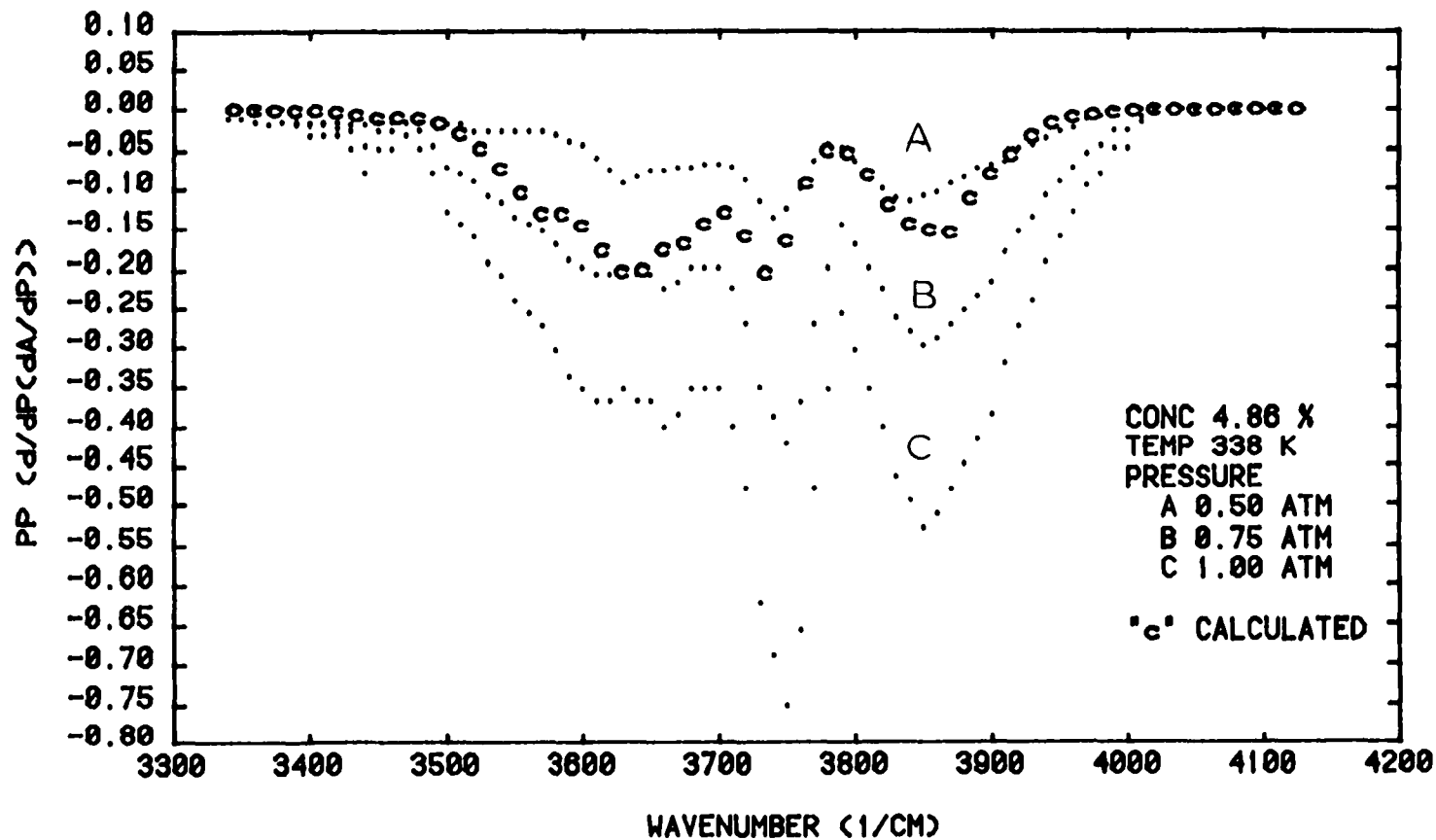


Figure 28

SECOND DEIVATIVE OF 2.7 MICRON BAND ABSORPTION

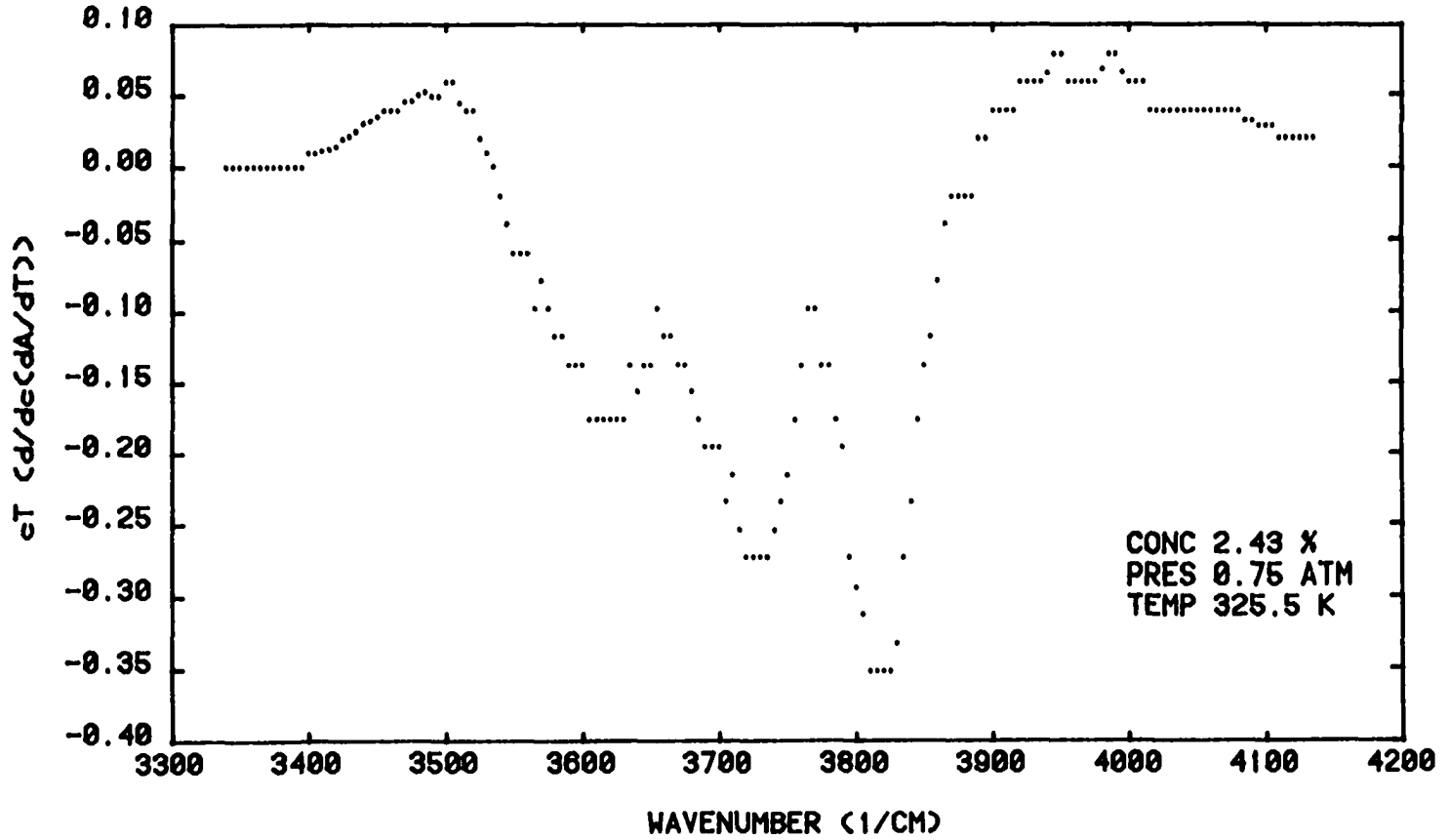


Figure 29

of the second derivative, PPA(PP).

Figure 29 shows $cT A(cT)$ versus wavenumber. The temperature dependence of the absorptance is again exhibited.

E. DYNAMIC MODE RESULTS

This section presents the most important result of our experiment: for the water vapor molecule no such results, experimental or theoretical, are available in the literature. The introduction of the fluctuations in the thermodynamic variables modulate the mean transmitted intensity. We can obtain the experimental adiabatic first derivative of the absorption with respect to the pressure from

$$(\partial A / \partial P)_{ad.} = -(1/I_0) (\delta I / \delta P). \quad V - (8)$$

First we discuss the results for a constant δP of 5.57 mm, peak to peak.

Figure 30 shows the adiabatic partial derivatives of the absorption times P for concentrations of 0.81% and 1.62% at 288°K and 293°K respectively. The calculated adiabatic derivative is found using calculated first derivatives,

$$P (\partial A / \partial P)_{ad.} = P (\partial A / \partial P) + 0.28 T (\partial A / \partial T). \quad V - (9)$$

Again, the calculated first derivatives at the experimental temperatures are obtained using calculated first and second derivatives, as was done in the case of static derivatives. The curves marked "c" are the calculated spectra. The agreement between experimental and calculated values is excellent.

ADIABATIC DERIVATIVE OF 2.7 MICRON BAND ABSORPTION

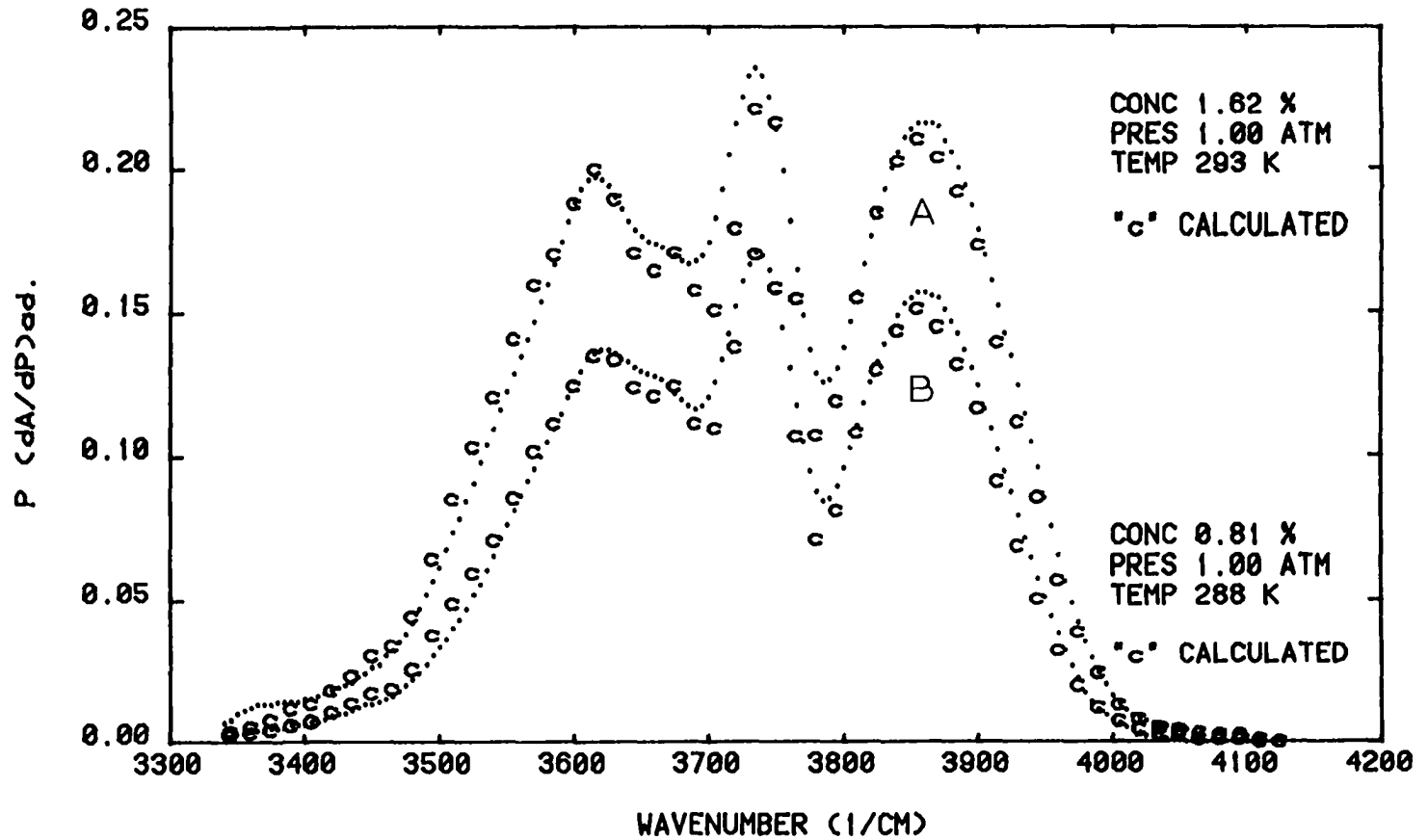


Figure 30

ADIABATIC DERIVATIVE OF 2.7 MICRON BAND ABSORPTION

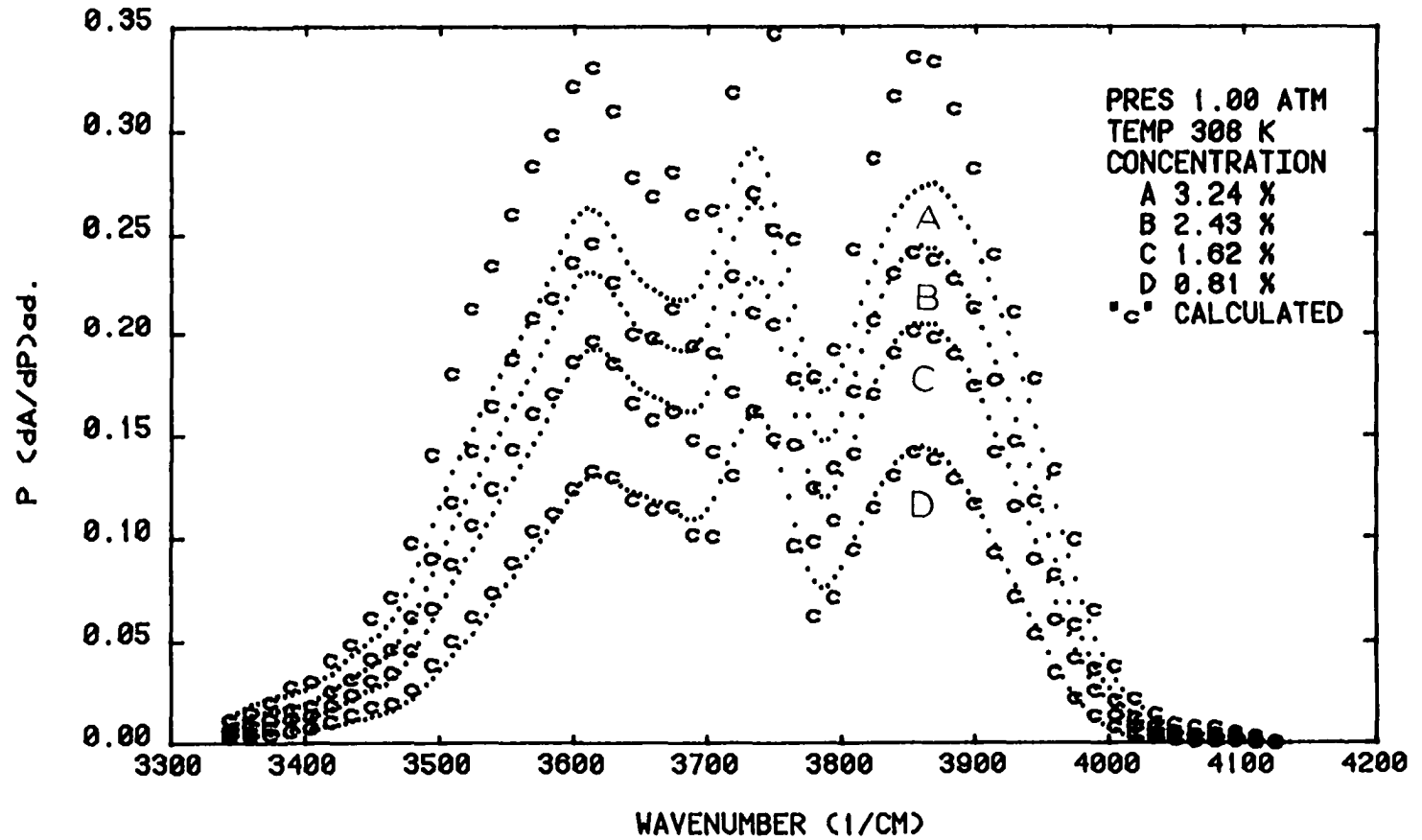


Figure 31

ADIABATIC DERIVATIVE OF 2.7 MICRON BAND ABSORPTION

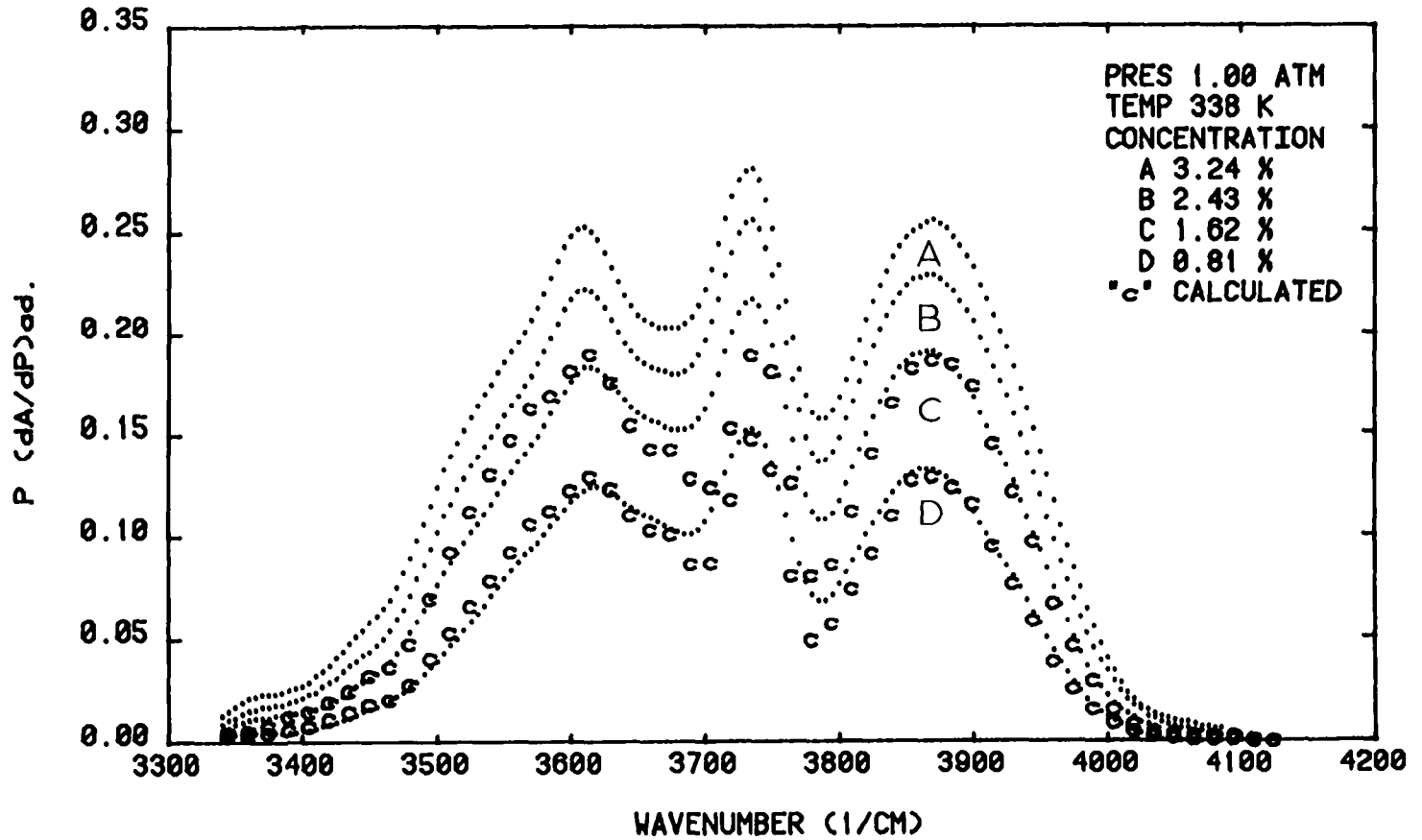


Figure 32

ADIABATIC DERIVATIVE OF 2.7 MICRON BAND ABSORPTION

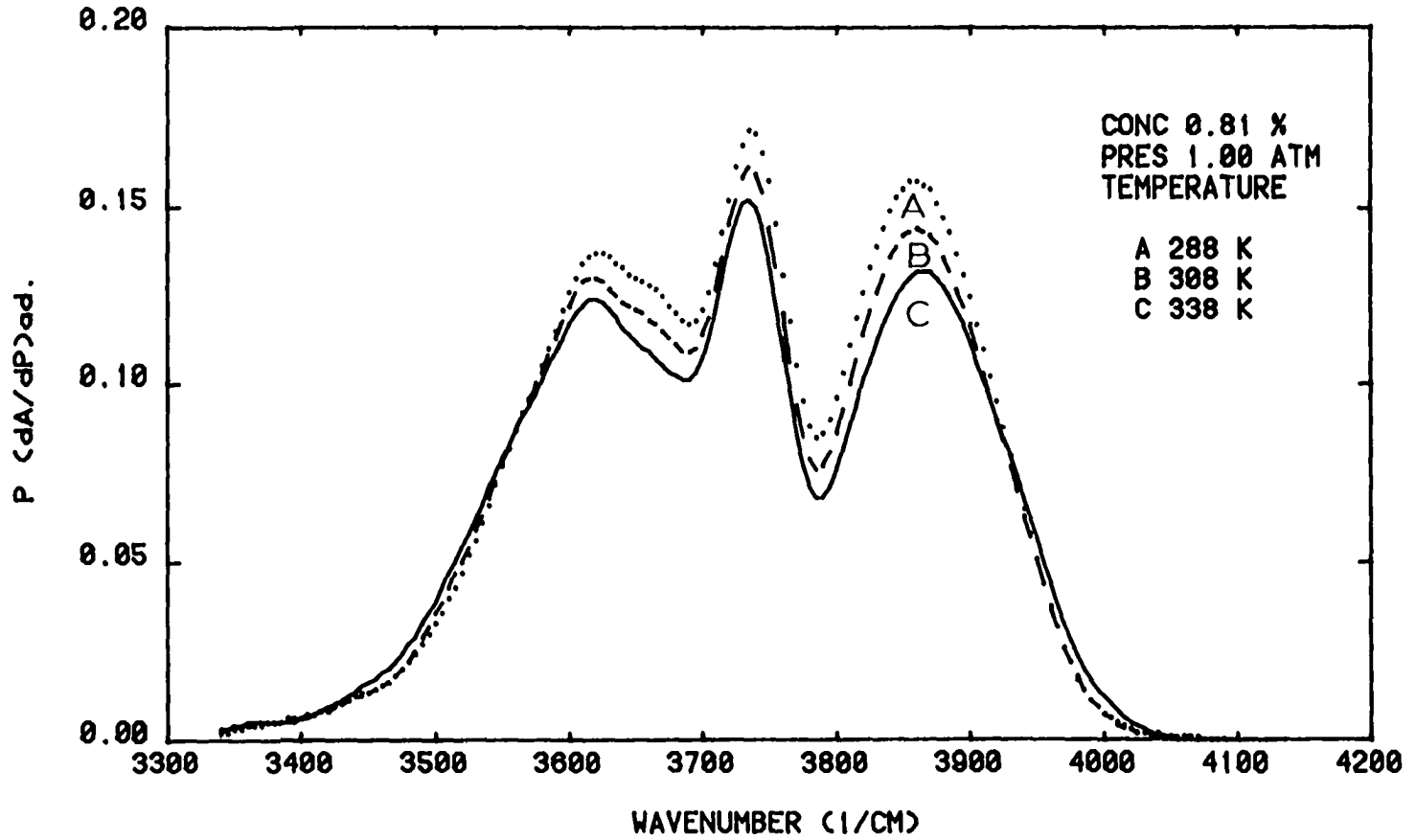


Figure 33

ADIABATIC DERIVATIVE OF 2.7 MICRON BAND ABSORPTION

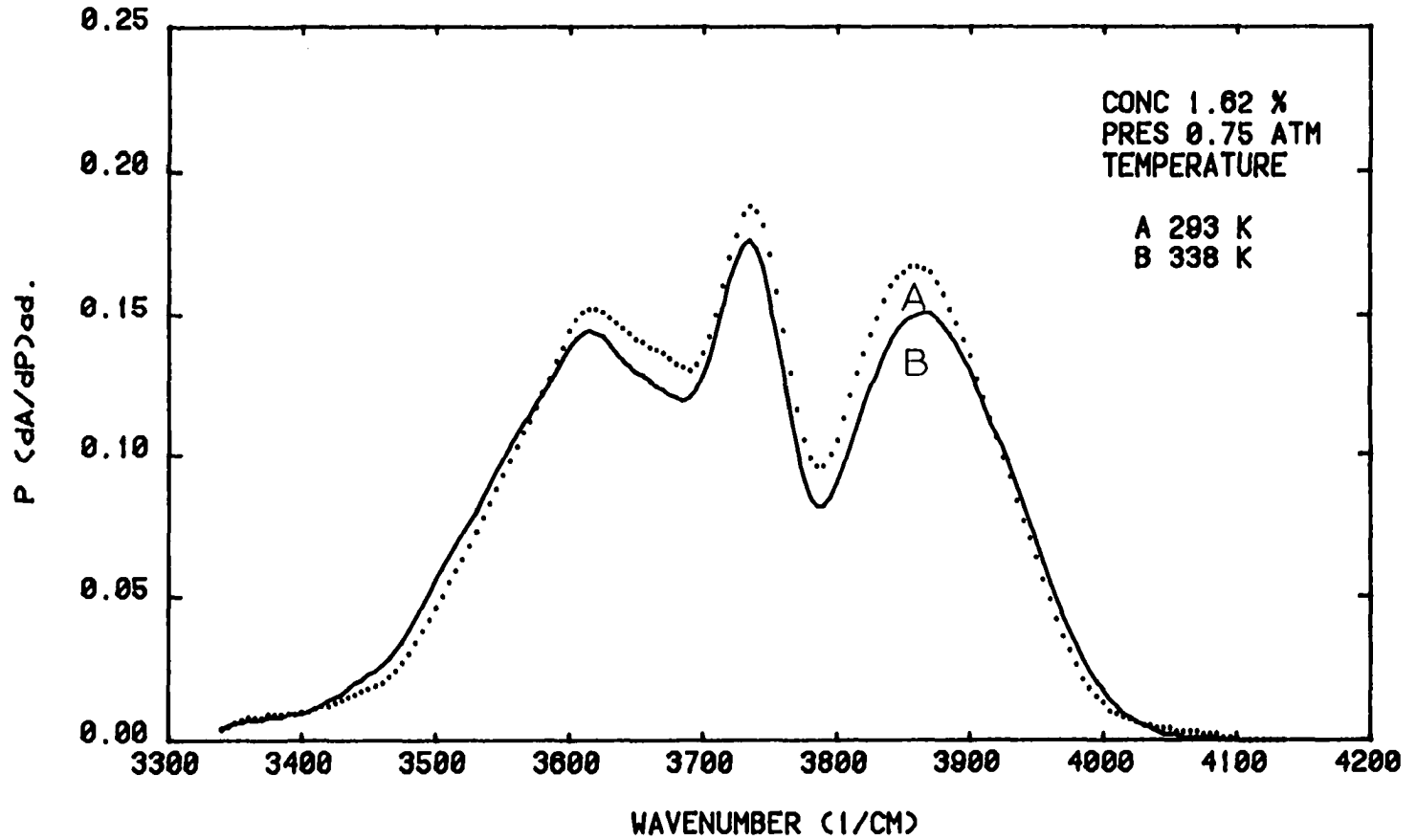


Figure 34

ADIABATIC DERIVATIVE OF 2.7 MICRON BAND ABSORPTION

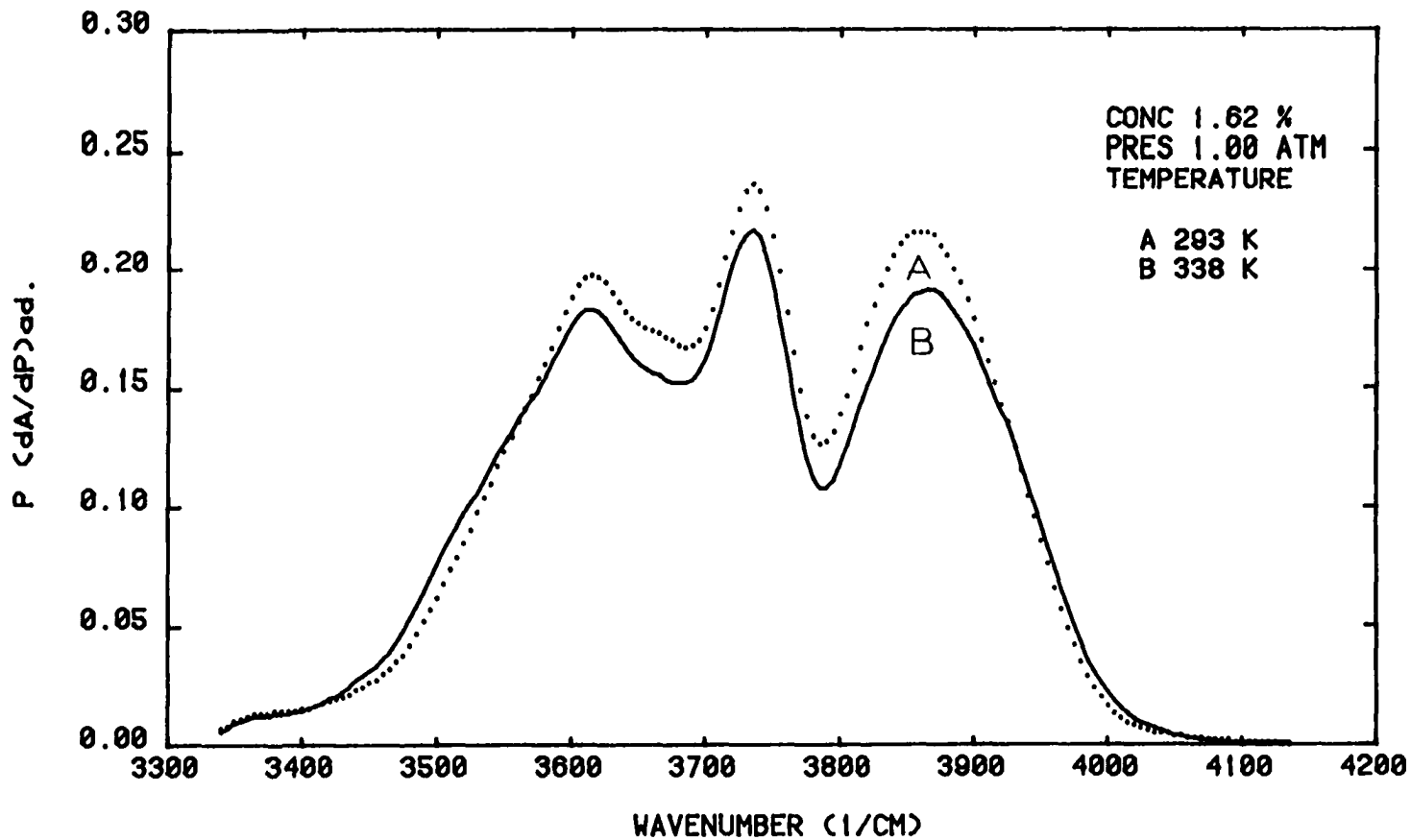


Figure 35

ADIABATIC DERIVATIVE OF 2.7 MICRON BAND ABSORPTION

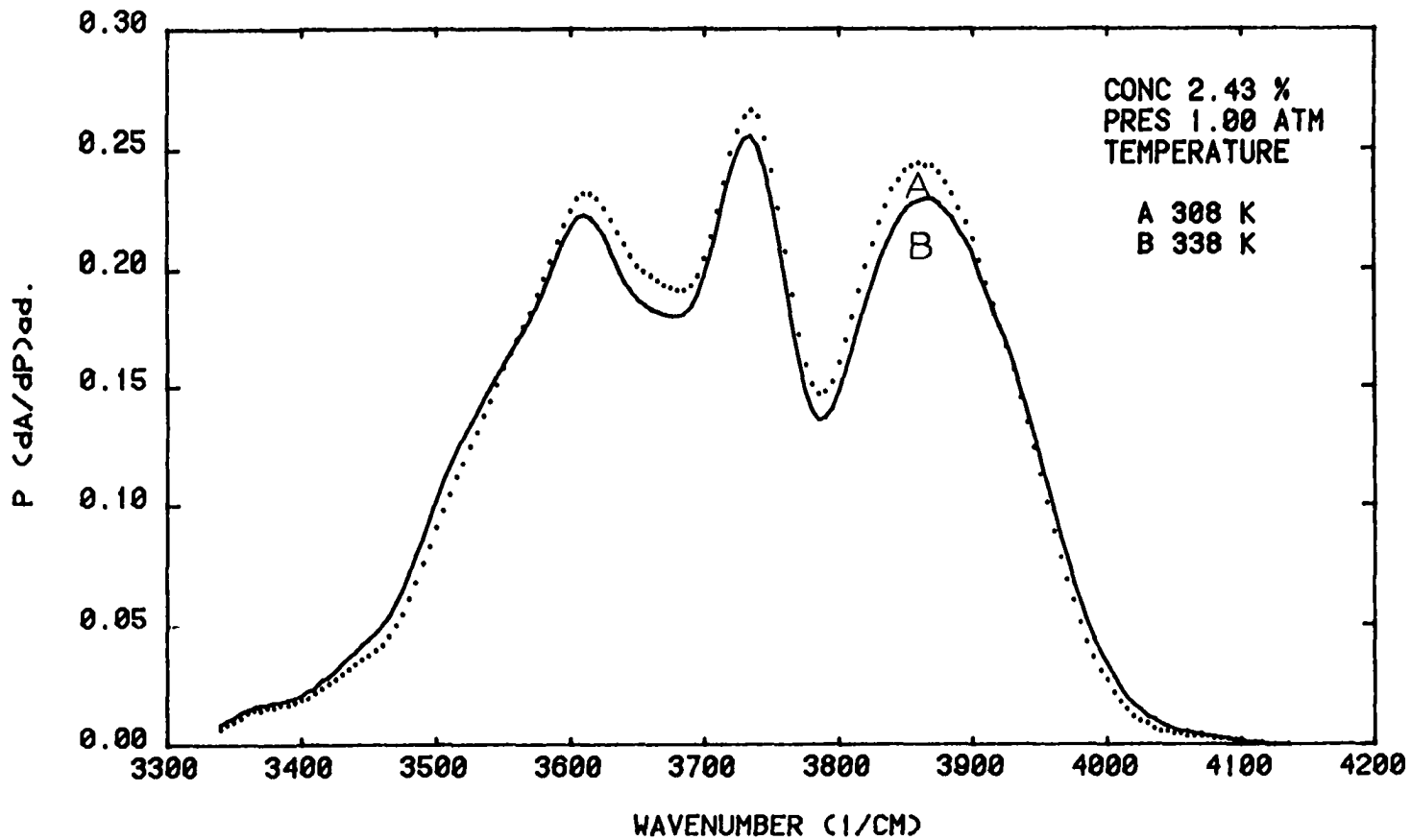


Figure 36

Figure 31 and 32 show $P (\partial A / \partial P)_{ad.}$ versus wavenumber with the concentration of the sample gas, c as a parameter at 308°K and 338°K respectively. The calculated spectra for the experimental temperatures are computed from the calculated $PA(P)$, $TA(T)$, and the second derivative, $PTA(PT)$. The agreement between the experimental and calculated values is good. A close look at these figures reveals an interesting phenomenon: as the concentration increases in equal steps the dependence of $P (\partial A / \partial P)_{ad.}$ on the concentration becomes smaller.

Figures 33 through 36 show $P(\partial A / \partial P)_{ad.}$ versus wavenumber for various values of concentration and pressure, with temperature as a parameter. These figures show that there are two regions in the wings of the band where $P (\partial A / \partial P)_{ad.}$ is independent of the temperature of the sample gas. These are the crossover regions at about 3575 cm^{-1} and 5910 cm^{-1} . Between the crossover points the effect of temperature on the $P (\partial A / \partial P)_{ad.}$ is negative, while in the wings, outside the crossover points, it is strong and positive.

Figure 37 shows $P (\partial A / \partial P)_{ad.}$ versus wavenumber with pressure as a parameter, for a concentration of 1.62% and temperature of 295°K . The curve marked "c" is the calculated spectrum.

Figures 38, 39, and 40 are computer plotted $(\partial A / \partial P)_{ad.}$ versus wavenumber with pressure as a parameter. These graphs show that the dependence of $(\partial A / \partial P)_{ad.}$ on the pressure is minimal in the wings of the band and small and negative in the core of the band. This is an important result: in each wing of the $(\partial A / \partial P)_{ad.}$ curve, we have a region, where $(\partial A / \partial P)_{ad.}$ depends only on the concentration of the sample gas.

ADIABATIC DERIVATIVE OF 2.7 MICRON BAND ABSORPTION

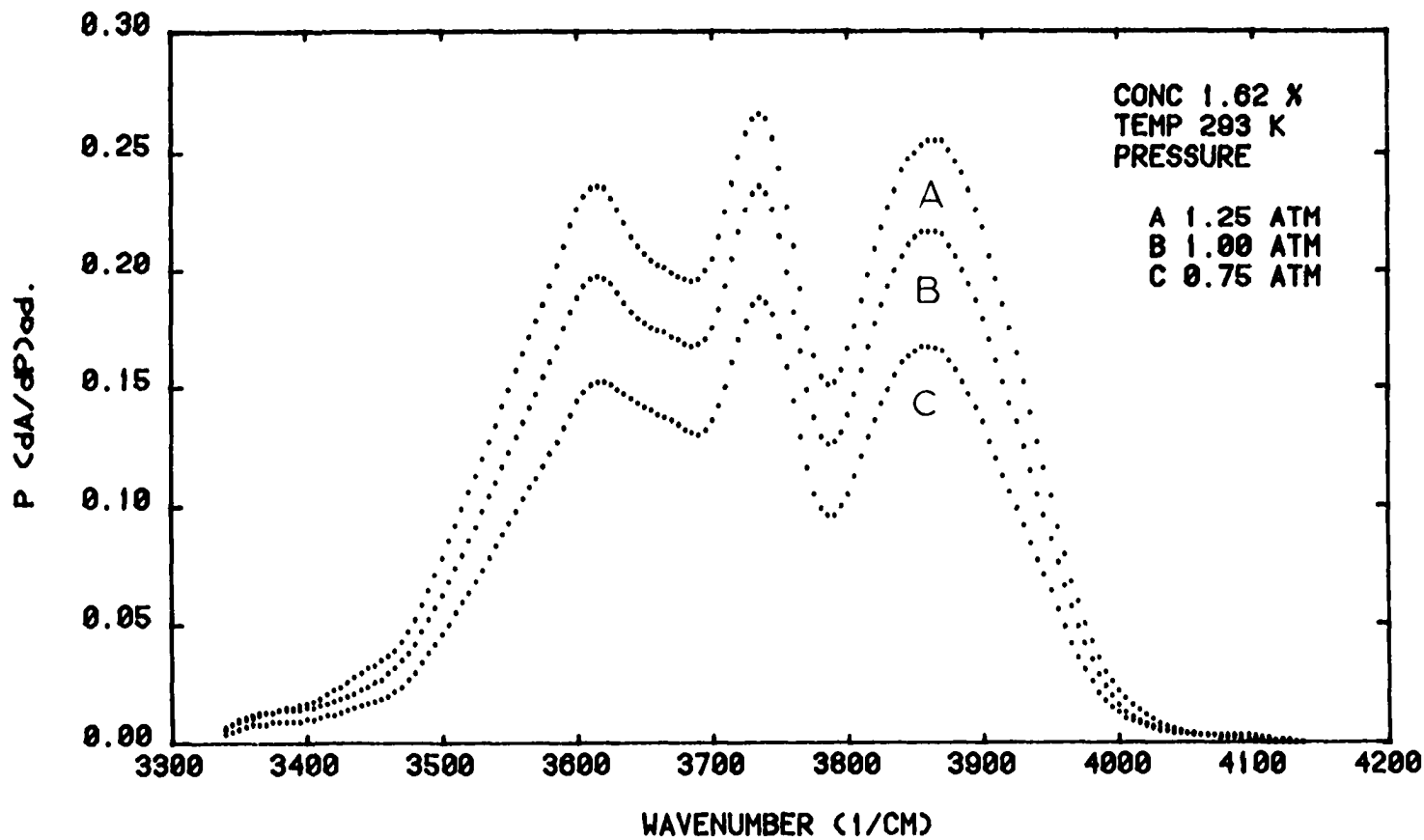


Figure 37

ADIABATIC DERIVATIVE OF 2.7 MICRON BAND ABSORPTION

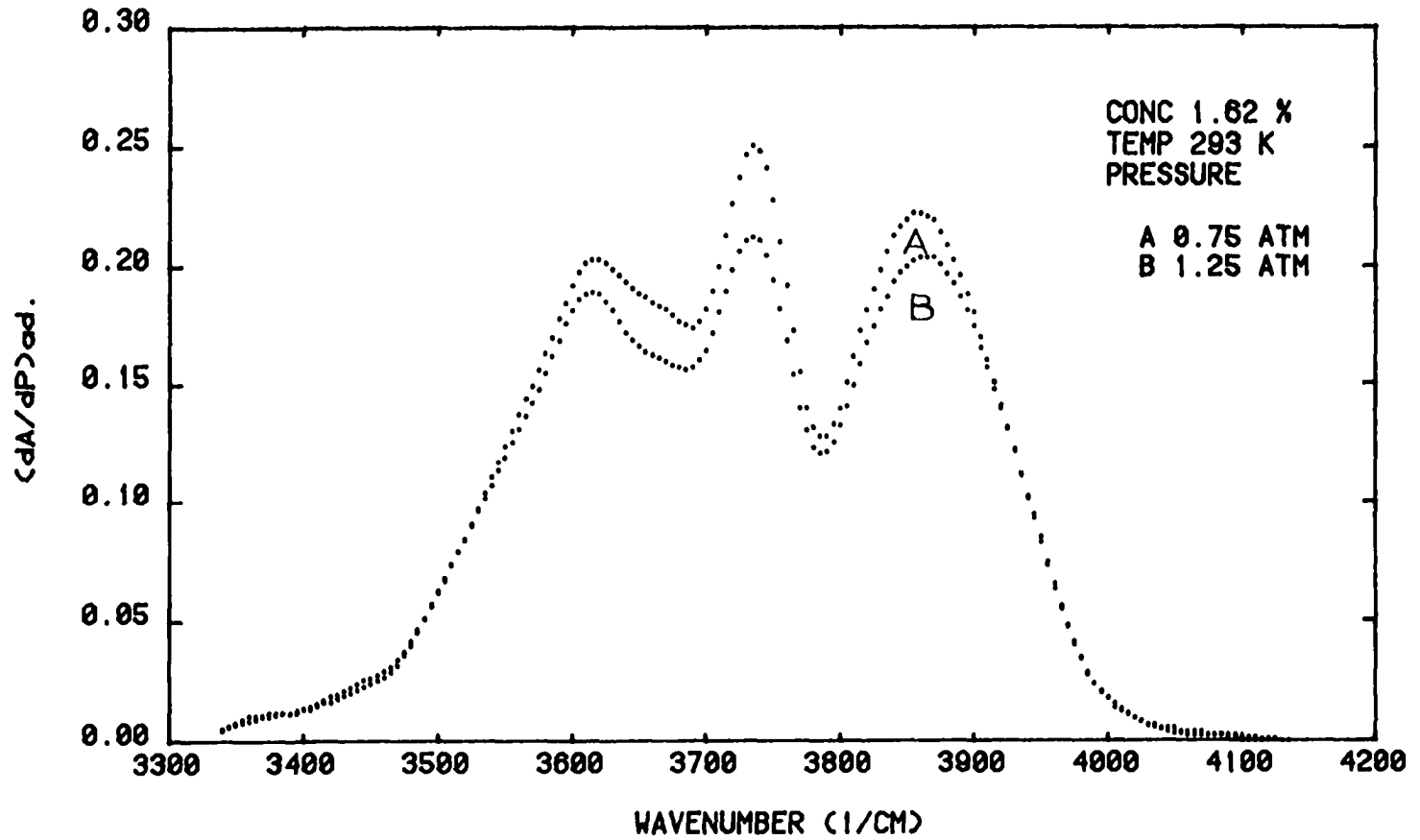


Figure 38

ADIABATIC DERIVATIVE OF 2.7 MICRON BAND ABSORPTION

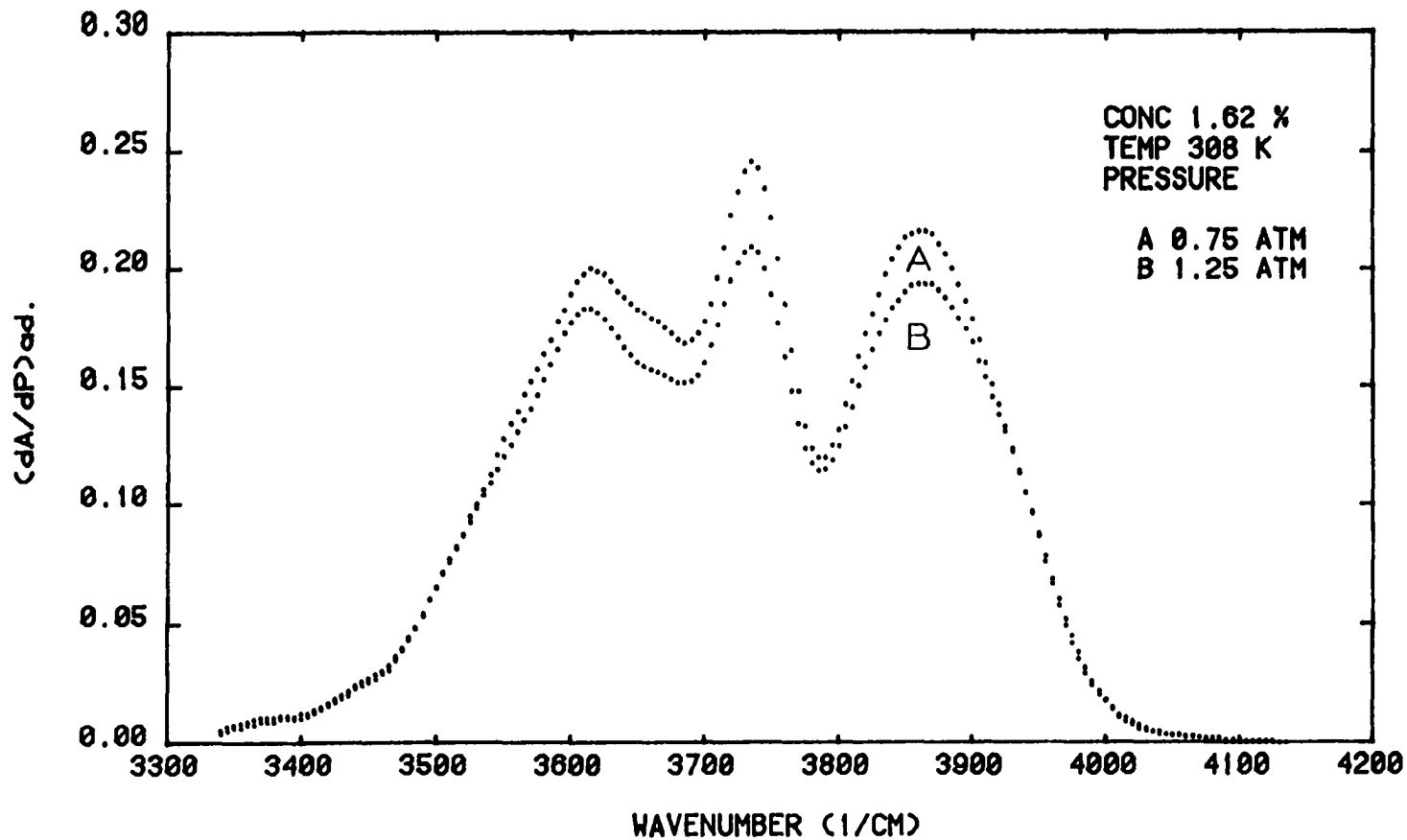


Figure 39

ADIABATIC DERIVATIVE OF 2.7 MICRON BAND ABSORPTION

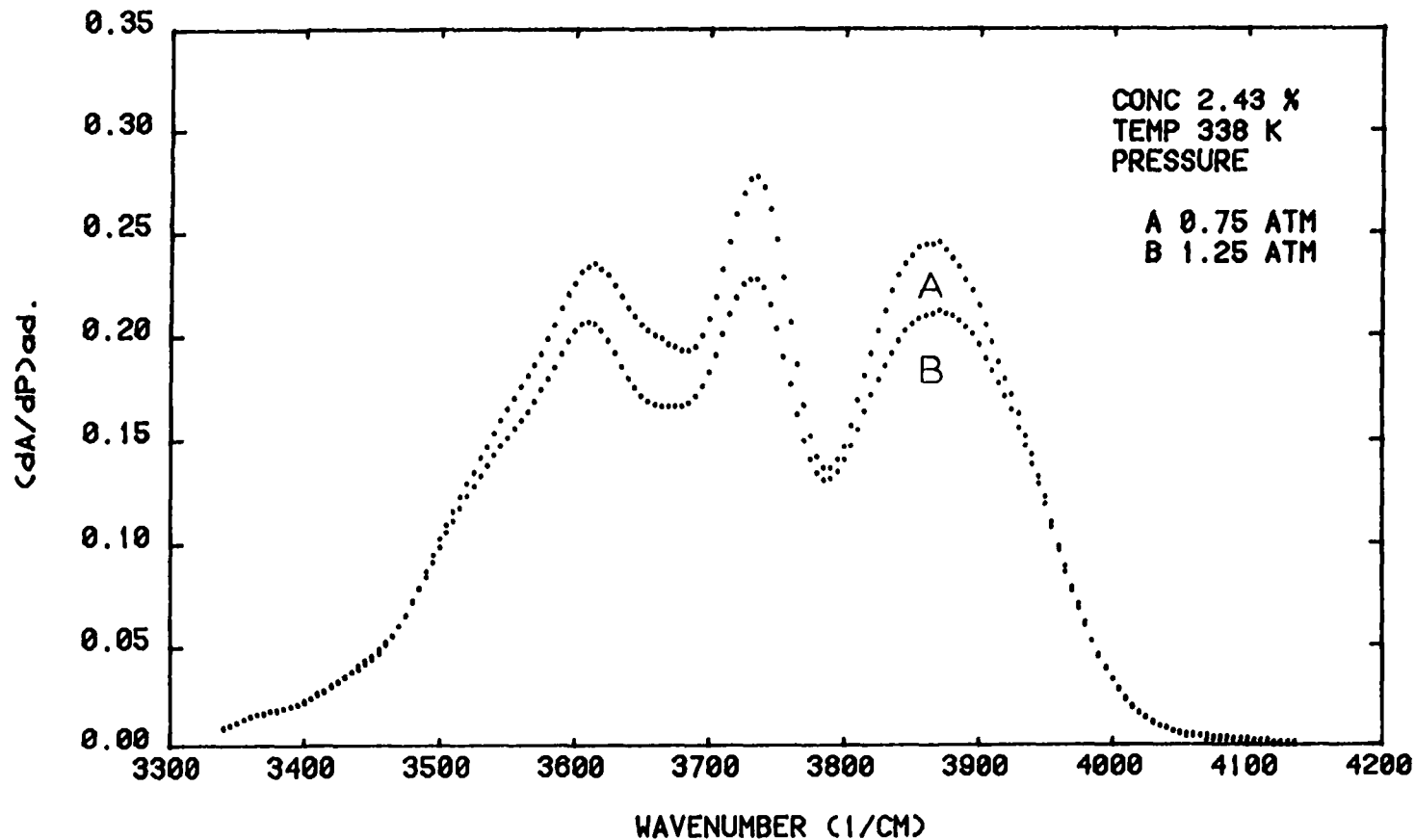


Figure 40

Experimental Second Derivatives

As in the static case, we obtain the second derivatives by using two $P (\partial A/\partial P)_{ad.}$ curves, with midpoints serving as reference points for c , P , and T .

Figure 41 shows the partial derivative, $cP (\partial/\partial c (\partial A/\partial P)_{ad.})$ versus wavenumber, where the "c" marks are the calculated values. Again, the agreement between the calculated and experimental values is good. This figure shows strong c dependence over the entire 2.7 micron band.

Figure 42 shows the partial derivative, $PP (\partial/\partial P (\partial A/\partial P)_{ad.})$ versus wavenumber. This figure shows that its value is zero or very small in the wings of the band, unlike the $cP(cP)$ curve.

Figure 43 shows the partial derivative, $PT (\partial/\partial T (\partial A/\partial P)_{ad.})$ versus wavenumber. The temperature dependence of the $P (\partial A/\partial P)_{ad.}$ curves is exhibited in this curve also. Again the calculated spectrum is plotted as "c" marks, by the computer.

F. VARIABLE δP ANALYSIS

A limited study was made concerning the dependence of the fluctuating intensity as a function of the fluctuating pressure, i.e., δI vs. δP .

Figure 44 shows $P (\partial A/\partial P)_{ad.}$ with δP as a parameter, for a concentration of 3.24%, pressure of 1 atmosphere and temperature of 338^oK. This curve shows that $P (\partial A/\partial P)_{ad.}$ remains almost a constant for every value of δP , as is to be expected. Figure 45 shows δI versus wavelength in microns, with δP as a parameter for $c = 3.24\%$, $P = 1$, and $T = 338^{\circ}K$. The I values in this figure are not degraded, unlike all the other spectra,

ADIABATIC DERIVATIVE OF 2.7 MICRON BAND ABSORPTION

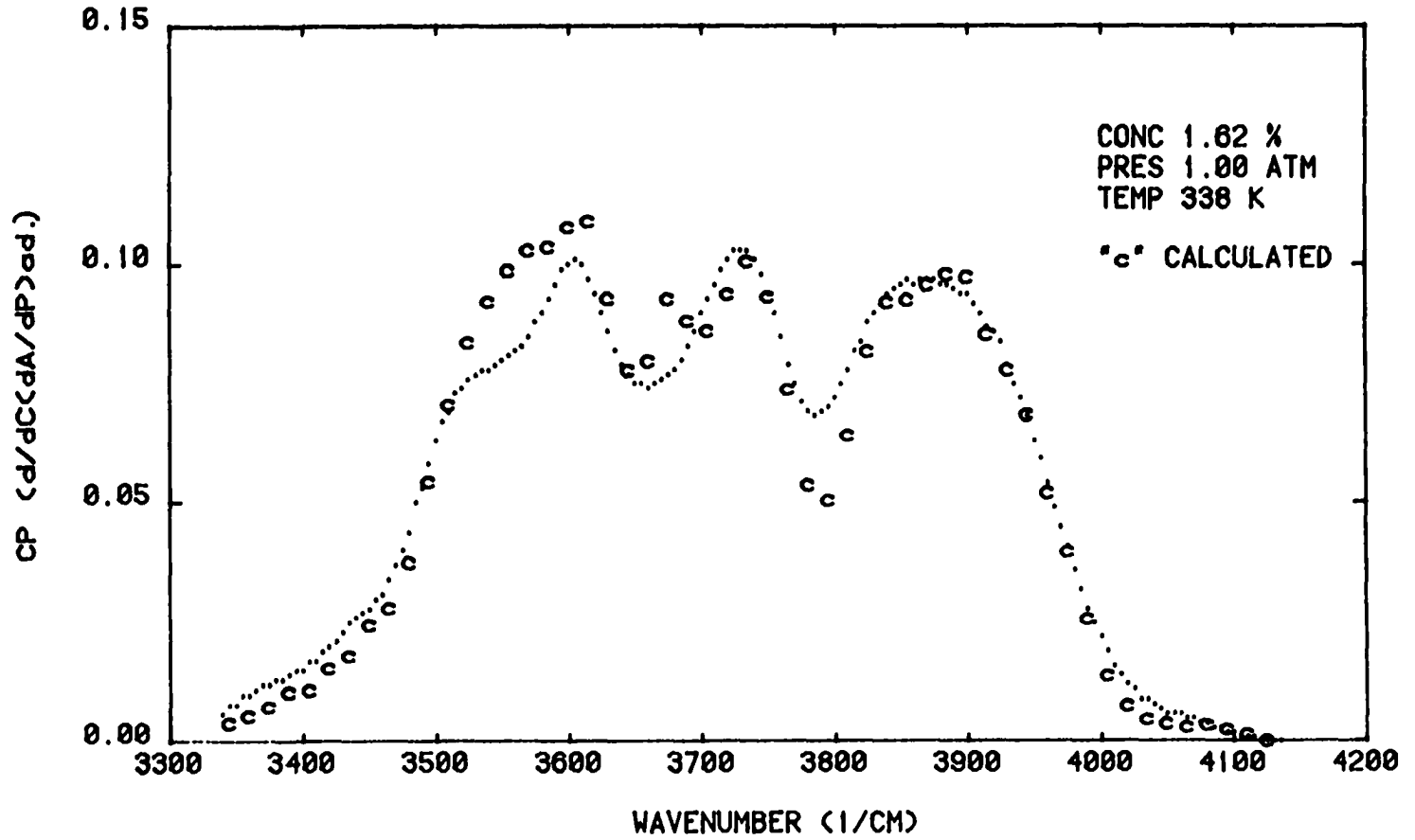
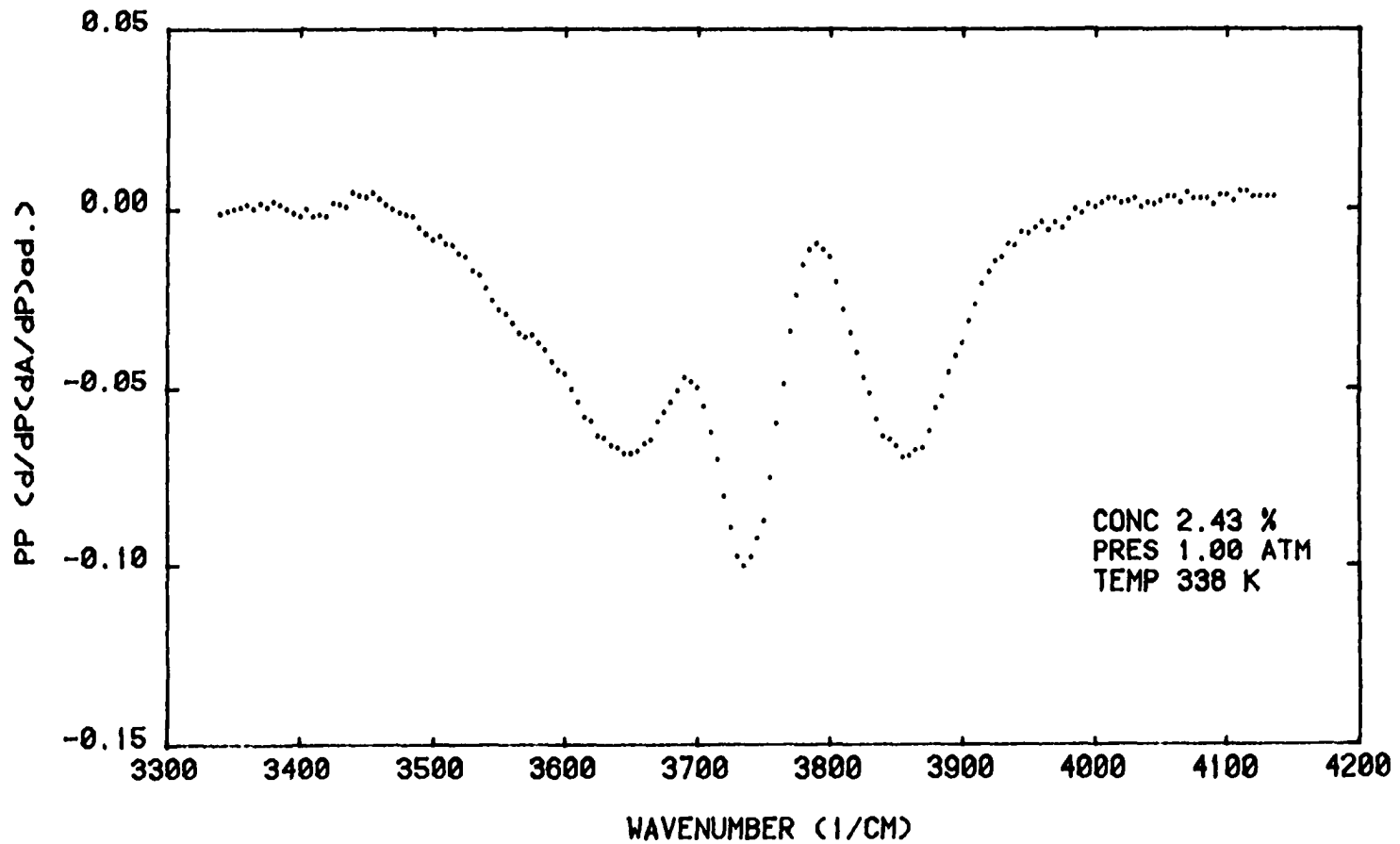


Figure 41

ADIABATIC DERIVATIVE OF 2.7 MICRON BAND ABSORPTION



100

Figure 42

ADIABATIC DERIVATIVE OF 2.7 MICRON BAND ABSORPTION

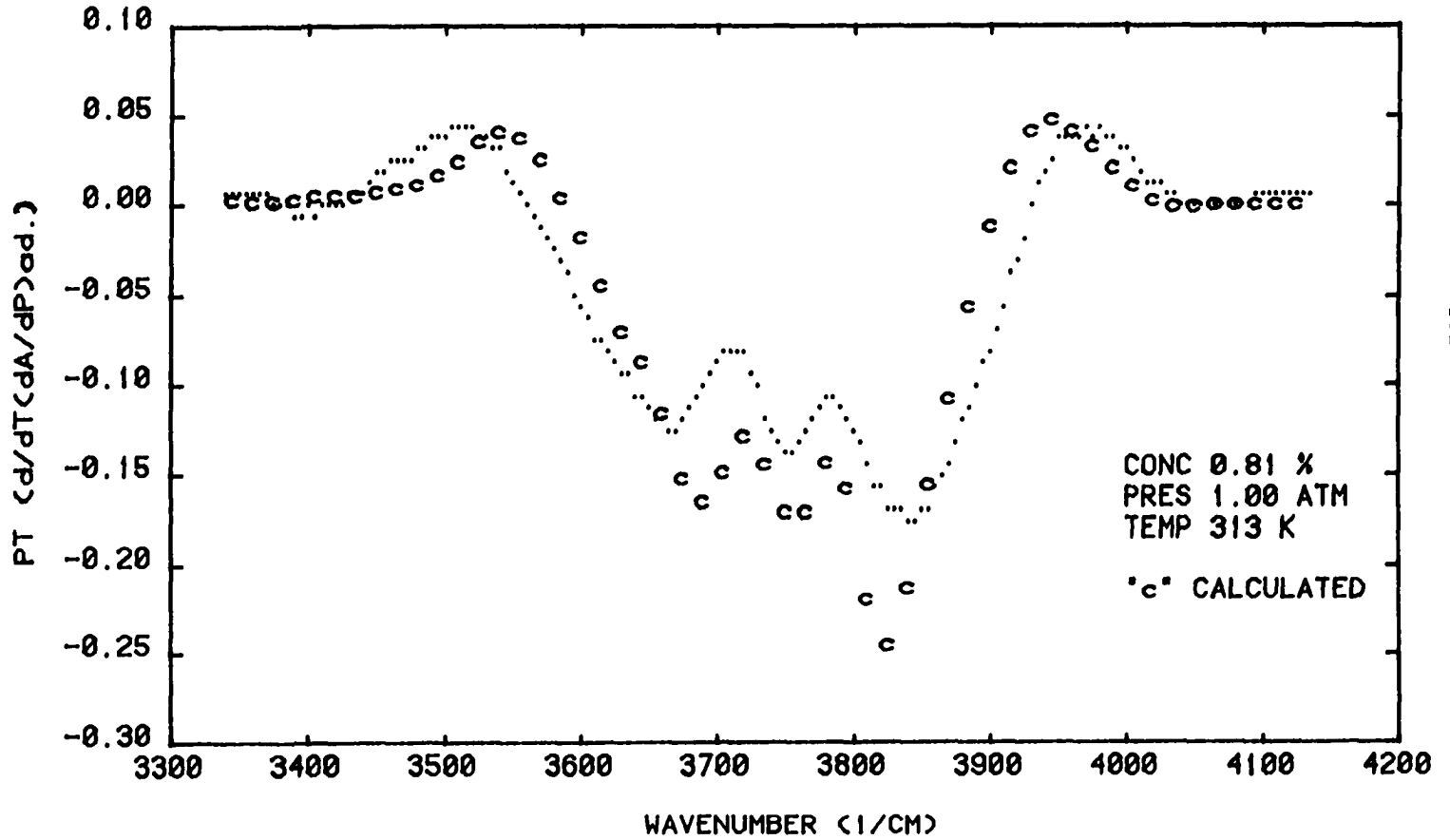


Figure 43

P (dA/dP)_{ad.} AS A FUNCTION OF dP

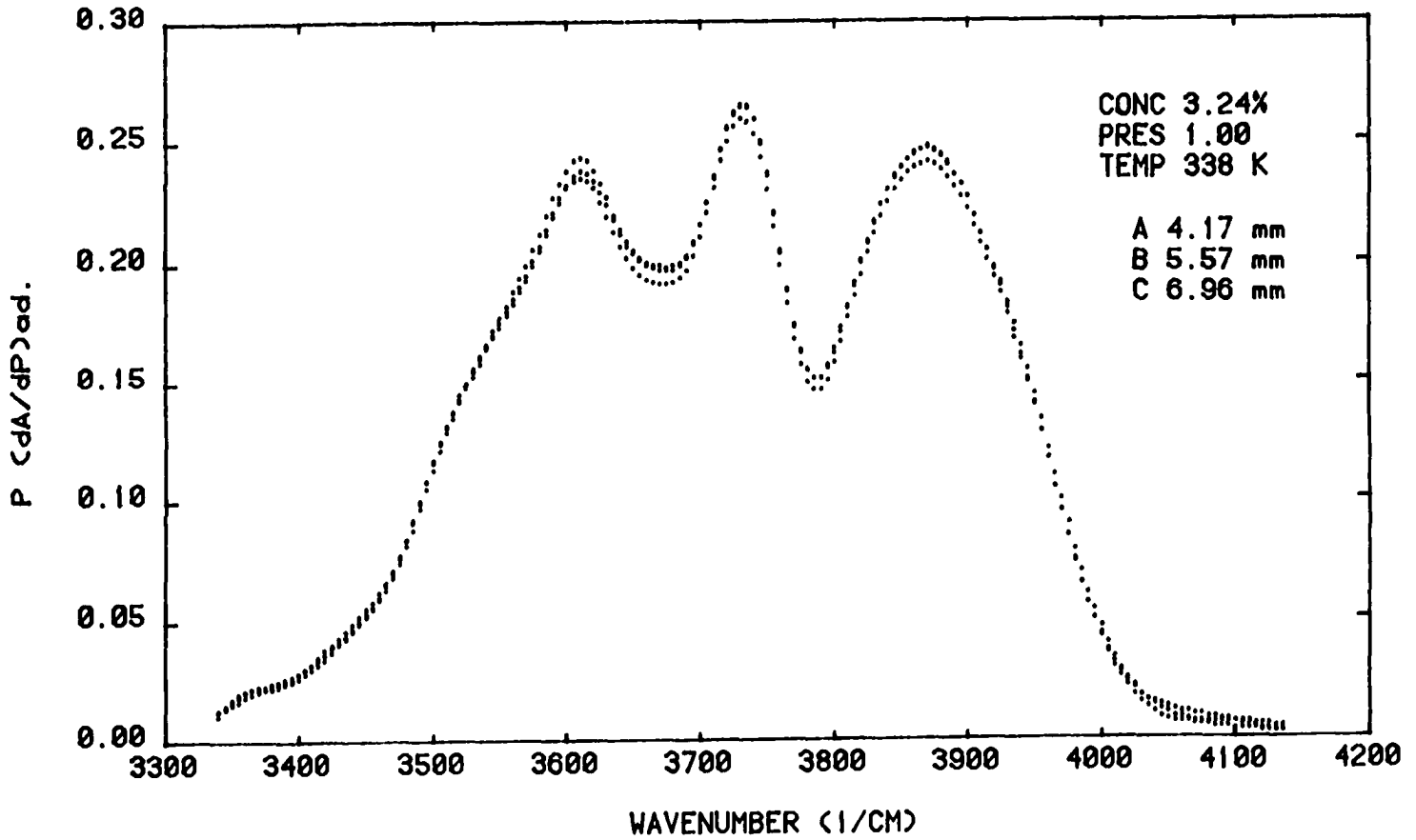


Figure 44

FLU. INTENSITY WITH FLU. PRESSURE AS A PARAMETER

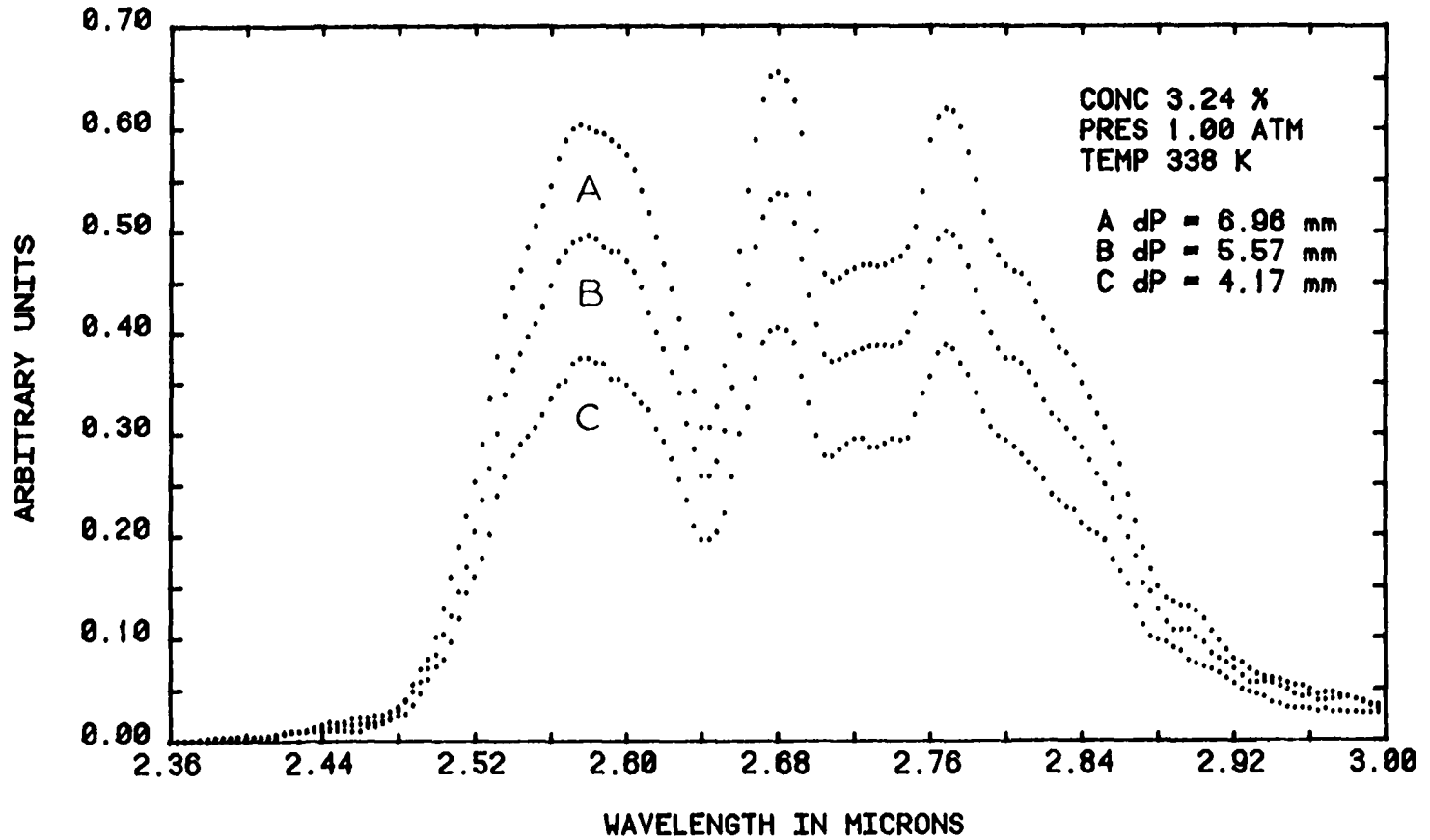


Figure 45

and this figure is typical of the experimental spectra obtained on the chartpaper.

G. DISCUSSION OF RESULTS

The basic aim of this experiment was to find spectral regions in the water vapor spectrum where the absorption or one of its derivatives may be expressed as a simple function of the thermodynamic variables, concentration, pressure, and temperature of the sample gas. In particular, we desired to express it as a function of only one of the three thermodynamic variables.

We have obtained the crossover points and thus isolated a region where the absorption depends upon two thermodynamic variables only. Examining the $(\partial A/\partial P)_{ad.}$ curves, we notice that in the crossover region, the pressure dependence is also minimal. Thus, for the $(\partial A/\partial P)_{ad.}$ spectra, there is a region which depends only on the concentration of the water vapor sample. A measurement at this region will enable us to determine the concentration of the water vapor. We have also found that near 3975 cm^{-1} and near 3525 cm^{-1} , the pressure dependence of the $(\partial A/\partial P)_{ad.}$ spectra is still negligible, but that there is a strong temperature dependence. Since we already know the concentration, the temperature of the water vapor can be obtained by a second measurement at this region. Finally a third measurement anywhere in the core of the band will yield the pressure of the water vapor. Thus, at least in principle, the $(\partial A/\partial P)_{ad.}$ spectra can be used for a spectral inversion to measure the thermodynamic variables, concentration, pressure, and temperature of

the sample gas.

H. 3.46 MICRON HYDROGEN CHLORIDE ABSORPTION AND ITS DERIVATIVES

Results for the calculation of the HCl fundamental band are presented in this section. The spectra are calculated for one atmosphere pressure and 300°K and are degraded to 30 cm⁻¹.

Figure 46 is a plot of the absorption versus wavenumber with the absorber mass, u , in units of g/cm², as a parameter. The absorber mass, u , can be related to the concentration, pressure, and temperature of the sample gas by

$$u = \text{constant} \times \frac{P_t}{T} \times c,$$

where $c = p/P_t$, p being the partial pressure of the sample gas and P_t being the total pressure of the sample gas and the foreign gas combined. We will use them both interchangeably in this section.

Figure 47 shows the calculated absorption spectrum for $u = 3.5687$ ($P^2\lambda = 1$), indicated by the solid line, compared with the values of Reference 39; λ is the path length of the absorber medium. The curve marked by the error bars is the measured spectrum, with an integrated absorptance of 57.2 cm⁻¹. The dashed line curve is the result of a theoretical calculation by Stull and Plass³⁹, with an integrated absorptance of 50.9 cm⁻¹. Our calculation yields an integrated absorptance of 60.1. Our calculated spectrum fits the experimental curve quite well, much better than the other calculations of Reference 39. Finally, the dash-dot-dash line curve is the result of an isolated

3.46 MICRON HCl BAND ABSORPTION

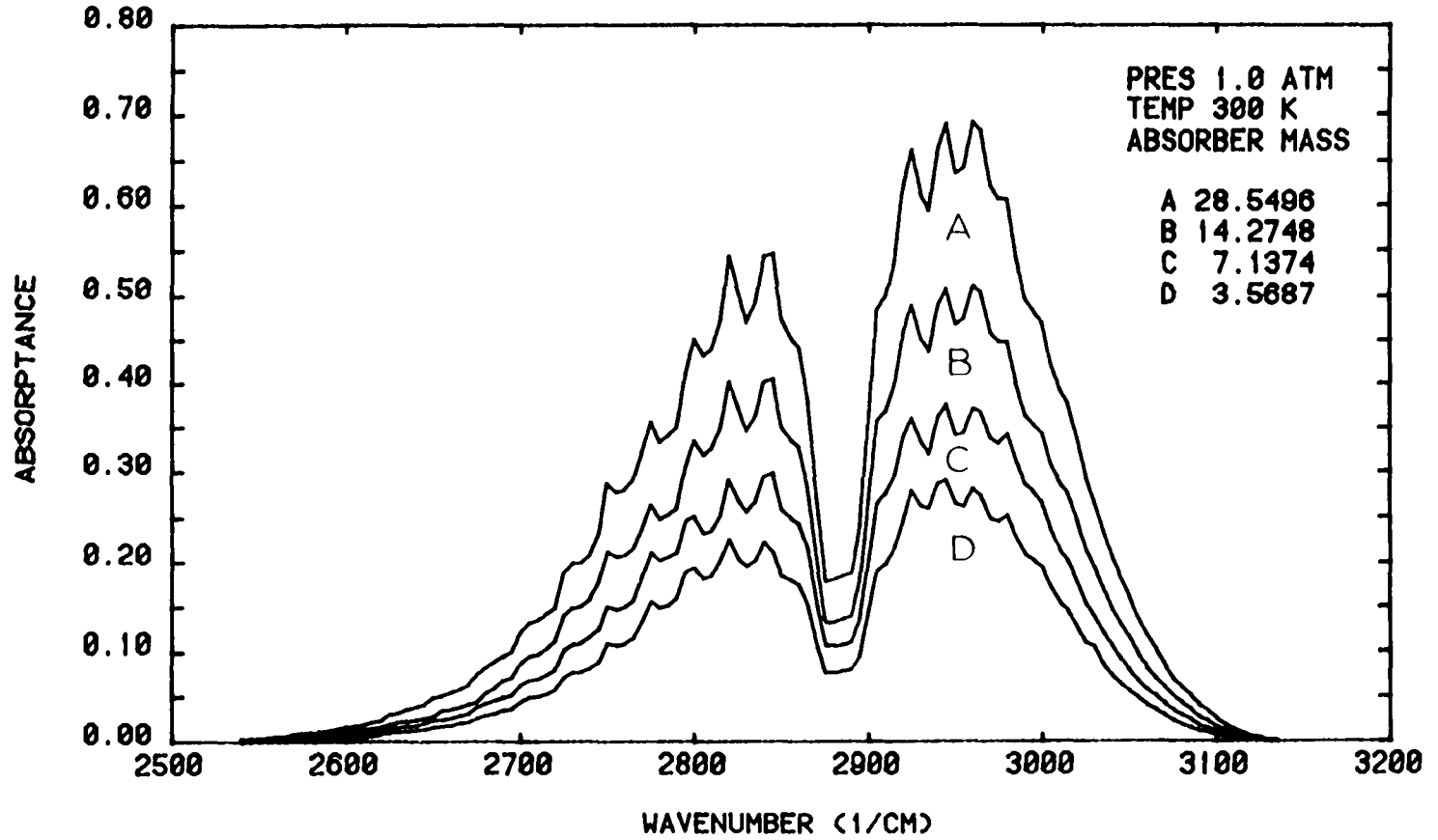


Figure 46

3.46 MICRON HCl BAND ABSORPTION

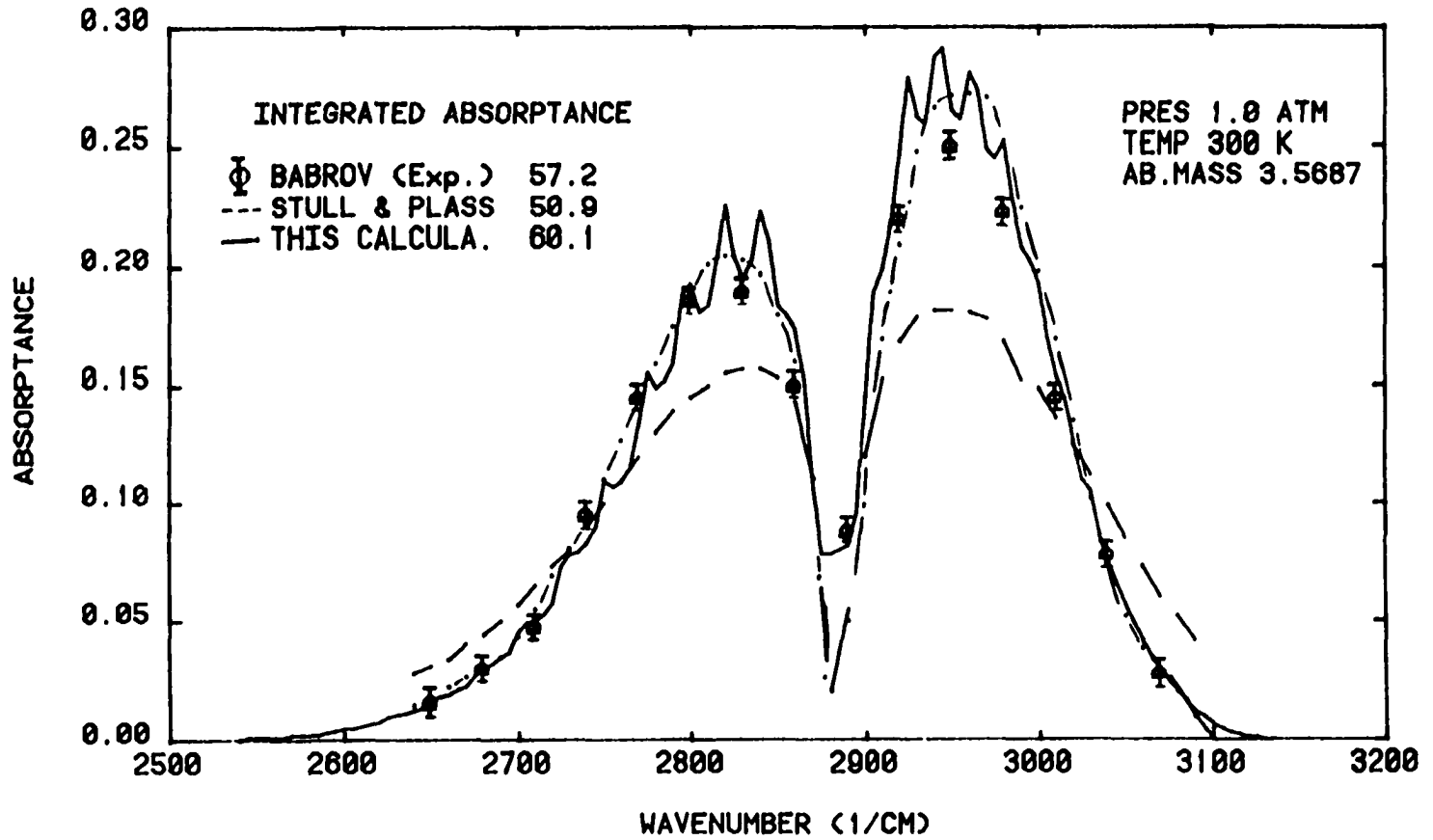


Figure 17

CALCULATED AVERAGE ENERGY

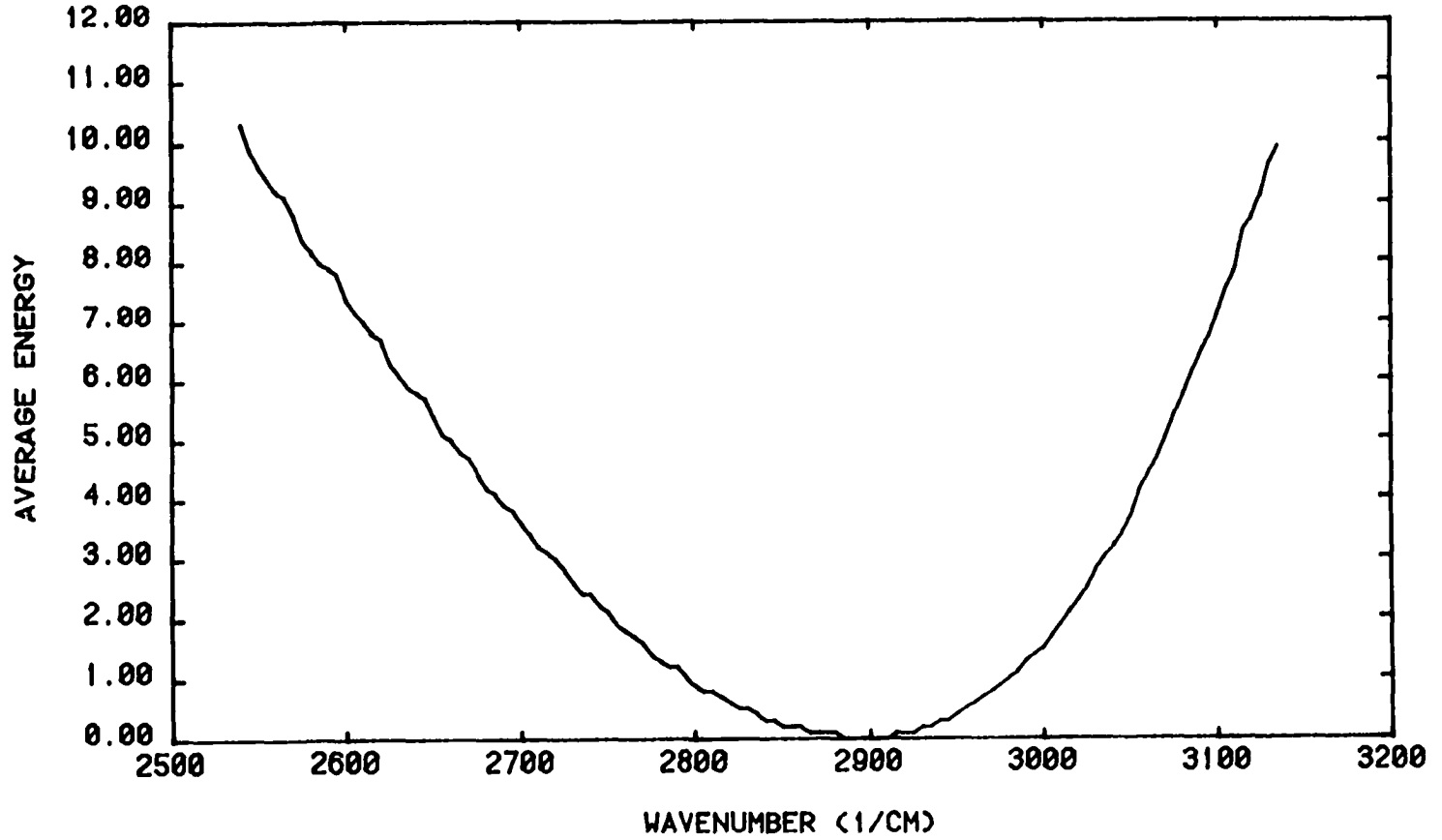


Figure 48

DERIVATIVE OF 3.46 HCl BAND ABSORPTION

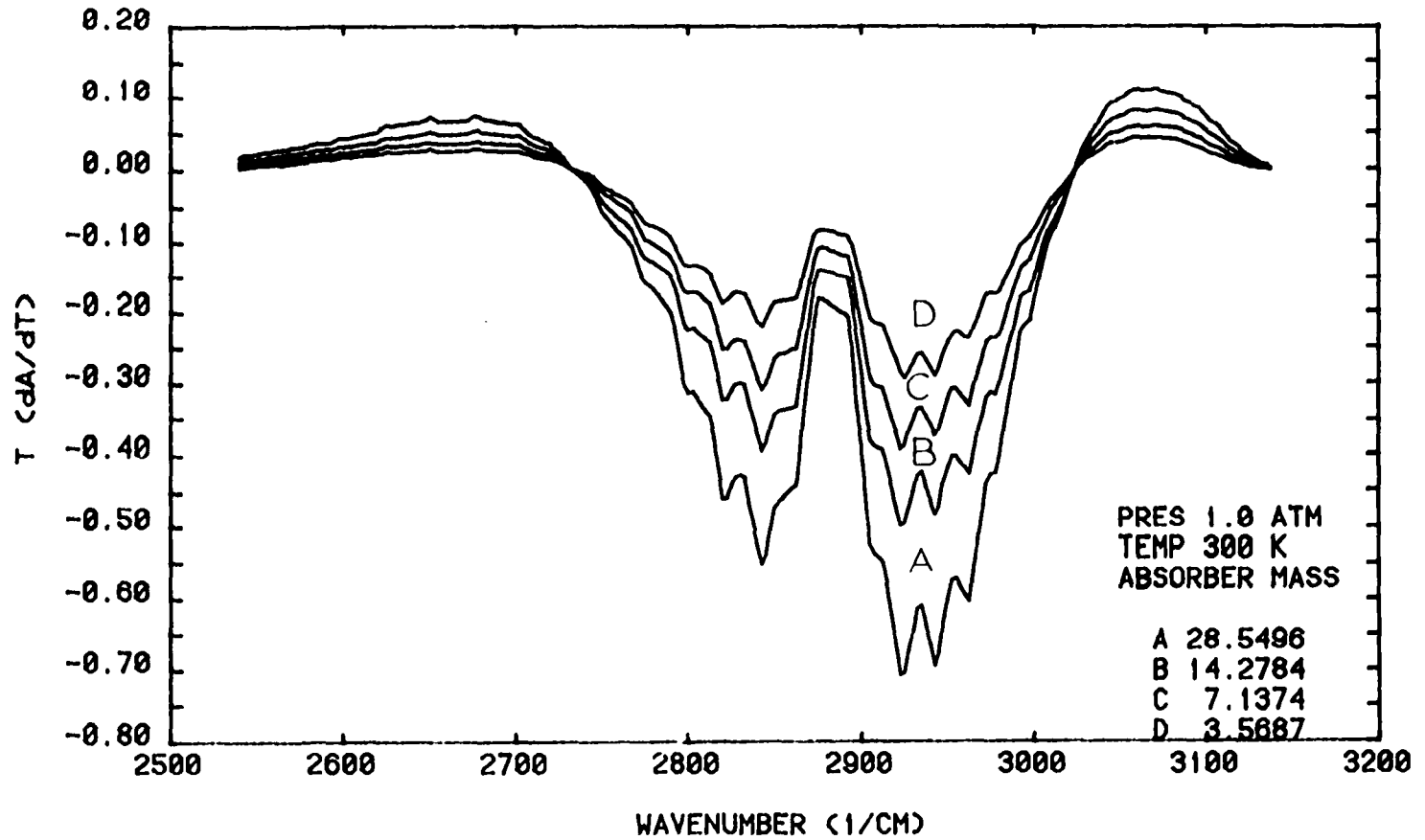


Figure 19

DERIVATIVE OF 3.46 MICRON HCl BAND ABSORPTION

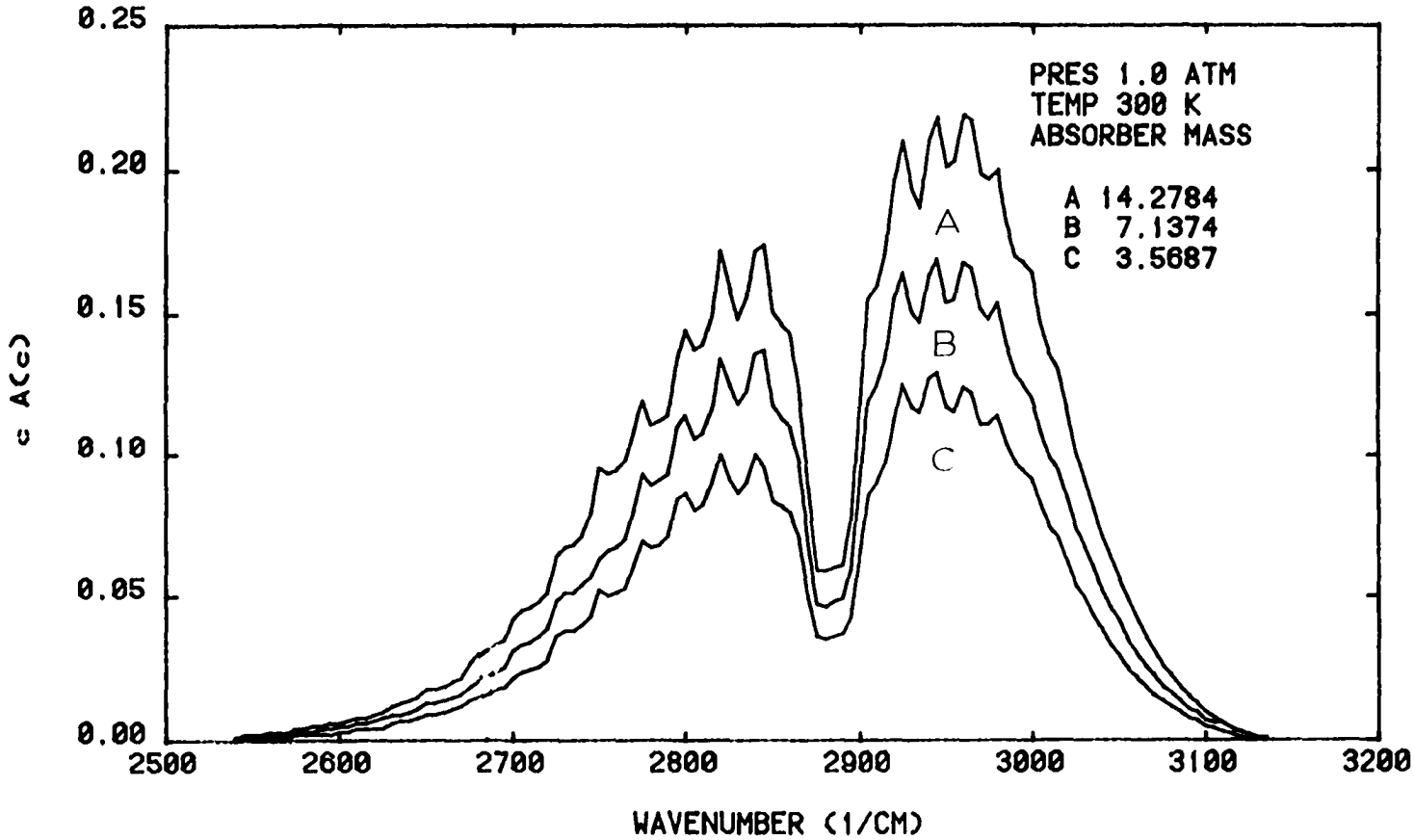


Figure 50

DERIVATIVE OF 3.46 HCl BAND ABSORPTION

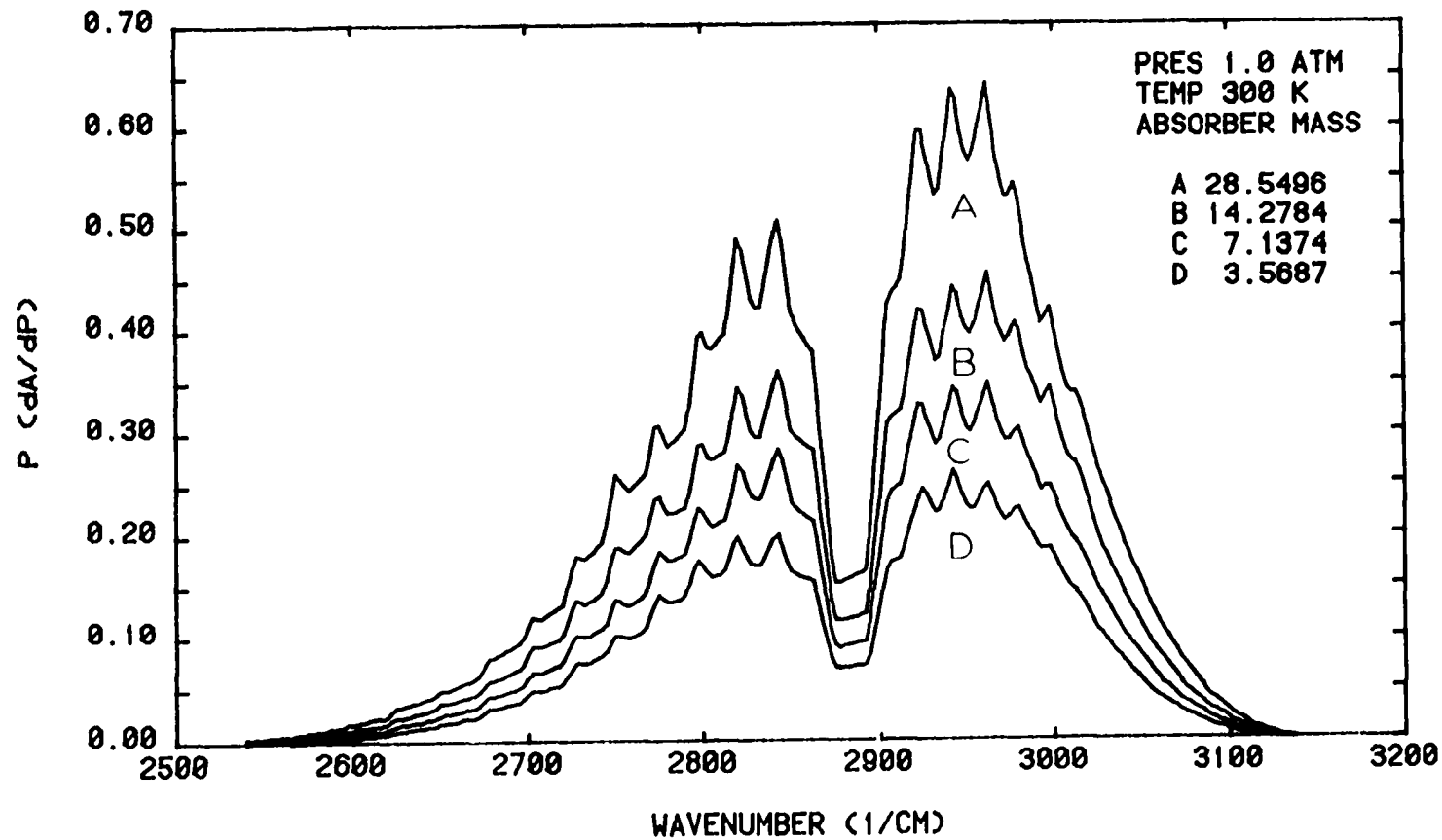


Figure 51

ADIABATIC DERIVATIVE OF 3.46 HCl BAND ABSORPTION

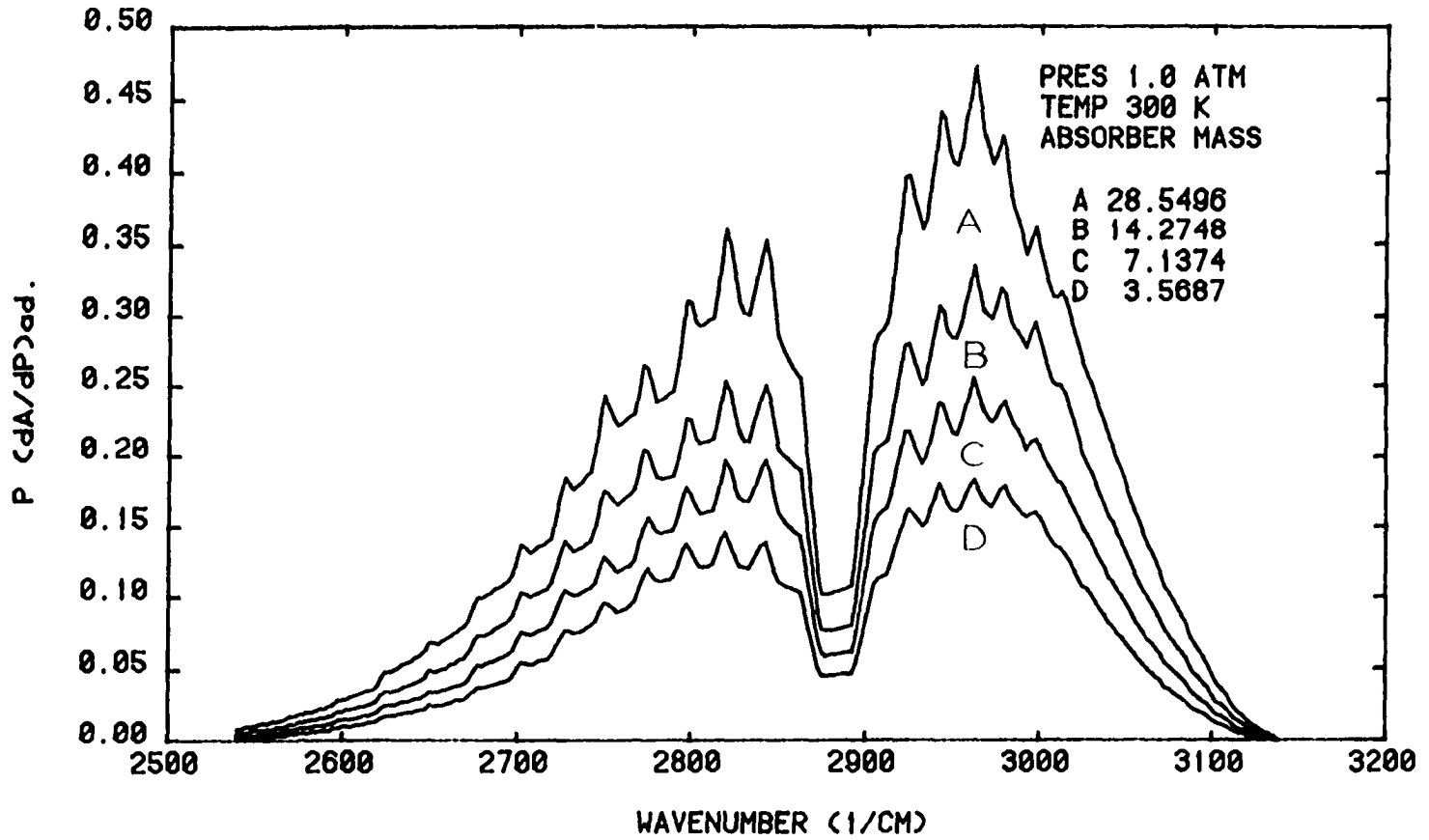


Figure 52

ADIABATIC DERIVATIVE OF 3.46 HCl BAND ABSORPTION

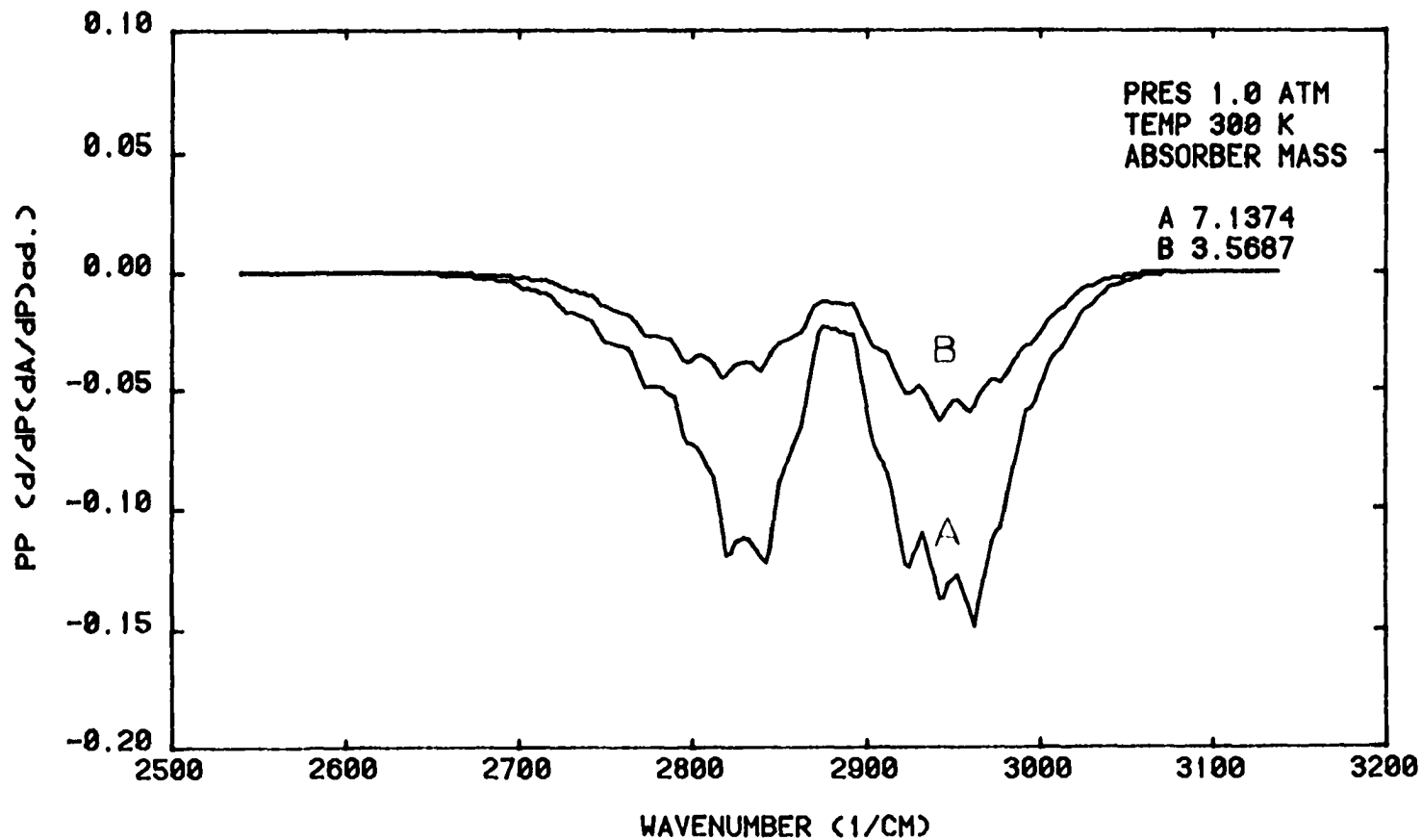


Figure 53

ADIABATIC DERIVATIVE OF 3.46 HCl BAND ABSORPTION

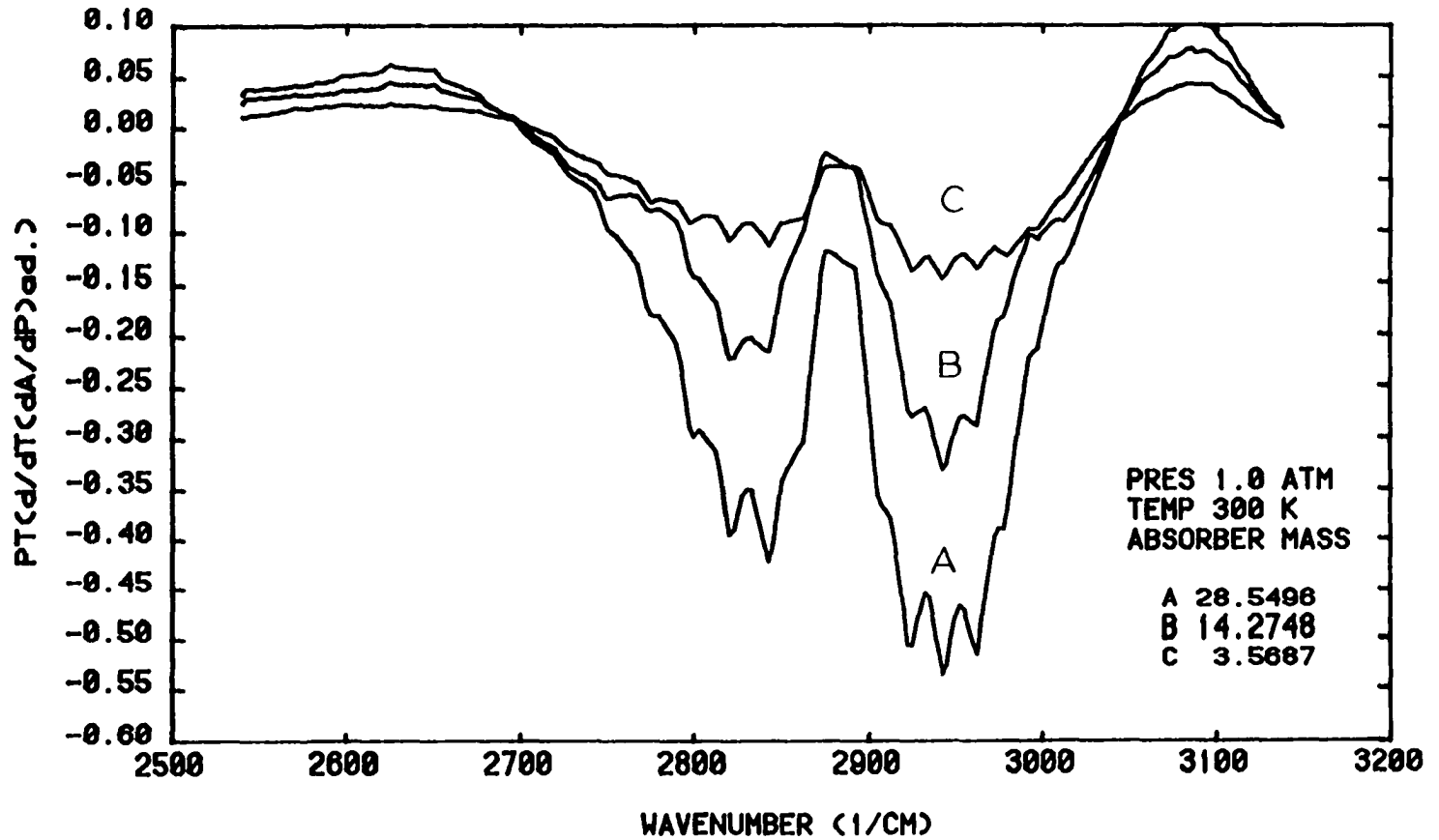


Figure 54

ADIABATIC DERIVATIVE OF 3.46 HCl BAND ABSORPTION

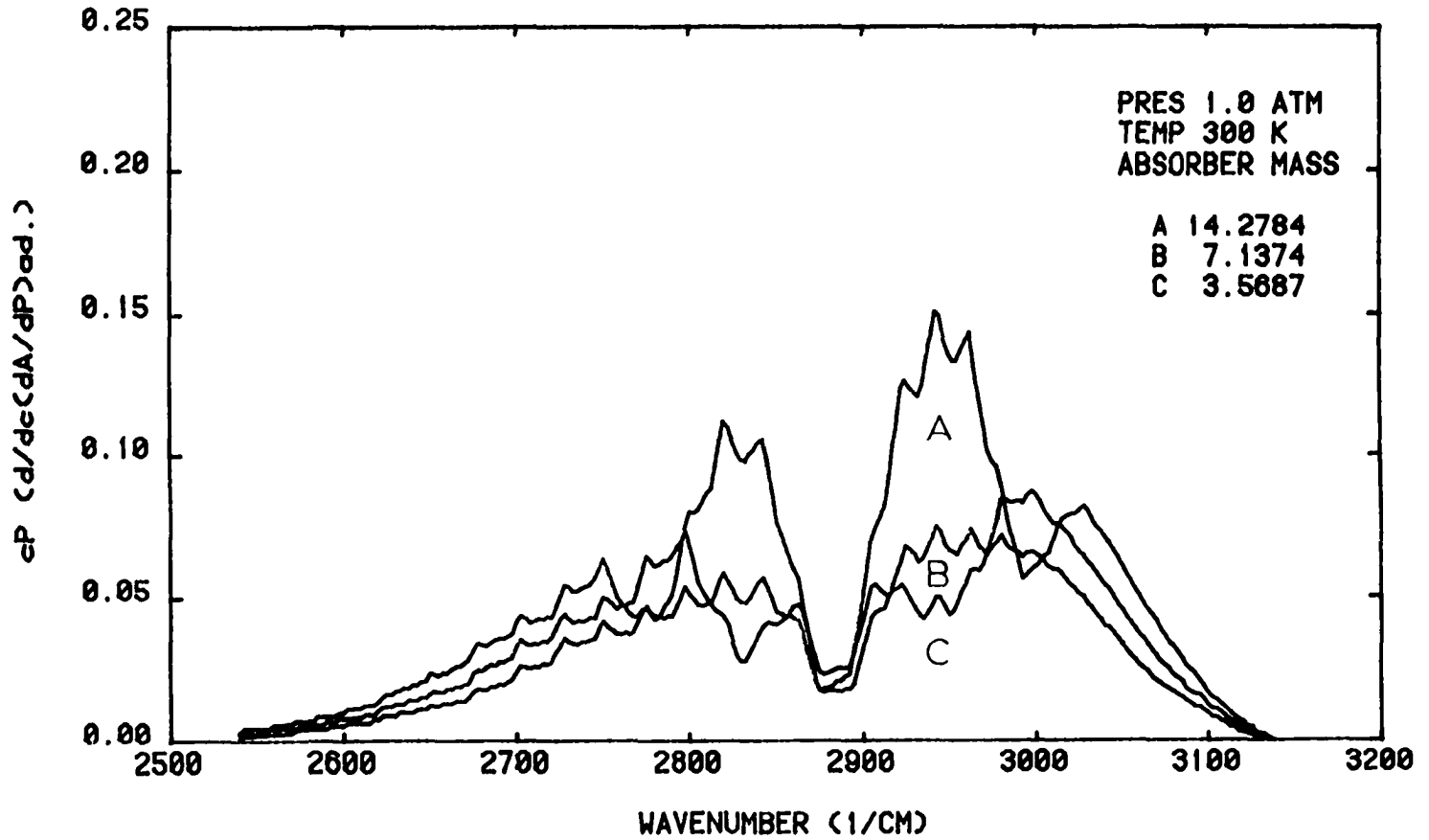


Figure 55

line theory calculation of Reference 39.

Figure 48 shows the average energy weighted by the absorption plotted against wavenumber. The absorptance equation of Reference 1 requires $(\partial A/\partial T)$ to be zero around the region of $E = 2.2$, which is the sum of the exponent of T in the expression for the rotational partition function, $m = 1$ for HCl, and a constant of about 1.2. This corresponds to two regions at about 2743 cm^{-1} and 3015 cm^{-1} .

Figure 49 shows $TA(T)$ versus wavenumber with u as a parameter. As expected, all the curves cut the X-axis at about 2730 cm^{-1} and 3025 cm^{-1} . Since the general thermodynamic dependence of the absorption and its derivatives of HCl are essentially the same as that of water vapor given earlier in this chapter, it will not be repeated here verbally.

Figure 50 and 51 show the other two first derivatives for HCl. Finally, Figures 52 through 55 show the adiabatic derivatives obtained using Table V.

CHAPTER VI

CONCLUSIONS

The use of the absorption and its thermodynamic derivative spectra of gases as a function of concentration, pressure, and temperature has been discussed by different authors^{2, 40}. We have shown that the thermodynamic derivative spectra of water vapor can be accurately measured in the laboratory using a vapor cross-flow system. We have also shown that these spectra can be calculated reliably from the individual line parameters of the vibration-rotation spectrum.

We agree with Babrov and Casden and Maclay that the line strengths compiled by the N.B.S. Monograph 71, for the 2.7 micron water vapor band should be corrected. We propose for the ratio of the measured line strengths to rigid rotator line strengths of the N.B.S. publication, the so called F factor, the function

$$F = (0.92 + Z_m)^2$$

where $m = J + 1$ for the R branch and $m = -J$ for the P branch; J is the rotational quantum number of the lower state. Furthermore, Z is given by -0.025 . Using the corrected line strengths, we obtained the absorption spectra which agreed within 4% with our experimental results and those of Reference 36.

The fluctuations in the thermodynamic variables obtained using acoustic excitation, were sufficient to produce measurable fluctuations in the transmitted intensity. Our experimental results agreed very well with the theoretical calculations using the corrected line strengths.

In the regions near 3575 cm^{-1} and 3910 cm^{-1} , in the wings of the 2.7 micron water vapor band, the dependence of the absorption and its adiabatic derivative with respect to pressure, upon the temperature is minimal, with a negative effect in the core of the band and a positive effect far in the wings of the band. We have also shown that the $PP \left(\frac{\partial}{\partial P} \left(\frac{\partial A}{\partial P} \right)_{\text{ad.}} \right)$ is very small in the wings of the band, while the $cP \left(\frac{\partial}{\partial c} \left(\frac{\partial A}{\partial P} \right)_{\text{ad.}} \right)$ is significant and can be used to measure the concentration of water vapor at a given location.

REFERENCES

1. Broersma, S., and Walls, W. L. "Thermodynamic Derivatives of Infrared Absorptance," Journal of the Optical Society of America (JOSA), Vol.64, No. 8, 1974, p. 1111.
2. Fisher, M. J., and Krause, F. R. "The Crossed-Beam Correlation Technique," Journal of Fluid Mechanics, Vol. 28, 1967, p. 705.
3. Nielsen, J. R., Thorton, V., and Dale, E.B. "The Absorption Laws for Gases in the Infrared," Rev. of Modern Physics, Vol. 16, No. 4, 1944, p. 307.
4. Gates, D. M., Calfee, D. F., Hansen, D. W., and Benedict, W. S. "Line Parameters and Computed Spectra for Water Vapor Bands at 2.7 Micron Region," N. B. S. Monograph 71, 1964, U. S. Dept. of Commerce.
5. Herzberg, G. Molecular Spectra and Molecular Structure: Vol. 2. Infrared and Raman Spectra. Van Nostrand Co., 1945.
6. King, G. W. Spectroscopy and Molecular Structure. Holt, Rinehart, and Winston, Inc., 1964.
7. Darling, B. T., and Dennison, D. M. "The Water Vapor Molecule," Physical Review, Vol. 57, 1940, p. 128.
8. Wyatt, P. J., Stull, V. R., and Plass, G. N. "The Infrared Transmittance of Water Vapor," Applied Optics, Vol. 3, 1964, p. 229.
9. Slawsky, Z. I., and Dennison, D. M. "The Centrifugal Distortion of Axial Molecules," The Journal of Chemical Physics (JCP), Vol. 7, 1939,p.509.

10. Allen, H. C., and Cross, P. C. Molecular Vib-Rotors. John Wiley and Sons, Inc., 1963
11. King, G. W., Hainer, R. M., and Cross, P. C. "The Asymmetric Rotor," The Journal of Chemical Physics, Vol. 11, 1943, p. 27.
12. Pugh, L. A., and Rao, N. K. "Spectrum of Water Vapor in the 1.9 and 2.7 Micron Regions," Journal of Molecular Spectroscopy, Vol. 47, 1975, p. 403.
13. Burch, D. E., Gryvnak, D. A., and Patty, R. R. "Scientific Report: Absorption by H₂O between 2800 and 4500 cm⁻¹ (2.7 Micron Region)," Publication No. U-3202, Aeronutronic Division of Philco Corporation, Ford Motor Co., Newport Beach, California(1965).
14. Howard, J. N., Burch, D. E., and Williams, D. "Infrared Transmission of Synthetic Atmospheres: I. Instrumentation," JOSA, Vol. 46, 1956,p. 186.
15. Wyatt, P. J., Stull, V. R., and Plass, G. N. "Infrared Transmission Studies, Final Report: Vol. II. The Infrared Absorption of Water Vapor," Publication SSD-TDR-62-127-Vol.II, Aeronutronic Division of Philco Corporation, Ford Motor Co., Newport Beach, California(1962).
16. Stephens, J. B. Private Communication, George C. Marshall Space Flight Center, N. A. S. A., Huntsville, Alabama.
17. Rank, D. H., Rao, B. S., and Wiggins, T. A. "Molecular Constants of HCl³⁵," Journal of Molecular Spectroscopy (JMS), Vol. 17, 1965, p. 122.
18. Mills, I. M., Thompson, H. W., and Williams, R. L. "The Fundamental Vibration-Rotation Band of Hydrogen Chloride," Proceedings of the Royal Society(London), Series A218, 1953, p. 29.
19. Herzberg, G. Molecular Spectra and Molecular Structure: Vol. 1. Spectra of Diatomic Molecules. Van Nostrand Co., 1950.

20. Toth, R. A., Hunt, R. H., and Plyer, E. "Line Strengths, Line Widths, and Dipole Moment Function of HCl," JMS, Vol. 35, 1970, p. 110.
21. Benedict, W. S., Herman, R., Moore, G. E., and Silverman, S. "The Strengths, Widths, and Shapes of Infrared Lines," Canadian Journal of Physics, Vol. 34, 1956, p. 850.
22. Varanasi, P., Saranji, S. K., and Tejwani, G.D.T. "Line Shape Parameters for HCl and HF in a CO₂ Atmosphere," Journal of Quantum Spectroscopy and Radiative Transfer (JQRST), Vol. 12, 1972, p. 857.
23. Rank, D. H., Eastman, D. P., Rao, B. S., and Wiggins, T. A. "Breathths and Shifts of Molecular Band Lines due to Perturbation by Foreign Gases," JMS, Vol. 10, 1963, p. 34.
24. Levy, A., Piollet-Mariel, E., and Boulet, C. "Noble-Gas Broadening of Vibration-Rotation Lines Belonging to Diatomic Molecules-I. Experimental Results for HCl Lineshifts and Widths," JQRST, Vol. 13, 1973, p. 673.
25. Maclay, G. J. "Integrated Absorptance of Spectral Line Groups in the 2.7 Micron Bands of Hot Water Vapor, Including Effects of Centrifugal Distortion," JCP, Vol. 43, 1965, p. 185.
26. Babrov, H. J., and Casden, F. "Strengths of Forty-two Lines in the ν_1 and ν_3 Bands of Water Vapor," JOSA, Vol. 58, No. 2, 1968, p. 179.
27. Babrov, H. J., and Healy, A. R. "Strengths of Twenty Lines in the ν_3 Band of Water Vapor," JOSA, Vol. 59, 1969, p. 779.
28. Benedict, W. S., and Calfee, D. F. "Line Parameters for the 6.3 Micron and 1.9 Micron Bands of Water Vapor," Environmental Science Service Administration, Professional Paper 2, U. S. Dept. of Commerce(1969).
29. Braslawsky, J., and Ben-Aryeh, Y. "First-Order Intensity Perturbations for the Vibration-Rotation Lines of Asymmetric Rotor: Theory

- and Application," JCP, Vol. 51, 1969, p.2233.
30. Cann, M. W. P. "An Optical Absorption Cell with Variable Path Length and Temperature," The Review of Scientific Instruments(RSI), Vol. 40, No. 4, 1969, p. 595.
 31. Hendrickson, P. E., Walls, W. L., and Broersma, S. "An Optical Absorption Cell with Vapor Cross Flow," RSI, Vol. 44, No. 3, 1973, p. 347.
 32. Cann, M. W. P. Instruction Manual: Absorption Calibration Cell, Illinois Institute of Technology Research Institute, Chicago(1969).
 33. Lysobey, D. J. "Infrared Correlation Spectroscopy with Application to CO₂ under Atmospheric Conditions," Ph. D. Thesis, The University of Oklahoma, Norman, 1972.
 34. Broersma, S., Hendrickson, P. E., and Walls, W. L. Technical Report: Thermodynamic Derivative Spectra of Infrared Absorption, The University of Oklahoma, 1973.
 35. Hendrickson, P. E., Walls, W. L., and Broersma, S. "6.3 Micron Water Vapor Band Derivatives," JOSA, Vol. 64, 1974, p. 1119.
 36. Plass, G. N., Yates, H. Handbook of Military Infrared Technology; Edited by Wolfe, W. L., Office of Naval Research, U. S. Printing Office, Washington D. C., 1965.
 37. Howard, J. N., Burch, D. E., and Williams, D. "Infrared Transmission of Synthetic Atmospheres: III. Absorption by Water Vapor," JOSA, Vol. 46, 1956, p. 242.
 38. Abramowitz, and Stegun(Editors). Handbook of Mathematical Functions, N. B. S., U. S. Dept. of Commerce, 1964, p. 914.
 39. Babrov, H. J. "Experimental and Theoretical Infrared Absorptance of HCl at various Temperatures," JOSA, Vol. 53, No. 8, 1963, p. 945.

40. Krause, F. R., Betz, H. T., and Lysobey, D. J. "Pollution Detection by Digital Correlation of Multispectral, Stereo-Image Pairs," *Journal of Atmospheric Environment*, Vol. 7, 1973, p. 455.